2012

Study on underground coal gasification combined cycle coupled with on-site carbon capture and storage

Peng Pei
University of North Dakota

STUDY ON UNDERGROUND COAL GASIFICATION COMBINED CYCLE COUPLED WITH ON-SITE CARBON CAPTURE AND STORAGE

by

Peng Pei

Bachelor of Engineering, North China Electric Power University, 2005

Master of Science, University of North Dakota, 2008

A Dissertation

Submitted to the Graduate Faculty

of the

University of North Dakota

in partial fulfillment of the requirements

for the degree of

Doctor of Philosophy

Grand Forks, North Dakota

December

2012

This dissertation, submitted by Peng Pei in partial fulfillment of the requirements for the degree of Doctor of Philosophy from the University of North Dakota, has been read by the Faculty Advisory Committee under whom the work has been done and is hereby approved.

Zhengwen Zeng, Chairperson

Steve Benson

Scott Korom

Richard LeFever

Vasyl Tkach

This dissertation is being submitted by the appointed advisory committee as having met all of the requirements of the Graduate School of the University of North Dakota, and is hereby approved.

Dr. Wayne Swisher
Dean of the Graduate School

11-19-2012
Date

Title Study on Underground Coal Gasification Combined Cycle Coupled with On-site Carbon Capture and Storage

Department Geology and Geological Engineering

Degree Doctor of Philosophy

In presenting this dissertation in partial fulfillment of the requirements for a graduate degree from the University of North Dakota, I agree that the library of this University shall make it freely available for inspection. I further agree that permission for extensive copying for scholarly purposes may be granted by the professor who supervised my dissertation work or, in his absence, by the chairperson of the department or the dean of the Graduate School. It is understood that any copying or publication or other use of this dissertation or part thereof for financial gain shall not be allowed without my written permission. It is also understood that due recognition shall be given to me and to the University of North Dakota in any scholarly use which may be made of any material in my dissertation.

Peng Pei
November 9, 2012

TABLE OF CONTENTS

LIST OF FIGURES

LIST OF TABLES

ACKNOWLEDGMENTS

First I would like to express my sincere appreciation to Dr. Zhengwen Zeng, my advisor, for his great efforts in helping and advising for my study for the Ph.D. degree. I would also like to express my appreciation to Dr. Steve Benson, Dr. Scott Korom, and Dr. Richard LeFever, for lots of their help and support to my research, dissertation and classes in the past several years. I would also thank Dr. Vasyl Tkach as the committee member at large.

During my study, I got numerous help from my colleagues, team members and friends around me. I am very grateful to Hong Liu, Jun He, Darin Buri and Dr. Joe Hartman from the Harold Hamm School of Geology and Geological Engineering; Melanie Jensen, Dr. Robert Cowan, Dan Daly, John Kay and Ed Steadman from the Energy and Environmental Research Center; Dr. Kegang Ling from the Department of Petroleum Engineering; Ed Murphy and Julia LeFever from the North Dakota Geological Survey; and Susan Tewalt from the United States Geological Survey.

My study has been partially supported through different projects funded by federal and state agencies (US DOE: DE-FC26-05NT42592 and DEFC26-08NT0005643; North Dakota Department of Commerce: Petroleum Research, Education and Entrepreneurship Center of Excellence; North Dakota Industrial Commission: NDIC-G015-031 and six industrial partners (Denbury Resources Inc., Great Northern Properties, Hess Corporation,

Marathon Oil Company, St. Mary Land & Exploration Company, and Whiting Petroleum Corporation). Special thanks to BP America Inc. for supporting Dr. Zeng's continuing commitment to advising me on my dissertation.

At last, I want to dedicate this dissertation to my parents, Liangui Pei and Qinglan Huang, who lost their education opportunities and dreams of achievement in the 1960s and 70s. Their silent love always gives me the integrity and courage to overcome the difficulties on my journey.

ABSTRACT

The North Dakota portion of the Williston basin holds huge, but economically unmineable lignite resources in the Fort Union formation. A technology coupling the underground coal gasification with carbon capture and storage (UCG-CCS) is proposed in this study to recover these lignite resources in North Dakota. The UCG-CCS system provides a cost-effective and environment-friendly approach to convert the lignite to electricity and beneficially utilize the by-product of CO_2 at the same time. The target coal seam is the Harmon lignite in the Fort Union formation in western North Dakota. The main objectives of this study are to set up the technology roadmap, conduct the preliminary feasibility study, and identify necessary future research works.

Based on literature review, three UCG candidate sites were screened out, located in Dunn, Golden Valley, and Slope Counties, respectively. The selected site in Dunn County has the best potential to host the UCG-CCS project because of its suitable geological conditions and proximity to oil fields. A three-dimensional geological model, a facies model and an aquifers distribution model were built. It is also estimated that the nearby oil fields have a CO_2 storage capacity of 18 million tones. So there exists a big market for beneficial utilization of CO_2 in the study area.

Environmental risks associated with UCG are always worth noting. The environmental risks usually result from the change of formation properties and the in situ stress field

during the gasification process. Good understanding to the geomechanical, petrophysical and hydrogeological characteristics of the coal-bearing formation is important. A laboratory geomechanical study was conducted by using rock samples of the Harmon bed. The results show that the low strength of the adjoining rock would be considered as a disadvantage for structural stability. On the other hand, the low-permeable adjoining rocks function as a hydraulic seal to prevent the escape of contaminants during gasification process. An analytical study and numerical modeling of a conceptual commercial scale UCG plant were also carried out to analyze the stability of the cavities and the mining recovery factor of the coal seam. The allowable size of the UCG cavities and reasonable spacing between the cavities were estimated based on the stress profile and safety consideration. The results indicate the mining recovery factor is significantly affected by the presence of discontinuity in the formation. The methodologies and results provide a convenient and fast approach to estimate the economics of a UCG plant, once the fundamental properties of the coal-bearing formation are known.

In the last part, the plant performance and cost of the UCG-CCS system were analyzed by analogue to an integrated gasification combined cycle (IGCC) plant with CO_2 capture. The results indicate that, as there is no surface gasifier and fuel handling system, the capital cost of a UCG-CCS system is significantly reduced by 50%, and the UCG-CCS system presents advantages over the IGCC plant.

Keywords: Underground coal gasification, CO_2 capture and storage, Fort Union lignite

CHAPTER I

INTRODUCTION

1.1 Importance of Coal

Coal is one of the most important energy resources in the world, and will remain so over the next several decades. According to the Statistical Review of World Energy 2012 published by BP [1], the world coal consumption in 2011 was 3,724.3 million tons oil equivalent, the global coal production in 2011 was 7,695.4 million tons, and the global proved coal reserves were 860,938 million tons. In other words, the global proved reserves of coal in 2011 were sufficient to meet 112 years of world production, by far the largest reserves-to-production (R/P) ratio for any fossil fuel. Regarding the United States, coal consumption in the U.S. in 2011 was 501.9 million tons oil equivalent, the U.S. produced 992.8 tons of coal in 2011, and the proved reserves were 237,295 million tons. The U.S. has a coal R/P ratio as high as 239 years, and this number is much higher than other major coal consumers in the world, such as the European Union (R/P ratio=97), China (R/P ratio=33) and India (R/P ratio=103).

The U.S. is home to the largest recoverable reserves of coal in the world. The U.S. Energy Information Administration (EIA) provides more detailed information about the importance of coal in the U.S. energy sector. About 93% of coal consumption in the US is

in the electrical power sector. In 2010, coal was the fuel for about 42% of the 4 trillion kilowatt-hours (kWh) of electricity generated in the U.S., comparing to natural gas: 25%, nuclear: 20%, hydropower: 8%, window power: 3%, biomass: 1%, solar: less than 1%, and geothermal: less than 1% [2]. The share of electricity generated from coal is expected to decrease by 2035. But the growing demand for electricity is expected to lead to an increase in the actual amount of coal used.

Through EIA's statistic data, coal consumption in 2010 totaled 951.2 million tons, up 5.1% from the 2009 consumption level of 904.9 million tons. This increase can be attributed to higher consumption in the electric power, manufacturing, and coke sectors. Coal is produced in 25 states spread across three coal-producing regions, but approximately 72% of current production originates in just five states: Wyoming, West Virginia, Kentucky, Pennsylvania, and Montana [3]. Figure 1 shows the map of major coal producing areas in the U.S.

Anthracite accounts for less than 0.5% of the coal mined in the U.S., and all the anthracite mines are located in northeastern Pennsylvania. Bituminous coal is the most abundant rank of coal found in the U.S., accounting for more than 45% of U.S. coal production. In addition to use in power generation, bituminous coal is also an important fuel and raw material for the steel and iron industries. West Virginia, Kentucky, and Pennsylvania are the top producers of bituminous coal. About 47% of the coal produced in the U.S. is subbituminous. Wyoming is the leading source of subbituminous coal.

Lignite accounts for 7% of total U.S. produced coal. Most lignite is mined in Texas and North Dakota. Lignite is mainly burned at power plants to generate electricity [4].

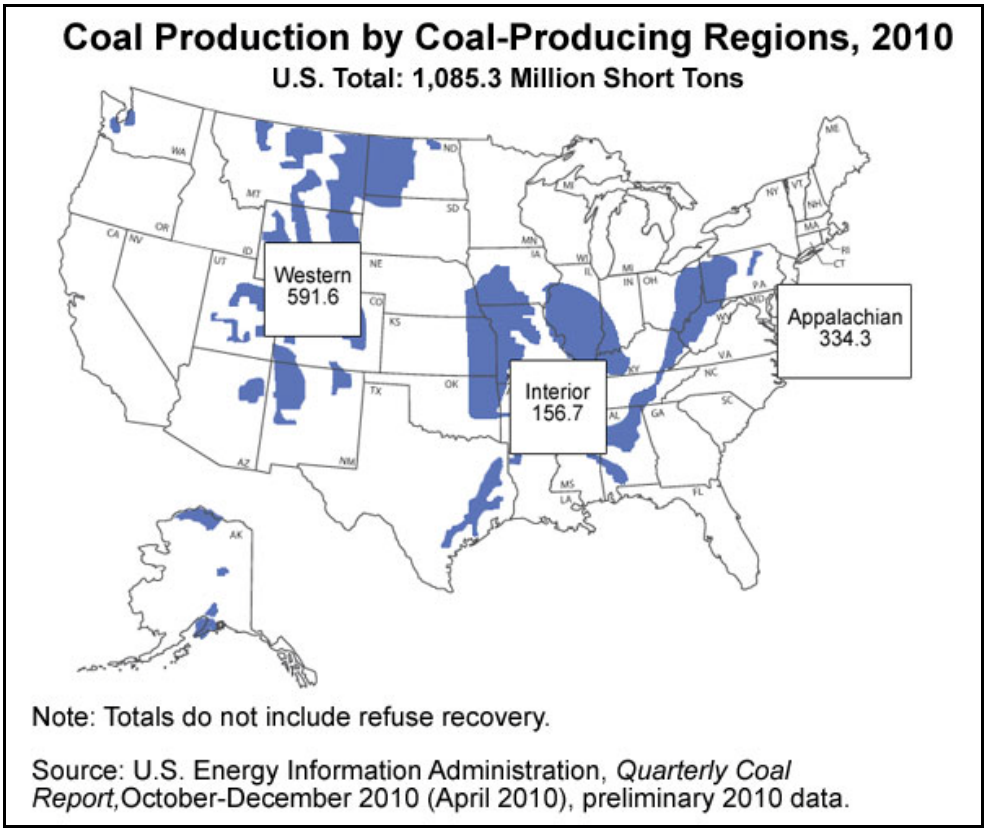

Figure 1. Major U.S. coal reserves and productions in 2010 [5].

From the above description, it is easy to conclude that there are huge coal resources and coal has been serving as a significant role in the energy sector. However, to facilitate the utilization of coals, some key barriers need to be addressed. Due to the limit of current coal mining technologies, 85% of the world coal resources are unmineable [6]. Coal mining introduces problems of safety, subsidence, groundwater contamination, surface pollution, and greenhouse gas emissions. Combustion of coal releases pollutants into the environment, including SO_x, NO_x, and particulate matter. The disposal of solid waste requires significant land use. In additions, the efficiency of most pulverized coal (PC)

power plants is less than 40%. This means current coal-based power generation systems have significant potential to improve their performance.

Coal-fired power plants are considered to be the biggest contributor of anthropogenic greenhouse gas emission. Coal accounted for 37% of the total U.S. emissions of CO_2 released into the Earth's atmosphere in 2010 [5]. In the special report issued by Intergovernmental Panel on Climate Change (IPCC) [7], it specifies that coal is currently the dominant fuel in the power sector, accounting for 38% of electricity generated in 2000, and coal is predicted to contribute 36% of electricity generation in 2030. As large stationary resources, coal-fired power plants have been listed as the primary target for CO_2 emission reduction. The introduction of carbon capture and storage (CCS) system will result in high energy penalties and significant cost increases to the power generation sector. Therefore, clean coal technologies that are able to utilize the huge coal reserves on the world or in the U.S. must be developed and applied to feed the need for energy in the next several decades.

1.2 Underground Coal Gasification Technology

Underground coal gasification (UCG) is a clean coal technology that converts coal in situ into a gaseous product, commonly known as synthesis gas or syngas through the same chemical reactions that occur in surface gasifiers [8]. The syngas primarily consists of CO, H_2, some CO_2 and minor amounts of CH_4. As indicated in Figure 2, wells are drilled to inject air or oxygen that drives combustion and gasification in situ, and to transport syngas to the surface for further processing, transport and utilization. The UCG process

can exploit coal deposits at depths greater than 100 meters (m), and where the coal seam thickness is greater than 2 m. The syngas produced from UCG typically has a relatively high content of CO and H_2, and is low in CH_4. Pollutants can be well controlled in the UCG process. Because of environmental concerns related to groundwater, the reactor cavity is usually operated at pressures lower than hydrostatic pressure, which brings water into the gasification reaction zone in situ [9].

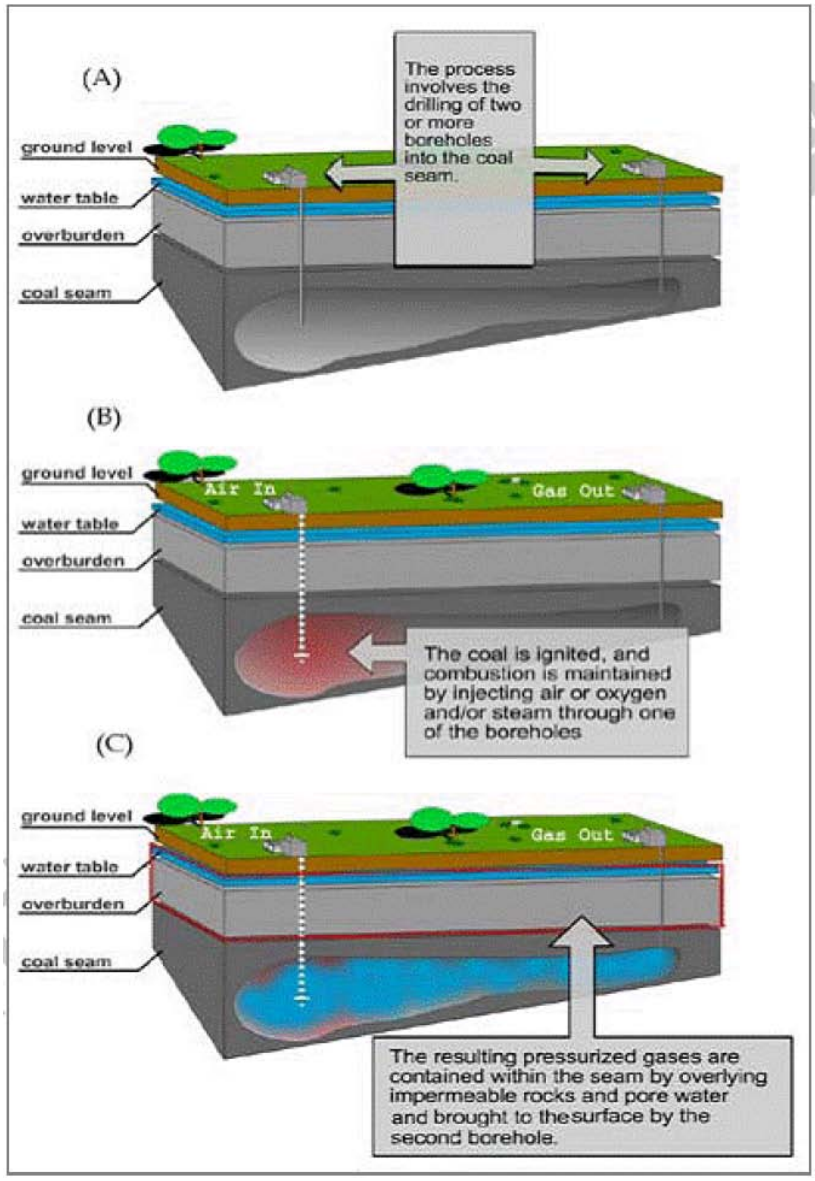

Figure 2. The UCG process [6].

As mentioned earlier, 85% of world coal resources are not economically mineable due to the limits of conventional mining approaches. The UCG process can utilize coal seams that are too deep to be economically mined, thereby significantly increasing global recoverable coal reserves. Linc Energy [6] estimated that there is over 5 million petajoule (PJ) of resource of UCG syngas in the U.S., over 1 million PJ of gas currently available and an additional 1.3 million PJ estimated to be available in Australia, 1.9 million PJ of UCG gas available in India, and over 2.2 million PJ of UCG syngas in China. It also stated that by using UCG technology, the recoverable reserves could be increased by at least three to four times. This means that 1.45 trillion tons of unminable coal in U.S. could be recovered. The UCG holds several advantages such as lower capital investment costs (due to the absence of a manufactured gasifier and coal preparing equipment), no handling of coal and solid wastes at the surface (ash remains in the underground cavity), no human labor or capital for underground coal mining, no minimum surface disruption, no coal transportation costs, and direct use of water and feedstock available in situ [10]. If the produced syngas is used to generate electricity with CO_2 capture, the cost of electricity is about $24 per megawatt hour (MWh), compared $77 for integrated gasification combined cycle (IGCC) and $52 for supercritical PC power plants [11]. Recently UCG has received renascent interests because of its ability to combine with CCS. The UCG Association [12] lists current UCG projects on the world as shown in Figure 3. Interests in the UCG technology and projects at different levels have recently occurred in most coal producing regions of the world, led largely by Australia who is interested in the potential for power generation and gas to liquids conversion. Other countries and regions of UCG activity include New Zealand, South Africa, China, U.S.,

Eastern Europe, India, Indonesia, Vietnam, Pakistan and the UK, which has recently issued a number of licenses to exploit UCG offshore.

Figure 3. Global UCG activities in recent years [12].

During the utilization process of the produced syngas, CO_2 can be separated and injected into adjacent coal seams which are not suitable for UCG operation (Figure 4). An example could be that the syngas is used in the gas turbine for electricity generation with a pre-combustion carbon capture process. In such a process, the raw syngas is cleaned first, and then treated with a water gas shift (WGS) reaction, which converts the CO in the syngas into CO_2 and generates more H_2. CO_2 is captured from the syngas, and the remaining H_2 is combusted to drive a gas turbine. The separated CO_2 is sequestered on site [13]. The UCG-created cavities, existing boreholes and hydraulic fractures may also provide extra potential CO_2 storage capacity.

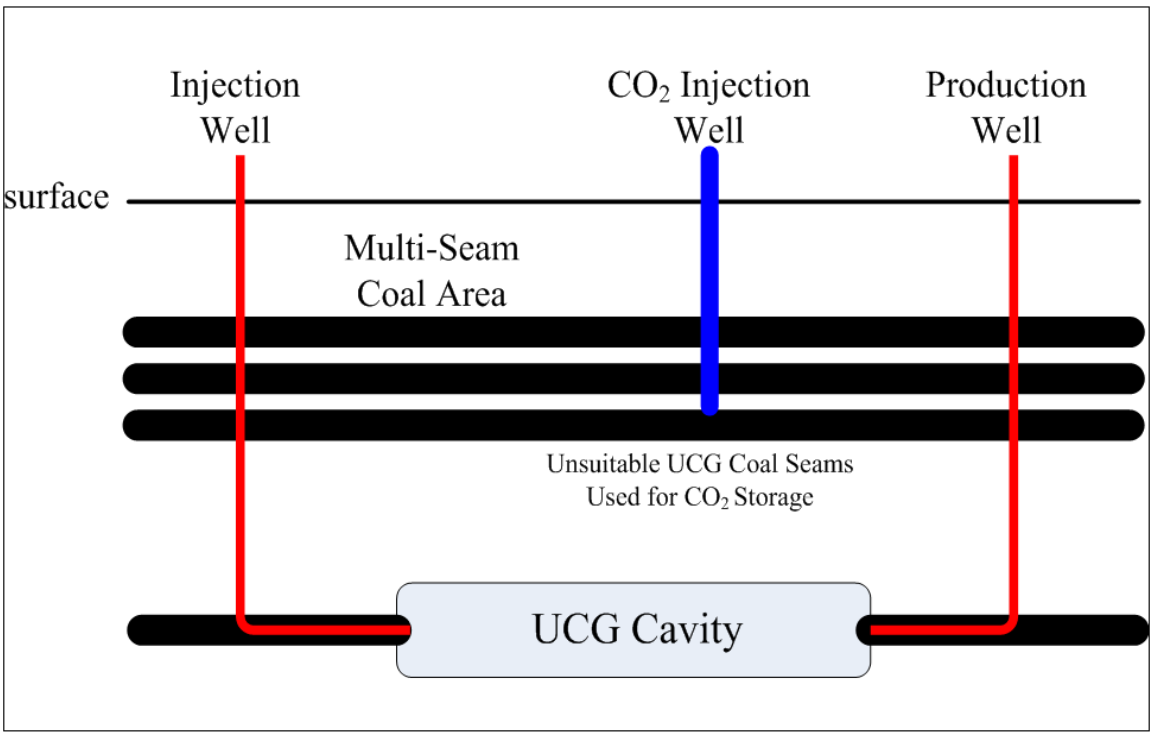

Figure 4. Underground process flow of the UCG with CO_2 storage in other coal seams.

Several key engineering and environmental issues need to be resolved to popularize the application of UCG technology. Based on the reviewed papers and documents, there are four key technical issues for a successful UCG project: combustion control, well linkages, site selection, and associated environmental issues. The UCG combustion process cannot be as well controlled as in the designed gasifiers on the surface. Process parameters like the rate of water influx, the distribution of reactants in the gasification zone, and the growth rate of the cavity, can only be estimated from measurements of temperatures and product gas quality and quantity. Variation of permeability affects the flow rate of injected reactants and products. Consequently, variation of the product volume and composition can introduce problems to the down flow processing and utilization equipments. Regarding possible environmental issues, the UCG may result in subsidence due to evacuation of coal seams, and groundwater contamination because of exchange of

underground fluids [8, 10].

Key technical issues in UCG involve combustion control, the linkage between injection and production wells, and product quality control. In a general scenario, the partial combustion of the coal happens first, and the released heat sustains the steam gasification process, resulting in the formation of a combustible product gas consisting of various proportions of H_2, CH_4, CO and CO_2 – syngas. The syngas flows through the porous coal seam, and is transported to the surface through the production well. Table 1 lists the fundamental reactions involving in the coal gasification. Reaction 1 (steam gasification) is the most important to produce the syngas (CO and H_2). Some coal is consumed by the exothermal Reactions 5 and 6 to release heat to sustain Reaction 1 [8].

The gasification cavity can be divided into an oxidization zone, reducing zone, and pyrolysis & drying zone (Figure 5). The oxidization zone is the first zone where Reactions 5 and 6 occur. The temperature in the cavity generated from the oxidation phase can be higher than 1500^oC. As oxygen is consumed in the oxidation phase, reduction takes place as Reactions 1 and 7. This is also called gasification process. Later in the drying zone, shift reaction and hydrogenating gasification occur. In this phase, coal also reacts with water to produce char and steam [14]. The reaction rates, from fast to slow, are ranked as: Reaction 6, Reaction 5, Reaction 1, Reaction 4, Reaction 7, Reaction 2, and Reaction 3.

The gasification process is governed by the laws of conservation of mass, energy and

transport of gas species, and by the Darcy's law. The flow in the cavity can be laminar or turbulent. It is believed that the mass and heat transfer are due to both natural convection and double-diffusive natural convection in which the temperature gradient and concentration gradient also drive the transportation. However, whether the concentration of each fluid and solid species on the coal wall happens as in laboratory tests is not well understood [15].

Table 1. Fundamental reactions for coal gasification (standard condition)

Reaction	Enthalpy
1.Steam gasification $C + H_2O = H_2 + CO$	ΔH =+118.5 kilojoule per mole (kJ/mol)
2. Shift conversion $CO + H_2O = H_2 + CO_2$	ΔH =-42.3 kJ/mol
3. Methanation $CO + 3\ H_2 = CH_4 + H_2O$	ΔH = -206.0 kJ/mol
4.Hydrogasification $C + 2\ H_2 = CH_4$	ΔH = -87.5 kJ/mol
5.Partial oxidation $C + 1/2O_2 = CO$	ΔH = -123.1 kJ/mol
6.Oxidation $C + O_2 = CO_2$	ΔH = -406.0 kJ/mol
7.Boudouard reaction $C + CO_2 = 2CO$	ΔH = +159.9 kJ/mol

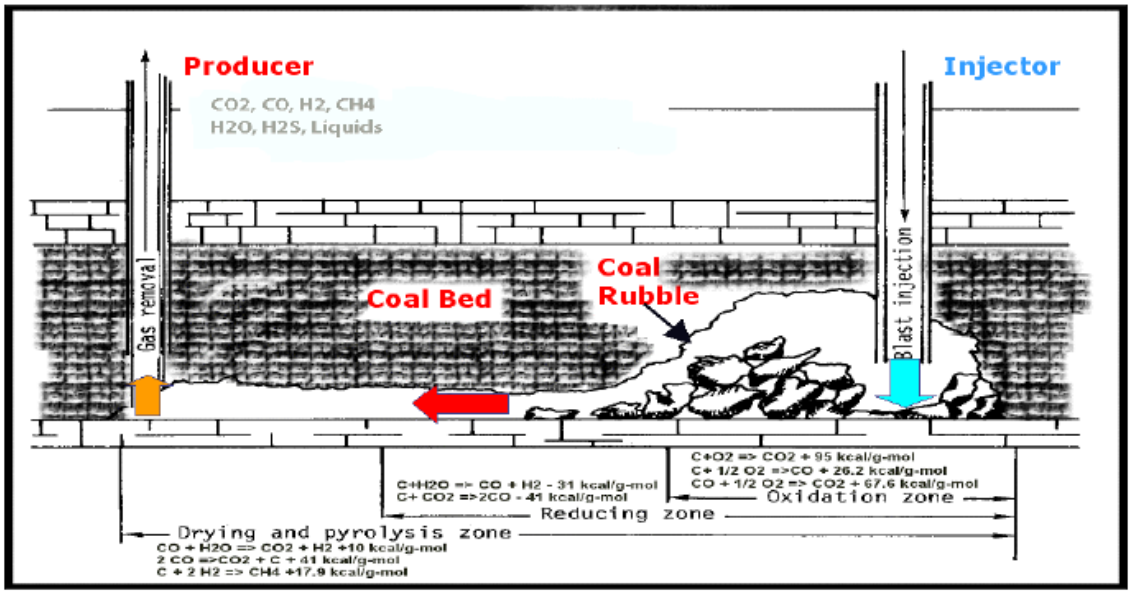

Figure 5. Chemical reactions during UCG process [14].

Regarding the gasification process, there are two different process configurations. The first, based on technology developed in the former Soviet Union, uses vertical wells and a reverse or forward combustion to open up the internal pathways in the coal. The second, called controlled retraction injection point (CRIP) technology, is being tested in European and American coal seams [16]. Techniques adapted from the petroleum industry, like horizontal drilling and hydraulic fracturing, are employed in UCG. Other techniques used include electricity linking, explosive fracturing, man-made in-seam channels, etc.

The first combustion linking configuration is shown in Figure 6. Two techniques are used: the Reverse Combustion Linking (RCL), and the Forward Combustion Linking (FCL). Coal is ignited in the injection well in FCL and the combustion propagates towards the production well. In RCL, the oxidant is injected through one well and coal is ignited in the other well so that combustion propagates towards the source of oxidant. The signal of successful linking of wells is the significant drop in the injection pressure which indicates

the creation of a low hydraulic resistance between the wells. FCL-created links have a pear-like shape, while those made by RCL are predominantly tube-like channels. In general, FCL is not as popular as RCL [17]. Currently, this technique is modified and used by the Ergo Exergy Inc, and called the εUCG process. So far, the RCL has been successfully used in the UCG projects in Chinchilla, Australia; and Majuba, South Africa [18]. However, as a proprietary process, detailed information of the εUCG has not been released.

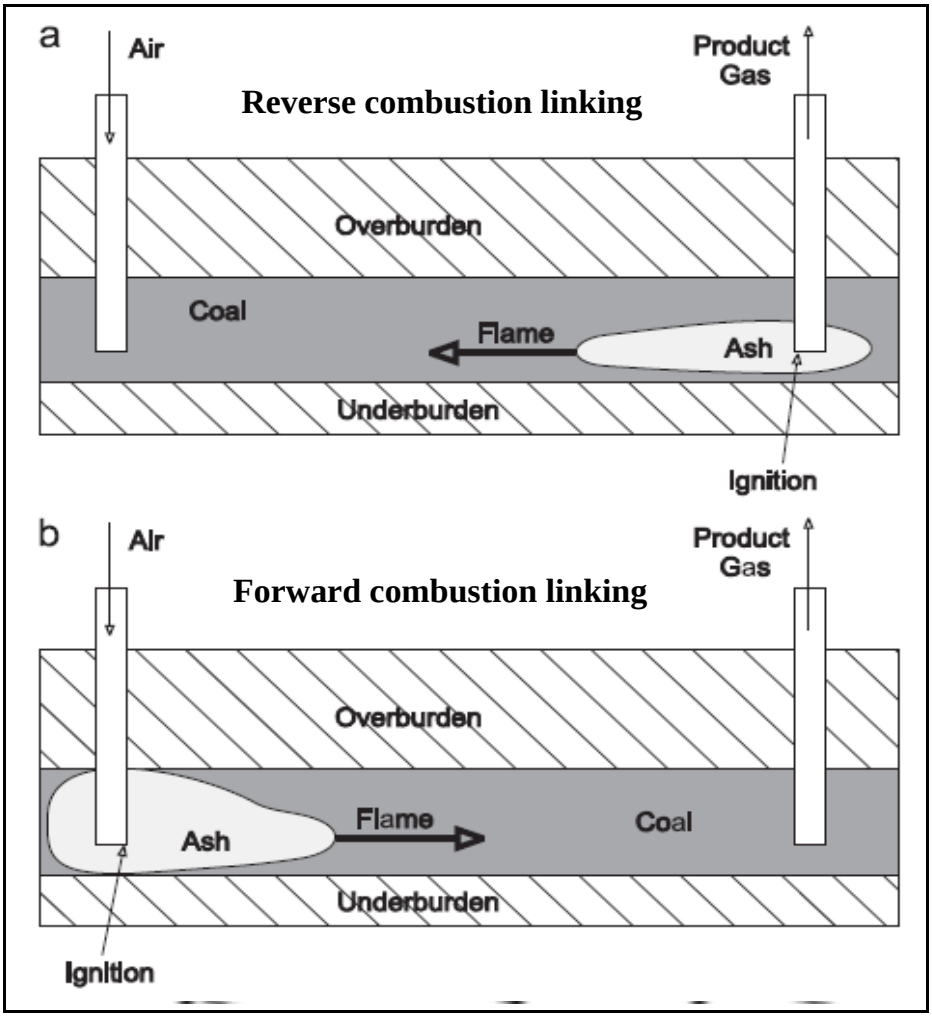

Figure 6. Schematic views of the reverse and forward combustion linking in UCG [18].

The CRIP technique was developed by researchers in the Lawrence Livermore National Laboratory (LLNL) in the USA. The process is shown in Figure 7. The production well is drilled vertically and the injection well is drilled directionally. The CRIP technique involves the use of a burner attached to coiled tube. Once the directionally drilled injection channel is established, a gasification cavity is initiated at the end of the injection well in the horizontal section of the coal seam. When the coal near the cavity is burned up, the injection point is retracted to start the combustion of fresh coal in the upstream location [8]. The CRIP technique was used in the Rocky Mountain 1 trial from November 1987 to February 1988, conducted in Carbon County, Wyoming, U.S. This project is considered to be the most successful UCG test in the U.S. The CRIP trial lasted a total of 93 days and gasified 10,024 tons of coal with average gas heating values of 10,693 kilojoule per cubic meter (kJ/m^3) [14].

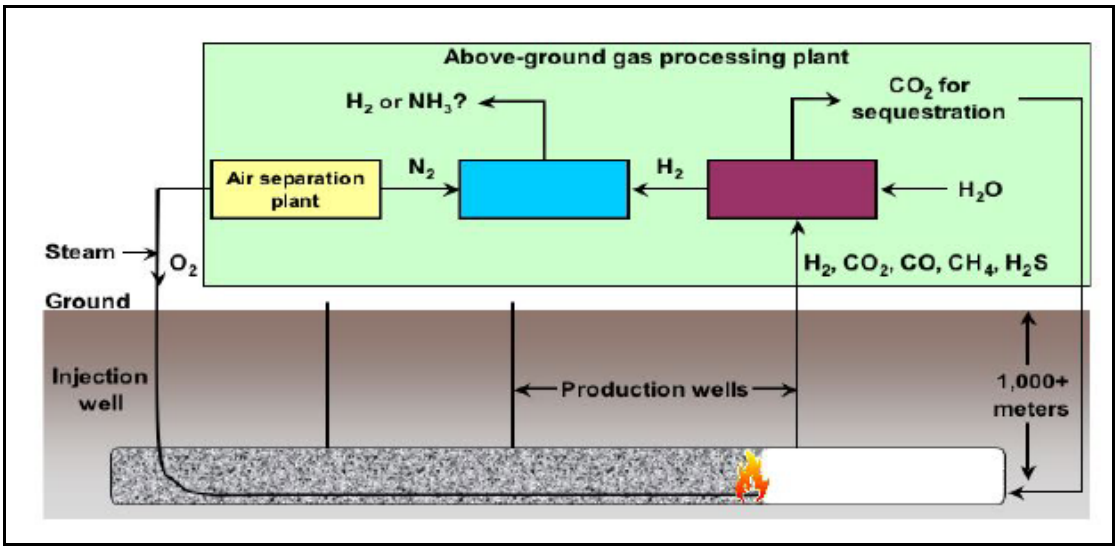

Figure 7. The CRIP process and surface gas processing [8].

Except the conventional CRIP layout, the directional production well and injection well can also be arranged parallel to each other to access coal seams located offshore [12]. In

such an arrangement, the injection and production wells are drilled from the platform on shore to reach offshore coal seams. The injection and production wells are retracted together at the same rate during gasification. This arrangement is shown in Figure 8.

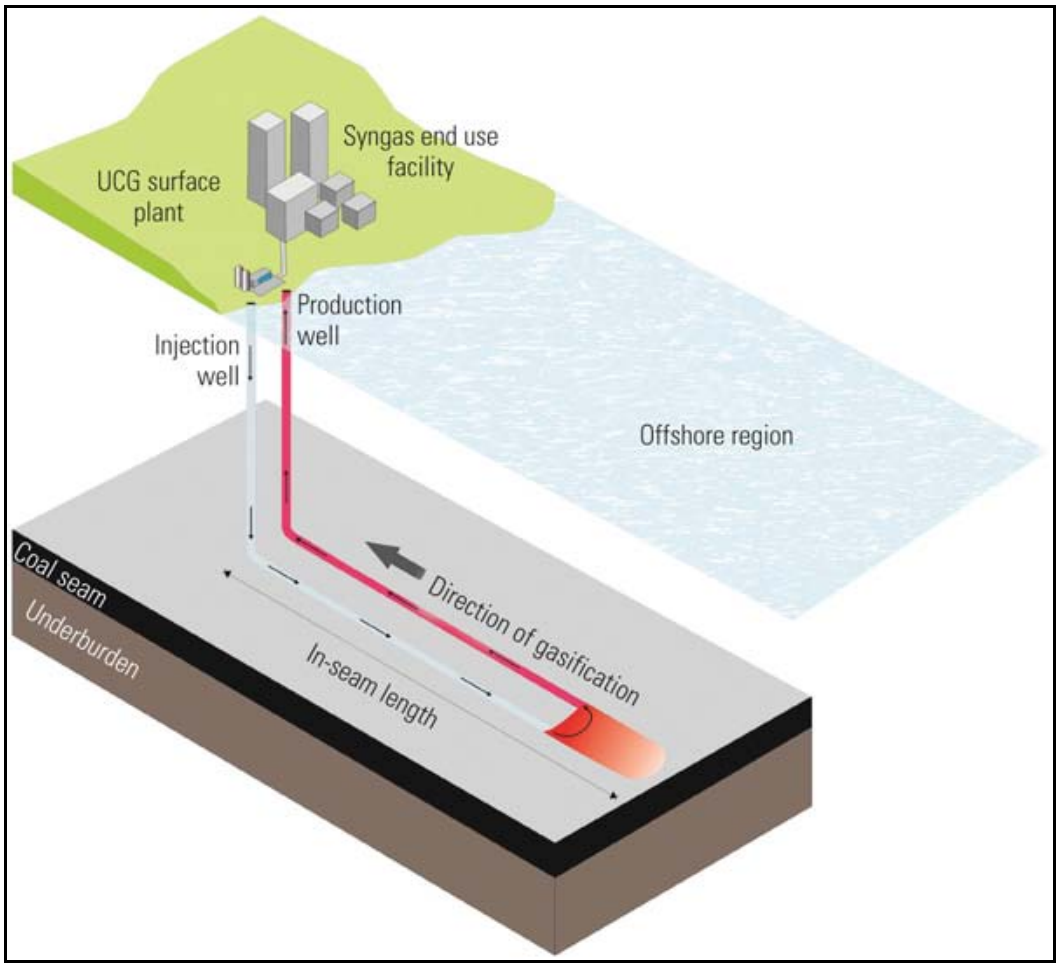

Figure 8. Parallel arrangement of injection and projection wells [12].

Water influx to a UCG reactor is important in affecting the process efficiency. Water influx is a result of drying of overburden rock, gravity drainage, depressurization of the coal aquifer, and reflux of condensate from product gas. Sometimes the in situ water influx can be utilized as a reactant in the gasification process, but it would not be easy to control the influx amount. If there is more water than what is needed in the reaction, heat

is lost in vaporizing the entering water, so less heat is available to support the gasification reaction [19]. To prevent undesired water influx, operational pressure of the reactor cavity can be maintained slightly lower than the hydrostatic pressure.

Conversion of coal to the syngas is directly reflected as the growth of reaction cavity. The cavity forms around the injection or ignition point, and grows upwards and outwards from the injection point (Figure 9). The growing process is determined by factors such as water influx, porous media flow, heterogeneous and homogeneous chemical reactions, radiative and convective heat transfer, and rock mechanics [19].

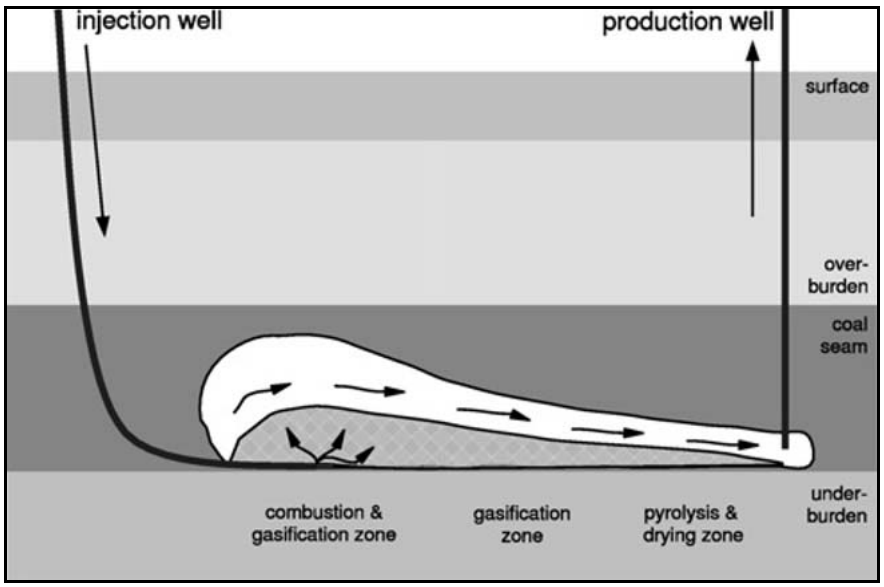

Figure 9. Schematic of an underground coal gasification cavity [15].

Except by being excavated, which is virtually impossible, the actual cavity geometry in field test can only be approximately inferred from post-burn coring, thermowell responses, electromagnetic and seismic mapping data, and material balance calculations. In most modeling studies, the cavity is modeled as an axisymmetric shape with a

cylindrical or rectangular cross-sectional shape. In the cavity, a porous bed of ash overlies the injection point with a void space created by removal of carbon and volatiles from the coal lying above. Due to the high permeability of the void space relative to that of the ash bed, the majority of the flow between the injection and production wells is expected to occur in the void space [15].

Thermodynamic conditions and the kinetics of a number of reactions and mass transfer to the reacting zones together control the gasification process. Different ignition and combustion processes and techniques including those mentioned above have been pursued and practiced to guarantee the stable quality of the products. However, challenges of obtaining constant product quality and product mass flow rates still remain unsolved. As the properties of the coal-bearing formation change in different locations, the process parameters, such as reaction pressure, temperature, oxidant injection rate also change. Variation of these gasification parameters significantly impacts the composition and quality of the product. For example, optimal pressure in the cavity is required to control the water flux from adjacent formations into the gasification zone and prevent contaminations. Careful monitoring during the process and detailed investigation and modeling are essential for the successful operations. Due to the complexity of the in situ conditions in the target coal seam, and sometimes lack of input data, accurate simulation to the process under actual environment is challenging. Sometimes the simulation data cannot provide reliable support for realistic projects. Improvement would require accumulation of project results and empirical data, as well as numerical processes of better performance.

In UCG practice and pilot tests, directional drilling, hydraulic fracturing and reverse combustion mentioned above are employed in seek of better flow connection between injection and production wells. Directional drilling is the practice of non-vertical wells (Figure 10). It has been well developed in the petroleum industry to satisfy special requirements, such as increasing the exposed area of the well to the reservoir, to reach locations which are inaccessible to vertical wells, vertical cross contact with fractures to enhance transit of fluids, and allowing multiple wellheads extending from one platform on offshore. This technique has also been well employed in coalbed methane (CBM) recovery. The interests in the CBM in U.S. started in 1990s, but exploitation activities once ceased due to poor performance of conventional vertical wells in the coal seams. With application of new technologies, especially the directional drilling, the CBM industry has gained great success [20]. In directional drilling, geomechanical characteristics of lithologies are important for assessing drillability and borehole stability. These characteristics include frequency and type of geologic discontinuities, orientations and magnitude of in situ stress, and permeability anisotropy [21].

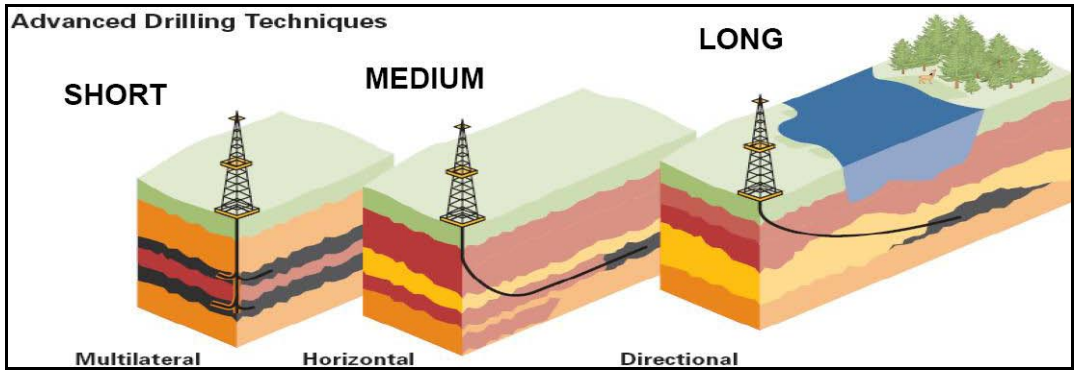

Figure 10. Directional drilling [22].

The gas transportation via only natural permeability in the coal seams is not reliable in many cases. Reverse combustion, hydraulic fracturing and directional drilling are used to address this problem. Besides, during the combustion process, the coal shrinks as loss of water content, and this may result in increase of the permeability in the coal seams. On the other hand, caking phenomenon may block permeable channels. If there are no low permeability seals like in the petroleum trap, production gas can easily lost into the surrounding formations. Hydraulic fracturing is a process of development of discontinuities in the rock mass element due to the change of geohydromechanical situation resulted from filtration of fluid under pressure. Fluid is injected through a selected section of the well to create high pressure. When the effective pressure exerted by the injected fluid is over the rock tension strength, failure will happen; therefore fractures are opened to increase the permeability of the rock (Olovyanny, 2005). Sometimes the opened fractures will close when the injected fluid is shut down. To prevent this from happening, proppants are injected with fluid into the fractures to hold the fractures open. The hydraulic fracturing technique has been widely used in stimulating petroleum production. There are concerns that the hydraulic fracturing process may induce environmental risks, such as fracturing fluid could contaminate water supplies, impact rock shelf causing seismic events or lead to surface subsidence. In 2004, the Environmental Protection Agency (EPA) indicates that the hydraulic fracturing conducted in coal seams are safe, because there was “no unequivocal evidence” of health risks, and the fluids were neither necessarily hazardous nor able to travel far underground [24].

The UCG process has the potential to result in hydrologic and geomechanical changes in the area surrounding the coal seam. As coals are converted into product gases, underground volumes are evacuated and the risks of subsidence are introduced. Factors influencing the magnitude of subsidence include the depth and thickness of the coal seam, stiffness and yield strength of the rocks, fracture density and orientation, and in situ stresses [19]. Subsidence can be controlled by leaving adequate pillars in the coal seam to support the overburden stresses. This is accomplished by distributing the multiple gasification reactors (cavities) properly underground. It is also recommended that selecting a seam at great depth and good characterization and understanding of the overburden unit can mitigate the subsidence of the overburden. In general, if the depth of the coal seam is greater than 200 m, the impact to the surface is minimized.

1.3 Syngas in Power Generation Coupled with CO_2 Capture

If the produced syngas from UCG is used for power generation, the process will be similar to the IGCC process. The IGCC power generation system is an innovative power generation technology combining with coal gasification and combined power generation cycle. An IGCC power plant usually has the following major components: the gasification island, the gas cleanup island, and the power island. A conceptual diagram of an IGCC system is shown in Figure 11. Coal or other fuels like petroleum coke is gasified in the gasifier to produce the syngas, and after cleaning of impurities components, the syngas is then combusted and expanded in a gas turbine to produce power. The heat from exhaust gas is recovered in a heat recovery steam generator (HRSG) to generate high pressure steam to drive another steam cycle [25].

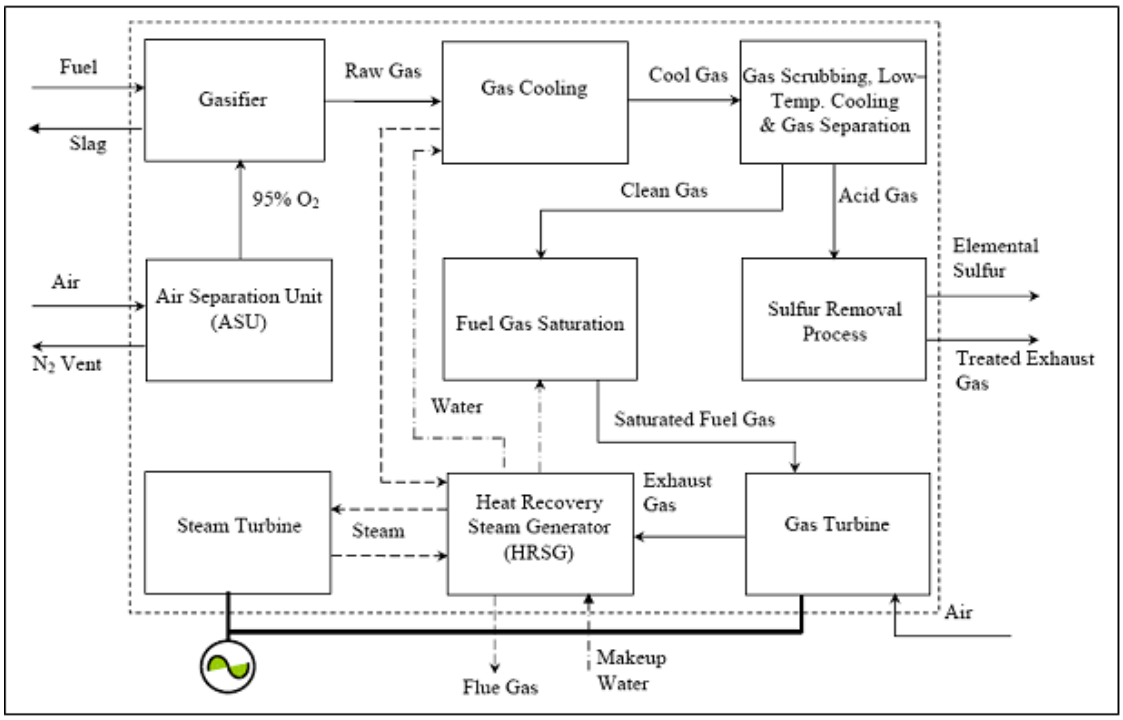

Figure 11. Flow diagram of an IGCC power plant [25].

The IGCC process is considered to be promising if carbon capture process is introduced. Comparing with other power generation processes, the IGCC shows a lower cost and lower energy penalty to integrate with the pre-combustion CO_2 capture process (Figure 12). The syngas is cooled, cleaned of particulate matter, and shifted to primarily H_2 and CO_2 in sour water–gas shift (WGS) reactors. After further cooling, H_2S and CO_2 are separated from the syngas through the acid gas absorption process in two stages, usually via physical solvent like Selexol. The CO_2-rich solvent goes through a stripping tower to release CO_2 and regenerate the solvent. Elemental sulfur can be generated by the Claus plant. Later, the CO_2 stream is dried and compressed for pipeline transport and underground sequestration. After the above process, pure H_2 is obtained and combusted in the gas turbine [26].

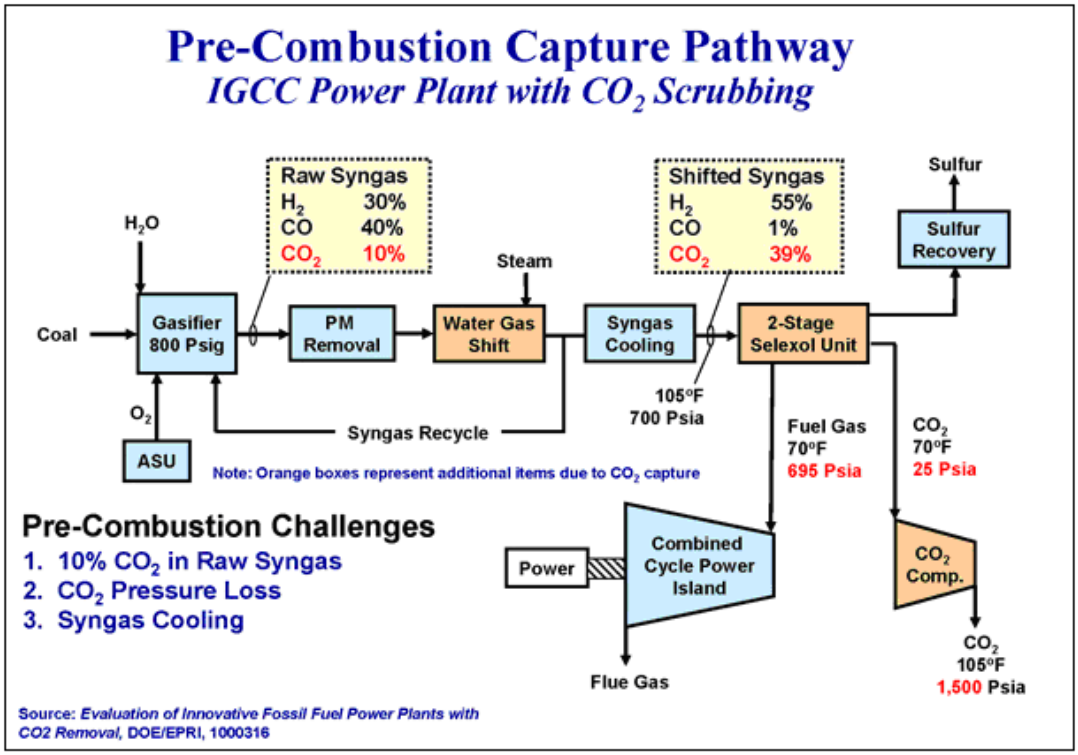

Figure 12. IGCC with pre-combustion carbon capture [26].

A UCG process coupled with combined cycle power generation and CO_2 capture, utilization and storage is proposed as Figures 13 and 14. The process is referred to as underground coal gasification coupled with carbon capture and storage (UCG-CCS) system in this dissertation. The UCG-CCS system adopts the features of the IGCC plant. Except the gasifier part and on site CO_2 injection, the gas utilization section is very similar to the IGCC process. The produced syngas from the UCG is cleaned and pollutants are removed. Following the WGS reaction, the CO_2 is separated and H_2 is then combusted in the power generation island.

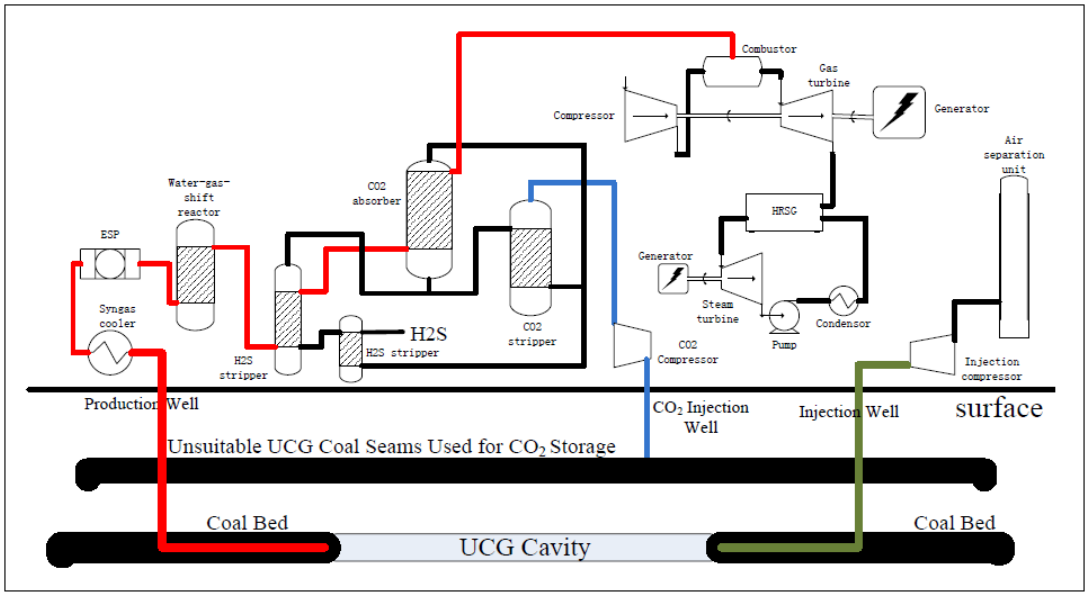

Figure 13. The proposed UCG-CCS system with CO_2 storage in coal seam.

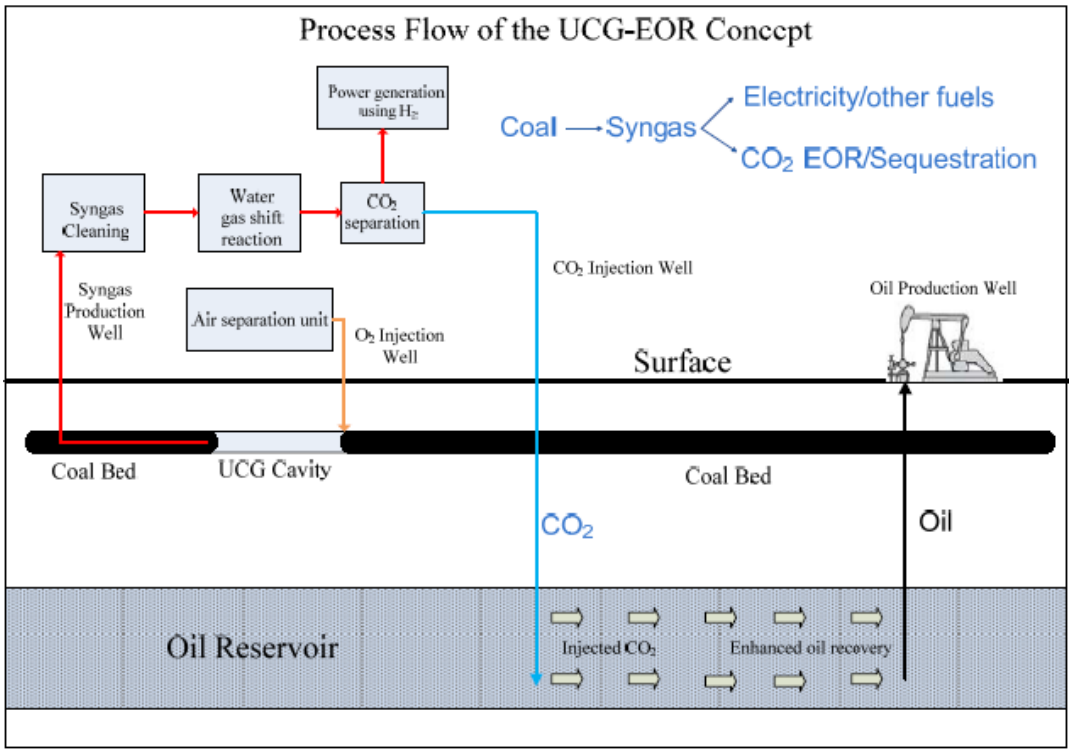

Figure 14. Concept of the UCG-CCS system with CO_2 enhanced oil recovery (EOR).

The CO_2 captured from this process can be injected in the adjacent coal seams which are not economic for UCG process, or used for EOR. Injection of CO_2 into the adjacent coal

seams is actually the same as enhanced coalbed methane recovery, which produce coalbed methane as a byproduct. Compared with IGCC, the UCG-CCS process has smaller land occupation due to the removal of the surface gasifier and coal preparing equipments. A significant part of the gasification ashes will be deposited in the UCG cavity, so the load of the gas cleaning process can be reduced. Regarding to the cost of UCG-CCS system, Blinderman et al. [11] estimated that if the produced syngas is used to generate electricity, the cost of electricity is about $24 per MWh, comparing $77 for IGCC plants, and $52 for supercritical PC power plants. Another reasonable prediction can be made based on the cost components of an IGCC plant. The coal handling equipments and the gasifier contribute about 30% to 40% of the total capital cost of an IGCC plant [27, 28]. Comparing with IGCC, the power generation system coupled with UCG has no coal handling system and gasifier, as well as transportation cost. Considering the investment of drilling wells, it could be reasonable to suggest that UCG-CCS system can save around 30% of capital cost.

Except being combusted to the drive gas turbine, the middle heating value syngas is a flexible source gas to manufacture a broad range of high value-added products. This has been regarded as a major advantage of the coal gasification process. Using syngas as a source gas, possible products include synthetic natural gas (SNG, methane), naphtha, waxes, jet fuels, diesel, ammonia, diemthyl ether (DME), methanol, acetic acid, methyl acetate and so on [29]. Polygeneration can greatly extend the product chain, expand the market and reduce waste disposal. There are successful experiences and examples of polygeneration based on coal gasification like the Dakota Gasification Plant in North

Dakota, the Eastman's gasification plant in Kingsport, Tennessee, U.S.

1.4 Risks of Groundwater Pollution Associated with UCG

Groundwater pollution is the biggest environmental concern associated with UCG process. Previous researchers have conducted studies to investigate contaminants, production mechanisms, transport mechanisms and mitigation approaches. Burton et al. [8] reviewed the development of the UCG process and described the details of each technology part, as well as lessons and experiences from previous tests and commercial operations in the world. Their paper presents assessment criteria for the hydrological conditions of the UCG sites, and practice on groundwater protection. Estimation of the environmental threats posed to groundwater resources as a result of UCG involves several mechanisms as follows: 1) generation of the contaminants within the burn chamber; 2) enhanced vertical hydraulic conductivity of the surrounding rock matrix as a result of collapse and fracturing; 3) buoyancy-driven upward flow due to differences in fluid density in the vicinity of the burn chamber; 4) thermally-driven upward flow of groundwater resulting from in situ burning of coal; 5) speciation and partitioning of some organic compounds probably would result in contaminant sorption to mineral surfaces; 6) bioattenuation of contaminant compounds that migrate into potable water aquifers.

It is suggested to give a quantitative rank (from most favorable to least favorable) for each of the above factors at the site assessment stage, therefore to facilitate comparison of different site scenarios.

During the Hoe Creek UCG test at Wyoming, which was conducted between 1976 and 1979, the collapse of the cavity had interconnected the three aquifers, and groundwater was recharging the reaction zone, and a broad range of organic combustion products had been introduced into the groundwater system. An opposite example would be the Chinchilla project conducted in Australia. In the Chinchilla project, the gasification pressure was maintained below the ambient pressure field. In such a case, water flowed from the host rock into the UCG cavity, preventing transport of contaminants into adjacent aquifers. Therefore, the contaminants were kept within the gasifier underground. Pressure control proved to be an effective method in reducing pollutants spread im UCG project. It is also suggested that the UCG site should be selected well below the portable fresh water table.

Liu et al. [30] proposed that the UCG process introduces pollutants to the groundwater in two ways: 1) dispersion and penetration of the pyrolysis products of the coal seam to the surrounding rock layers; and 2) the emission and dispersion of high contaminants with gas products after gasification and migration of residue by leaching and penetration of groundwater. If the gasification process is conducted at a pressure higher than the local hydrostatic pressure, some of the produced gases can escape into the surrounding permeable strata, or through cracks and faults. Volatile products are transported before condensing or dissolving in the groundwater. As the gasification process, groundwater would fill into the gasification zone. At the beginning of groundwater re-filling, most of the water becomes vapor due to the high temperature in the zone, and water vapor which contains contaminants can be pumped out through production wells and treated at the

surface. As the temperature drops down, returning water would fill up the gasification zone and the residual coal ash is leached with the water as a carrying media. This could lead to buildup of contaminants radially near the gasification zone after the project. However, the contaminants can be adsorbed on the coal and strata, or reduced due to reactions with other species. In such cases, the surrounding strata around UCG cavity serve as a filtration to stop the migration of the pollutants.

The largest group of contaminants identified during and post UCG process are phenolic compounds. Other organic pollutants include aromatic carboxylic acids, aromatic hydrocarbons, ketones, aldehydes, pyridines, quinolines, isoquinolines, aromatic amines, naphthalene, o-xylene, 2-methyl pyridine and o-cresol. Observed inorganic contaminants are calcium, sodium, sulfate, bicarbonate and uranium. It is concluded that the inorganic compounds are introduced by soluble ash components carried by groundwater.

To understand pollutions mitigation, flow modeling and water quality models are used to predict the fate of the contaminants. During the field test, the self-restoration mechanism was observed. Studies show that the improved water quality was due to adsorption and ion exchange properties of surrounding strata, precipitation reactions, dilution and dispersion by natural ground-water flow and biological conversion reactions. It is also supposed that adsorption of organic matter by clay and lignite is an effective removal mechanism. Some control and mitigation methods to the pollutants are suggested, such as maintaining the operation pressure below the hydrostatic pressure, identifying a permanently unsuitable zone, setting a hydraulic barrier and pumping contaminated water

out for surface disposal.

Yang and Zhang [31] proposed that contaminants transport associated with UCG process is mainly carried out in three ways: advection, molecular diffusion, and mechanical dispersion. For advection, groundwater is the carrier media, and if it is assumed that the contaminant traveling velocity is the same as that of the groundwater; the flow flux of the contaminants equals to the specific flow of the groundwater timed by the concentration. Both of the molecular diffusion and mechanical dispersion are controlled by the Fick's Law. Except the above three ways, absorption of the contaminants to the aquifer skeleton and coal seams also occur in forms of ion exchange; and this phenomenon is controlled by the Freundlich Equation. Yang's modeling result shows that, with the progress of gasification, the permeability between the coal-rock increases; the flow seepage velocity is increased; and temperature and pressure gradients decrease. After gasification, the temperature field expanded gradually, and thus its influence. As mentioned before, the variation of temperature in turn would change the parameters of water-bearing formation, therefore impact the behavior of water flow and contaminant transport.

Yang and Zhang [31] also conducted a contaminant transport model under nonisothermal condition and most of the coefficients involved in the governing equations are dependents of temperature. The values of these coefficients were either determined by experiments or obtained from literatures. Geological conditions of a UCG test site in China were applied to this model. Measured experimental data which were already known, such as temperature, pore water pressure, concentration of contaminants (phenol + CN^- + NH^+)

were used to form the initial condition. Modeling results include pore water pressure fields, temperature fields, and contaminant concentration fields in the gasification panel after 11, 20, and 36 months, respectively. The results show that, as the progress of gasification, the permeability of the coal-rock increases; the flow seepage velocity increases; and temperature and pressure gradients decrease. After gasification, the temperature field expanded gradually, so as its influence. The variation of temperature in turn would change the parameters of the water-bearing formation, therefore impact the behavior of water flow and contaminant transport.

Following the Hoe Creek I and Hoe Creek II UCG experiments, measurement of contaminants was carried by the LLNL at the project site in Wyoming [32]. The investigation looked at the changes in groundwater quality due to the residual gasification products. In general, it was found that the contaminant concentrations decreased with distance from the burn zone and time after gasification. As the groundwater returned to the burn zone, dissolution and leaching of the residuals leaded to the formation of a plume of contaminated groundwater, which began to move through the coal seam. If there are fissures and overburden collapse destroys the seal of the gasification zone, additional channels for the escape of the pollutants would exist.

The Hoe Creek I test was in a small scale, with 118 tons of coal gasified, at a depth of 38 m, below the static water table. Groundwater returned and filled up the burn zone after the test. Phenolic materials were found to increase in large amounts as a result of the test. Measured data indicated that the phenol concentrations decreased rapidly with time and

with distance from the gasification zone. The decrease of concentration was interpreted as that the contaminants were adsorbed by the coal seam and around rocks. This interpretation was also confirmed by laboratory sorption experiments.

The Hoe Creek II test was larger than the Hoe Creek I test. Two thousand and ninety tons of coal were gasified. However, this test failed as it induced roof collapse and inadvertent gasification of an overlying coal seam. Such a failure created interconnection of three aquifers and two coal seams and possible subsidence on the surface. The interconnection was detected by hydraulic head measurements, water sampling, and post-burn coring and logging investigation. The head measurement showed that after gasification, water mounded up in the vicinity of the burn zone, and water head over there was higher than its pre-gasification level and above aquifers. It is believed to be one of the evidences of the interconnection between the gasifier and overlying aquifer, and such a connection had influenced ground-water flow rates and contaminant movement near the burn zone. The normal flow in the vicinity of the gasifier was largely replaced by a radially outward flow of greater velocity. However, due to larger water influx, the contaminant concentrations of the Hoe Creek II was smaller than the last project.

From the literature described above, it is known that inappropriate site selection and operation of a UCG project may result in severe environmental problems in groundwater pollution. However, some strategies can be applied to avoid the environmental risks. It is suggested that the target coal seam should avoid nearby aquifers. In the case that any nearby aquifers exist, the gasification pressure should be kept slightly below the

hydrostatic pressure of the coal seam [6, 8]. A successful example is the Chinchilla project in Australia. UCG pilot studies have shown the importance of operating within a critical range of injection pressure which is high enough to keep too much water from invading the combustion zone and quenching the burn, and low enough to minimize loss of product gas and spreading of contaminants from the reactor zone.

1.5 Motivations and Objectives

The UCG technology and UCG-CCS coupled system have gained interest around the world in recent years. The North Dakota portion of Williston Basin contains huge lignite resources in the Fort Union formation. The deep, thick, and relatively continuous Harmon lignite beneath southwestern North Dakota provides potential opportunities of using UCG technology. As the oil industry is booming in North Dakota, there is also a demand on CO_2 for EOR. The UCG-CCS system can be a suitable technology to exploit the vast fossil fuel resources in North Dakota. This concept enables the exploitation of deep lignite, beneficial usage of CO_2 to boost oil production, and mitigation of CO_2 emission.

Although the Fort Union Formation lignite resource in the Williston Basin of North Dakota has been investigated before, previous work was not focused on UCG applications. The coal-bearing formation has not been assessed and characterized from the view of UCG application. In addition, the fact that aquifers in the Fort Union Formation coincide with or close to the Harmon lignite bed means associated groundwater issues can impact the gasification process, which may limit the applicability of UCG. As mentioned above, appropriate site screening criteria and procedures, and

optimized operation process (parameters) are required to minimize the environmental risks and maintain a stable gas product quality. Detailed knowledge about the geology, hydrogeology, geomechanics and thermophysics of the target sites, based on extensive investigations and modeling work, is necessary. However, the needed information to investigate the Harmon lignite for UCG production is largely not available.

Based on primary consideration of resource abundance, the UCG technology is supposed to be applicable in North Dakota. But there are many challenges remain to resolve and answer before it can be concluded that the UCG technology can safely and economically work. This study targets at a feasibility study of applying UCG technology to the Harmon bed, identifying research roadmap, providing data and information for necessary research works in the future. Applicability of UCG in North Dakota has been investigated from different aspects, including geology, hydrogeology, safety, operation strategy, and economy. Results generated in this study can be used as a baseline reference for site selection, environmental risk prediction, and optimization of operation.

CHAPTER II

FORT UNION LIGNITE IN NORTH DAKOTA

2.1 Williston Basin and the Fort Union Lignite in North Dakota

Williston basin (Figure 15) is a large intracratonic sedimentary basin in eastern Montana, western North Dakota, northwestern South Dakota, southern Saskatchewan and southwestern Manitoba. The basin began to subside during the Ordovician Period, around 495 million years before present. Deposition in the Williston basin occurred during all periods of the Phanerozoic. The sediments in the basin are divided into six sequences based on the historical transgression events, and each sequence contains formations (Figure 16). These sequences are, in ascending order, the Sauk, the Tippecanoe, the Kaskaskia, the Absaroka, the Zuni, and the Tejas. Williston basin is roughly circular, deepest in its center, and the strata become shallower and thinner towards its margins. Major geological structural features in the North Dakota portion include the Nesson anticline, Little Knife anticline, Billings anticline, and part of the Cedar Creek anticline. The basin is known for its rich deposits of petroleum and coal resources. It contains more than 4,500 m of Cambrian to Quaternary age rocks. Most of the hydrocarbons produced in the Williston basin are from carbonate reservoirs that range in age from the Ordovician through the Mississippian.

Figure 15. Map of the Williston basin and its major structures [33, 34].

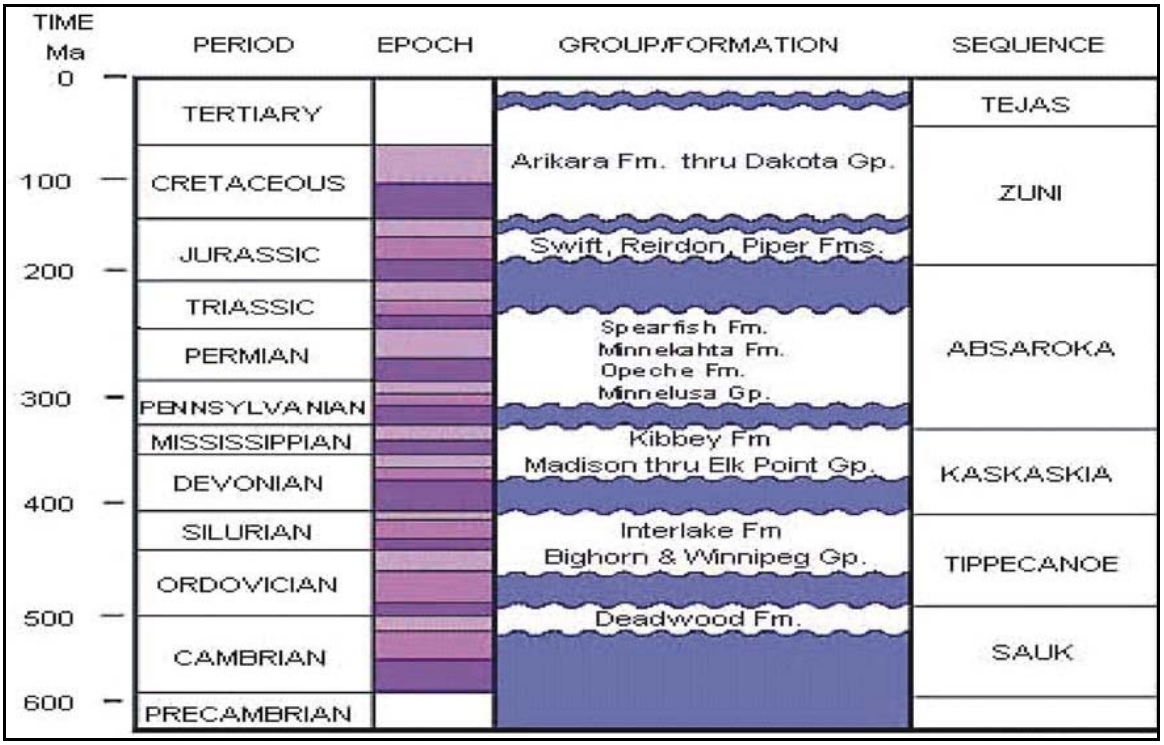

Figure 16. Stratigraphy and sequence of the Williston basin, North Dakota portion [35].

The Fort Union formation is primarily a nonmarine geologic unit of Paleocene age that extends from the Powder River basin in Wyoming to the Williston basin in eastern Montana and western North Dakota (Figure 17). The Fort Union strata make up the surface bedrock over much of the Williston Basin. The strata are conformably underlain by the Upper Cretaceous Hell Creek formation, conformably overlain by the Paleocene/Eocene Golden Valley formation, and unconformably overlain by Quaternary glacial till in the northern half of the basin (Figure 18). The four major members in the Fort Union formation are: Cannonball member, Ludlow member, Tongue River member, and Sentinel Butte member. The Fort Union formation is composed primarily of sandstone, siltstone, and mudstone; and subordinate carbonaceous shale, coal, and limestone. The sandstone and mudstone are common rock types of the formation. The Fort Union formation extends over 83,000 square kilometers (km^2) in the Williston basin in North Dakota.

The North Dakota portion of the Williston basin hosts significant coal resources of lignite rank in the Fort Union formation. Most of these lignite resources are contained in the coal zones named Harmon and Hansen in the southwestern part of the basin, and in the Hagel and Beulah-Zap coal zones in the east-central part. As Figure 19 shows, the Harmon and Hansen coal zones lay in the lowermost part of the so-called Tongue River member. The Hagel coal zone is in the lower part of the Sentinel Butte member. The Beulah-Zap coal zone is in the upper part of the Sentinel Butte member [36]. North Dakota currently contributes about three percent of the U.S. total coal production.

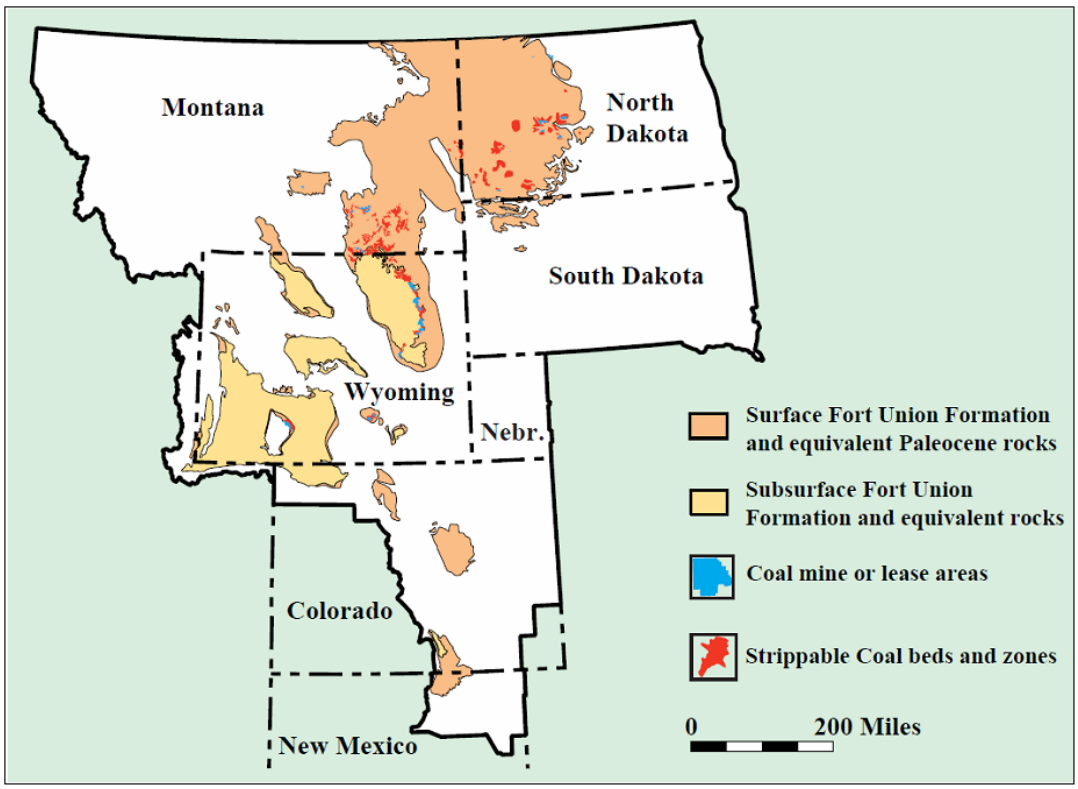

Figure 17. Map of the Fort Union formation [36].

Epoch	Zones (Nichols and Ott, 1978)	Williston Basin		
		U.S. Geological Survey	North Dakota Geological Survey	Saskatchewan, Canada
Quaternary		GLACIAL TILL DEPOSITS		
Eocene		Golden Valley Formation	Golden Valley Formation	
Paleocene	P6	Fort Union Formation: Sentinel Butte Member	Fort Union Group: Sentinel Butte Formation	Ravenscrag Formation
	P5			
	P4	Fort Union Formation: Tongue River Member	Fort Union Group: Bullion Creek Formation	
	P3			
	P2	Fort Union Formation: Ludlow Member / Cannonball Member	Fort Union Group: Slope Formation / Ludlow Formation / Cannonball Formation	
	P1			
Upper Cretaceous		Hell Creek Formation		Frenchman Formation
		Fox Hills Sandstone		Eastend Sandstone

Figure 18. Stratigraphy of the Fort Union formation and its neighboring formations [36].

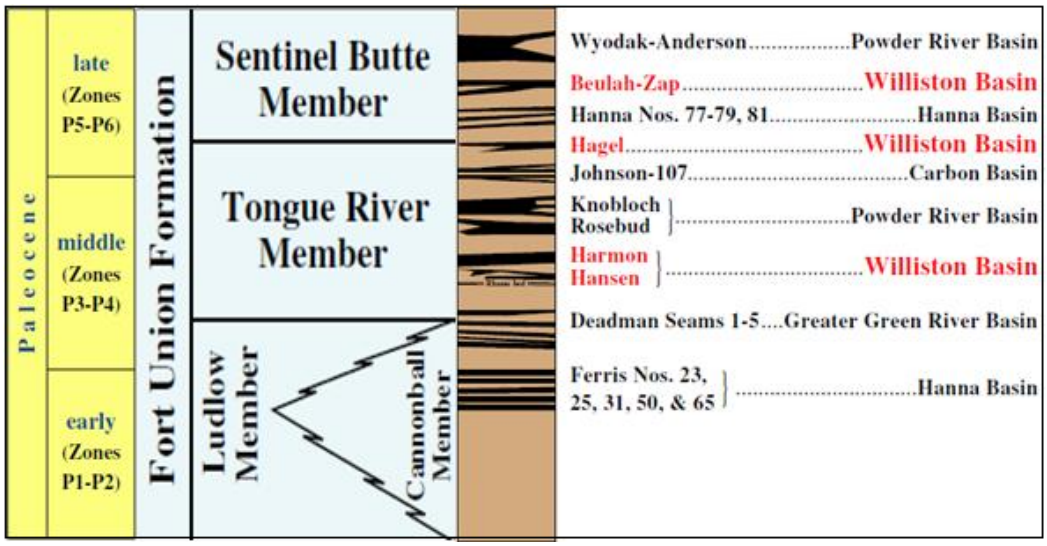

Figure 19. Stratigraphy and coal zones of the Fort Union formation, after [36].

Lignite resources in North Dakota have been investigated by the North Dakota Geological Survey (NDGS) and the United States Geological Survey (USGS) in detail. Reports and maps provide the depth, thickness, lateral structure of the lignite beds and locations of economically mineable reserves. The literature can be conveniently used in primary UCG site selection with regard to depth and thickness. Studies have indicated that there are about 1.18 trillion tonnes of resources of lignite in North Dakota. However, the economically recoverable reserve by surface mining is about 22 billion tonnes, or only two percent of the entire resource [37].

The Fort Union lignite in North Dakota has a low percentage of fixed carbon and calorific value. Its average calorific value is 15,128 kilojoule per kilogram (kJ/kg), and average sulfur and ash contents are 0.86% and 7.99%, respectively [38]. The thick coal beds in the Williston basin were deposited mainly in swamps related to fluvial and deltaic environments. The extensive areal distribution of these coal beds and zones reflects accumulation in raised swamps on abandoned alluvial platforms. Coals produced here

have been mainly used to feed local mine-mouth power plants or transported to other states [37]. The Harmon coal was mined in the Gascoyne surface mine, which was closed in 1996. The Hagel coal zone in the Sentinel Butte Member is mined in the Center and Falkirk surface mines. The Beulah-Zap coal zone in the upper part of the Sentinel Butte Member is mined in the Freedom surface mine north of Beulah and in the Knife River surface mine south of Beulah. The major coals that have been mined or proposed for mining in North Dakota are shown in Figure 20.

Figure 20. The major coals that have been mined or proposed for mining in North Dakota [37].

2.2 Depositional Environment of the Fort Union Lignite

The strata of the lower part of the Fort Union, the Ludlow and Cannonball members, were deposited mainly in deltaic and marine environments, respectively. Accumulation of Ludlow coal beds was directly influenced by eustatic sea-level rise and fall of the Cannonball Sea, which was situated mainly in the east-central part of the basin, current North Dakota and South Dakota. These eustatic sea-level changes were expressed as the transgressions (toward the west) and regressions (toward the east) of the sea, in which the marine Cannonball strata were deposited [39]. During transgressions, deltaic deposits from previous regressions were reworked by waves and tidal processes forming stacked, coarsening-upward parasequence sets of barrier bars [36]. Coal beds accumulated in those tidal-intertidal and back-barrier swamps usually are thin and common in North Dakota and South Dakota.

For the upper part of the Fort Union formation (Tongue River and Sentinel Butte members), the strata were interpreted as mainly fluvial and deltaic deposits. Thick coal seams like Harmon coal and associated sediments probably accumulated in swamps on abandoned deposits of fluvial-channel belts that migrated into nearby interfluvial areas. Merging and splitting of these coal zones attest to autocyclic processes associated with the fluvio-deltaic environments. The Harmon coal zone would be an ideal candidate for UCG utilization due to its abundant resource, sufficient thickness and good continuity in structure. However, because the depositional system is probably a mixture of inter-channel fluvial system and lacustrine swamp, the lignite may be overlain by impermeable sediments, and sandy sediments commonly encountered in channels. The

Harmon coal zone is interbedded with floodplain mudstone and siltstone, and overlain by fluvial channel sandstone and interfluvial silty sandstone, siltstone, and mudstone [36]. Lithological facies variation of the surrounding rocks can be great within a short distance.

Winczewski [41] interpreted the change of depositional environment from the view of flow direction switch. According to Winczewski's interpretation, during the deposit of the Fort Union formation, what is current Montana and Wyoming was constantly changing as uplift occurred in the west, and the Cannonball Sea covered today's North Dakota and part of South Dakota. The area in between was a series of rivers, floodplains, and lakes. The climate at that time was subtropical. Coal-forming plants grew along the rivers, and lake margins between rivers. As the Cannonball Sea retreated to the northeast, the Powder River system entered into current Williston basin at the same time. Sediments resources of Fort Union formation in the Williston basin was provided by the Powder River system. However, there was a switch of the flow direction, and the flow progressed to the north and east (Figure 21). Low-lying areas between the river channels remained below water level and supported peat swamps, where peat deposits were buried by younger sediments and eventually transformed into lignite. Coal beds that formed in these peat swamps are thin and laterally discontinuous. Peat deposits also accumulated in swamps once occupied by river channel, overbank, floodplain, and crevasse splay environments later abandoned by the river. Peat deposited in these environments formed thick and laterally extensive coal beds exemplified by the Harmon and Hansen coal. Therefore, coal first formed in the south and west, as a thick, single bed. On the other hand, later diffused flow patterns in the east created thin, multiple-bed coal (Figure 22).

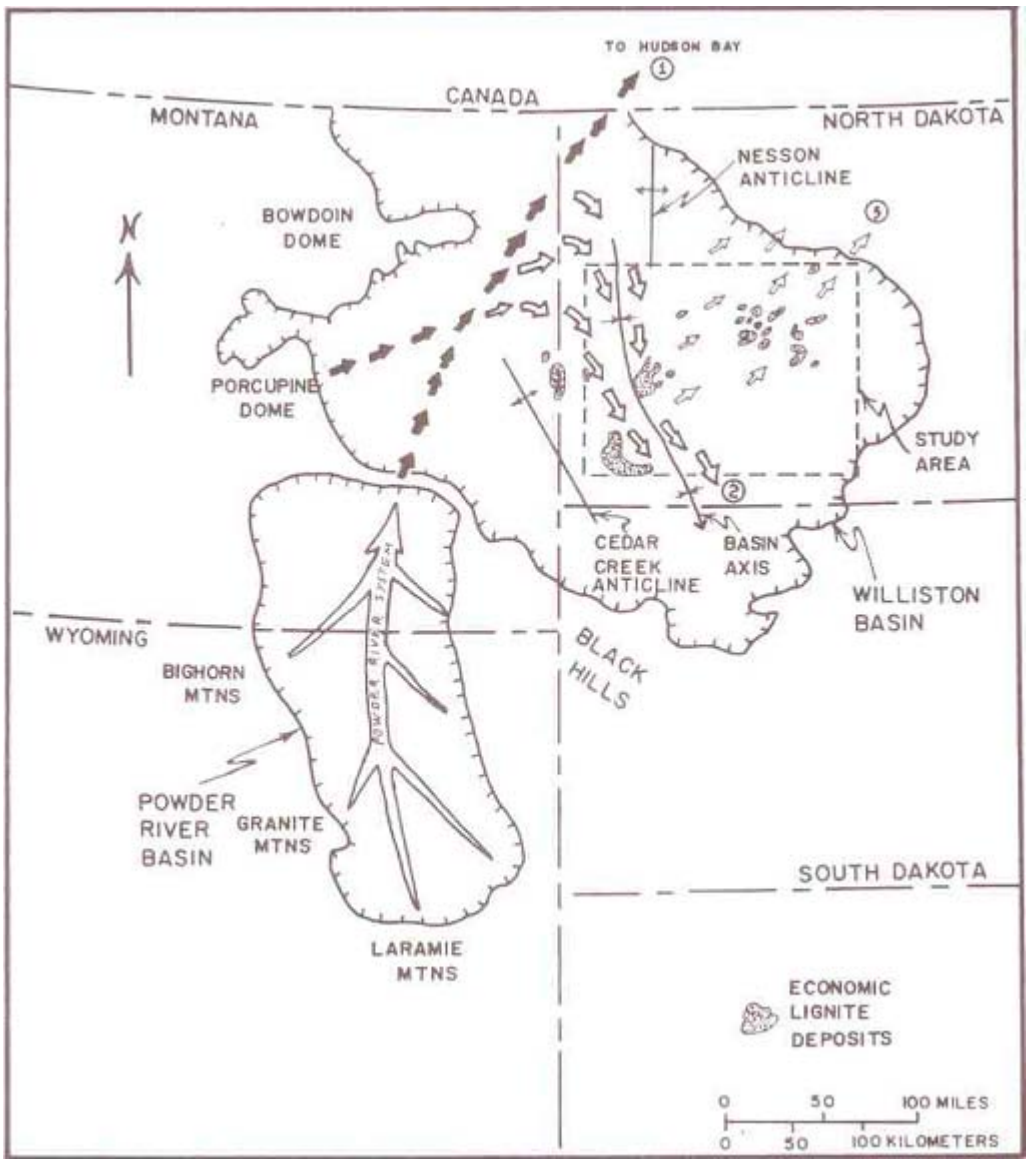

Figure 21. Flow direction progressed from south to northeast during Fort Union formation deposition [41].

Whatever the interpretation to the depositional environment is, the fact that the overlying lithology of the Harmon lignite zone is highly variable makes the UCG site selection process challenging. Detailed investigation and modeling to the surrounding rock with advanced simulation tools are necessary.

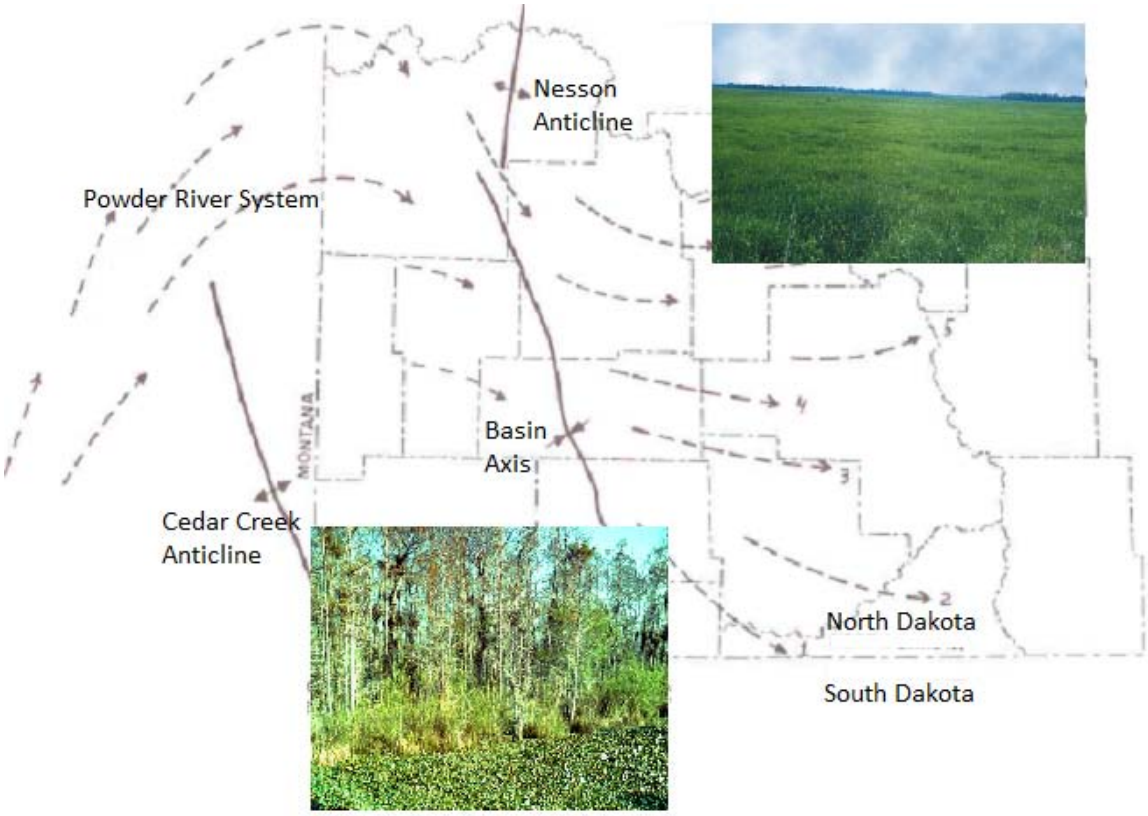

Figure 22: Different deposit environments created by the switch of flow direction, after [41].

2.3 CO_2 Utilization and Storage Potential in the Williston Basin

The Williston basin has significant potential as a geologic sink for sequestering CO_2. Except using CO_2 in EOR projects, geologic sinks that may be suitable for long-term sequestration of CO_2 include depleted petroleum reservoirs and deep saline formations, which are abundant in the basin. The basin is considered as neither structurally complex nor tectonically active, and the stratigraphy is well studied and documented. Fischer et al. [35] investigated the potential sequestration units based on the boundaries and rock properties of the formations (groups). Figure 23 shows the potential CO_2 sequestration units in the basin: sandstones and oil filed in the Deadwood formation, aquifers of

Winnipeg group, Red River oil fields in the Red River formation, aquifers and oil filed in the Madison group, aquifers in the Minnelusa group, the Dakota aquifer, and Fort Union coal seams. So stacked CO_2 storage potential exists in the Williston Basin.

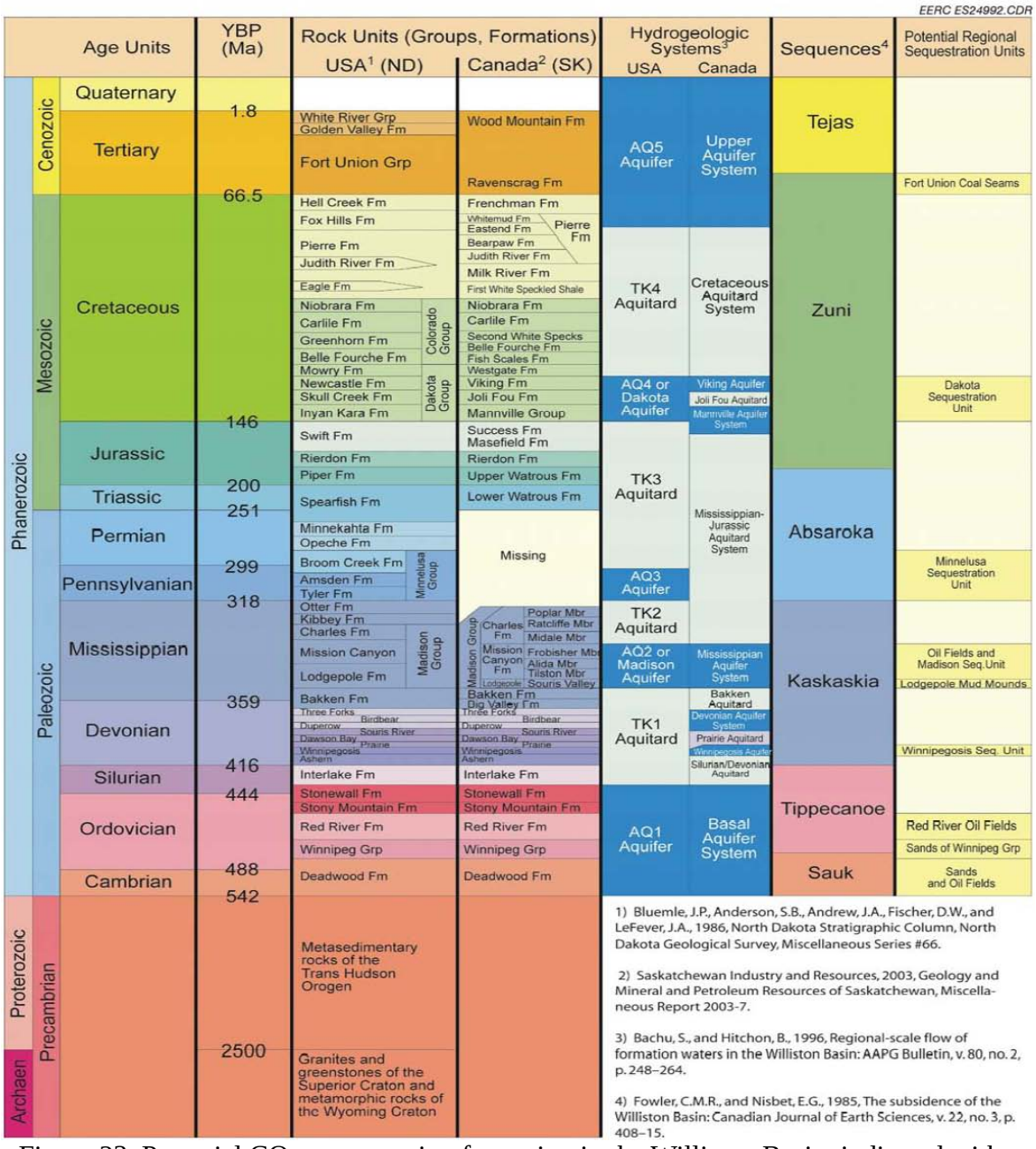

Figure 23. Potential CO_2 sequestration formation in the Williston Basin, indicated with geologic nomenclature [35].

Smith et al. [41] has conducted initial reconnaissance-level estimates for the CO_2 storage capacity in selected oil fields in the Williston basin. Two methods were used depending on the nature of the readily available reservoir characterization data for each field. The two methods are the EOR method and the volumetric method. The first method results in a CO_2 storage capacity based on the beneficial usage of CO_2 for EOR, and the second method gives the maximum storage capacity using the pore space of the reservoir. The result indicates that more than 22 oil fields in North Dakota have a market to utilize 114 million tons of CO_2, with the potential to produce more than 261 million barrel (bbl) of incremental oil through CO_2-flooding activities. These oil fields also have a maximum capacity to sequester nearly 371 million tons of CO_2.

Field Name	*Producing Pool (s)*	*Volumetric Capacity (million tons)*	*Enhanced Oil Recovery Capacity (million tons)*	*Incremental Oil Production (million stb)*
Beaver Lodge	Madison	111	21	44
	Devonian			
	Silurian			
	Ordovician			
Cedar Hills South	Red River B	49	21	43
Tioga	Madison	39	13	26
Big Stick	Madison	31	10	20
Charlson North	Madison	30	5	10
Antelope	Madison	19	7	14
	Devonian			
Newburg	Spearfish-Charles	18	6	12
Dickinson	Heath	15	4	7
North Elkhorn	Madison	14	3	7
Charlson South	Madison	11	1	1
Rough Rider East	Madison	11	2	4
Rival	Madison	11	5	9
Clear Creek	Madison	10	2	3
Blue Buttes	Madison	9	5	11
Fryburg	Heath-Madison	9	9	19
Lignite	Madison	7	2	4
Wiley	Glenburn	5	5	12
Bear Creek	Duperow	5	1	2
Medora	Heath-Madison	4	3	7
Fryburg South	Tyler	3	1	3
Mohall	Madison	3	1	2
Tracy Mountain	Tyler	2	0.5	1
Total		416	128	261

Figure 24. CO_2 storage capacity of selected oil fields in North Dakota [41].

CHAPTER III

CHARACTERIZATION OF THE SELECTED SITES

3.1 UCG Site Selection Criteria

UCG is a promising technology to recover the unmineable coal resources. However, associated environmental issues and improperly designed gasification processes could limit the applicability of UCG. Major environmental risks include subsidence and groundwater pollution [42]. Fractures may be generated due to high temperatures during gasification, reducing the integration and strength of the rock-mass, and providing transport paths for UCG-introduced contaminants. Thus the UCG design procedure is highly site specific. A successful UCG project would depend on good understanding of the natural properties and in situ geological/hydrogeological conditions of the target coal seam and its surrounding rocks. Since these parameters determine the gasification operation strategies and the composition of the product gas, they, in turn, govern the economic and environmental performances of the UCG plant. Therefore, appropriate site screening criteria and procedures, and optimized operation processes are required to minimize the environmental risks and maintain a satisfactory product gas quality. The site characterization work will provide detailed knowledge of the geology, hydrogeology, geomechanics and thermophysics of the target sites.

There is an extensive literature discussing UCG site selection procedure [8, 10, 42-43]. Selection criteria are based on considerations of resource abundance, mitigation of environmental risks and security of good product gas quality. Many characteristics of the coal-containing strata need to be investigated during the site selection process. In general, the UCG sites are primarily selected from coal zones which are considered to be economically unmineable using conventional technology. There are a variety of factors making a coal seam unmineable in the foreseeable future. Depending on specific local conditions, the definition of unmineable coal deposits may be different. Topez listed some common factors as follow [44]:

- Seam thickness: any seam under a thickness of 0.46 m is not likely to be mined.
- Location: a seam which occurs under a city or in a location where environmental considerations preclude any mining.
- Continuity-Depth-Quality: discontinuous seams or seams affected by excessive tectonic disturbances; excessive depth and dipping; and very low quality coal seams.

The NDGS [45] defined the economic coal deposits based on minimum criteria established by coal companies operating surface mines in the state of North Dakota. These economic criteria are: a minimum cumulative coal thickness of 3 m – typically occurring in no more than two beds, a minimum individual bed thickness of at least 0.76 m, a ratio of overburden to coal thickness of not higher than 10:1, a minimum of 7.6 m of overburden, and a maximum depth to coal of approximately 46 m.

Besides the formation structure, geomechanical, hydrogeological and thermal properties

of the coal-bearing formation should be well understood. Table 2 lists part of, if not all, the parameters of the target formation that should be investigated during the site screening, and their functions in the process design and operation control.

Table 2. Key formation properties and their major functions in UCG site characterization

Property	*Function*
Coal seam thickness and depth	Assessment of resource, well design and gasification module design
Coal seam structure and inclination	Gasification zone design, well design and assessment of contaminants migration
Coal permeability	Well linkage, transport of injected gases and gaseous products
Hydrostatic pressure and capillary pressure	Water influx control, gasification pressure and loss of products
Rock permeability	Water influx control and propagation of contaminants
Rock porosity, water saturation	Water available for chemical reaction
Rock thermal conductivity, thermal expansion coefficient	Temperature distribution, thermal stress and its effects
Rock strength, thermal expansion coefficient	Heat induced fractures, rock response and failure risks
Rock-quality designation (RQD)	Loss of product gas, transport of contaminants and rock failure risks

Deeper coal seams have advantages such as minimized risk of subsidence and the possibility to conduct the UCG process at higher pressure, which increases the heating value of the produced gas. Also, deeper seams are less likely to be linked with potable aquifers, thus avoiding drinkable water contamination problems. In assessing the UCG

potential in Indiana, Shafirovich [43] ranked the suitability of coal resources based on coal seam depth as: high (depth > 200 m), medium (depth between 60 m and 200 m, with high yield strength of overburden rocks), low (thickness between 60 m and 200 m, with low yield strength of overburden rocks), and unacceptable (depth < 60 m).

Hydrogeological issues are very important in UCG site selection and operation. If the coal seam coincides with an aquifer, special attention should be paid to the risk of groundwater pollution. Two methods can be applied to protect groundwater from pollution in a UCG project. The first method is to keep the gasification pressure below the hydrostatic pressure around the coal seam. In such cases, water from the aquifer enters into the gasification zone due to the pressure difference, and is involved in the reactions, particularly in the WGS reaction, increasing hydrogen content in the product gas [46]. However, water influx is also controlled by the permeability of the surrounding rocks, and could be higher than the desired quantity for chemical reactions. Excessive water influx would decrease the caloric value of the product gas. The second method is to select a site with shale-prone surrounding rocks. Shaly rocks have lower permeability than sandy rocks, and as a result, they can function as a seal to prevent propagation of contaminants from the gasification zone [42]. So we propose that the clay content of the surrounding rocks should be considered as an important factor in UCG site selection.

Since the physical variation of the strata is mainly controlled by the depositional environment, sedimentology reports about the target site can provide a rough, but fast, image of the isolation capability of the surrounding rocks. If coals were deposited in

deltaic or fluvial successions, they are likely to be overlain by permeable layers. If coals were formed in a lacustrine system, they are likely to be buried by shales or high-clay content rocks, therefore with good isolation. In addition to the primary permeability system, natural fractures and thermal-induced fractures during UCG operation should be well understood as they could be the major channels for fluid transport.

On the other hand, the target coal seam should have a sufficiently high permeability in order to transport injected oxidants and gaseous products. Other factors that need to be considered in site selection include impact to nearby mines and infrastructure for construction and product transportation. In general, a simplified UCG site screening procedure for coal seam in North Dakota is proposed in Figure 25.

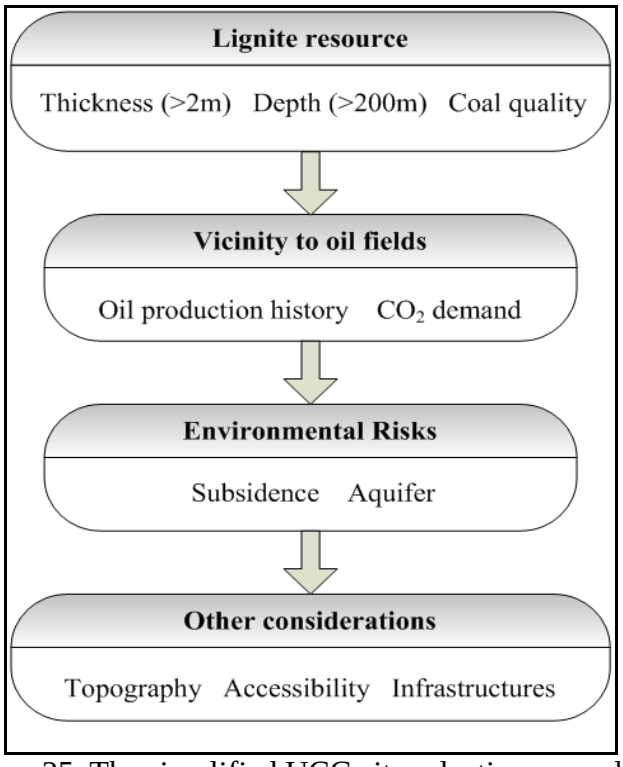

Figure 25. The simplified UCG site selection procedure.

An extensive literature review was conducted to look at the depositional history of the Fort Union formation, geological structure of the Fort Union strata, stratigraphy description, strippable coal map, coal resource estimation, water resource and aquifer investigation, petroleum resource report, petroleum production data, geological structure of the Williston basin, etc. The work is based on the data and documents available from the USGS and NDGS, combining specific consideration to local conditions. According to the coal resources assessment conducted by USGS [47], coal resources in beds thicker than 0.76 m in the Fort Union formation in seven counties in southwestern North Dakota have been evaluated: Adams, Billings, Bowman, Golden Valley, Hettinger, Slope, and Stark. The evaluated results are: Harmon and Hansen coal beds and zones—60.8 billion tonnes, Hagel coal beds and zones—4.0 billion tonnes, and Beulah-Zap coal beds and zones—4.8 billion tonnes. In general the Harmon coal zone has more resource. Another reference of lignite resources used in this study is the report of lignite reserve published by NDGS [37], where the lignite resources were evaluated at the county level in western North Dakota.

With the above literature, and discussion in Chapter II about the structure and deposit process of the Fort Union lignite, the Harmon coal zone is thicker and more continuous than other coal zone. Therefore, applying the primary site screening criteria, the Harmon coal zone in the Fort Union formation was selected as the target coal seam for the proposed UCG-CCS process. Three sites in North Dakota were chosen as the candidate sites. These sites are located in Slope County, Golden Valley County, and Dunn County, respectively, as shown in Figure 26. The detailed selection process and geological

modeling of the candidate sites are discussed in the following parts.

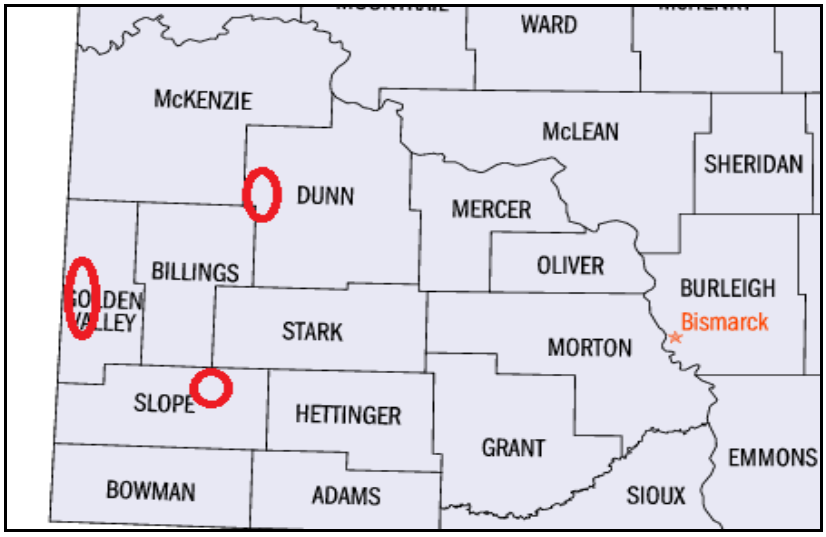

Figure 26. Selected candidate sites for UCG-CCS process.

3.2 Tools and Data in Site Screening

The Harmon lignite zone in the Fort Union formation, western North Dakota is considered to be the candidate coal seam because of its abundant resources. Our goal is to select a site suitable for UCG project and obtain detailed data in geology, hydrogeology and rock properties of the site. Available information used in this study includes reports, dissertations, conference and journal papers, lithological interpretation logs, and unprocessed well logs. Most of the literature and data are published by researchers in NDGS, USGS, North Dakota Industry Commission (NDIC), and The University of North Dakota (UND).

Two sets of logs were used in constructing the model: the lithological interpretation logs, and oil and gas electrical logs. The lithological interpretation logs in the Williston basin

are available from the USGS [48]. The stratigraphic data came from 6,033 locations in the basin, including oil and gas wells, coal drill holes, and outcrop measured sections which penetrated the Fort Union formation. Only the data from non-proprietary drill-holes are included in the open files. The database includes information on geographic location, stratigraphic measurements, lithologies, and stratigraphic nomenclature. The stratigraphic dataset is easy to use and covers extensive areas in the basin. Therefore, the dataset is used to deliver the coal seam thickness, depth, distribution, and surrounding rocks. After necessary processing, the logs were put into *Petrel* [49], a commercial simulator. As the selected sites are located in an area intensively drilled by the oil and gas industry, a significant amount of the electrical logs is obtainable. However, the Fort Union formation is not of interest to the oil companies, so most of the electrical logs were not run through it. As suggested by Murphy et al. [37], the lignites generally have readings of around 5 to 10 gamma counts per second, and the mudstone has counts around 20. The well logs were first digitized using *Petra* [50], a petroleum software package, and then the clay contents were interpreted by *Interactive Petrophysics* [51], another software package. The results were input into *Petrel* where the two sets of log data were compared with each other, and with lithology descriptions in other literature. Based on the comparisons, a well correlation was carried out; and finally a three-dimensional model of the Harmon coal seam and surrounding rocks was generated. It should be noted that although the Harmon bed may be split into several beds, only the thickest single bed is considered as the continuous part in our model. This model provides a visualized structural demonstration to the coal seam and surrounding rocks, and will serve as an input for further dynamic modeling of the gasification process.

In the USGS report [47], isopach maps of net coal thickness and overburden thickness of the Harmon coal zone in southwestern North Dakota are given (Figures 27 and 28). From the net coal thickness map, it can be seen that there are two major thick Harmon coal zones: one in the central parts of Slope County, and the other in the west-central part of Golden Valley County, with part thicker than 6.1 m, or 20 foot (ft). However, one should keep in mind that these are net thickness maps, not thickness maps of a single coal seam. As given in the report [47], the Harmon coal in Slope County is 11,793 million tonnes in total, and the Harmon coal in Golden Valley County is 6,532 million tonnes in total. Currently, there is no surface mining activity in the Harmon coal beds. In this study, two parts within the thicker Harmon coal zone have been selected as the evaluated segments, named as the Slope site and the Golden Valley site (Figure 29). Details of modeling works and discussion about these two assessment parts will be present later in this chapter.

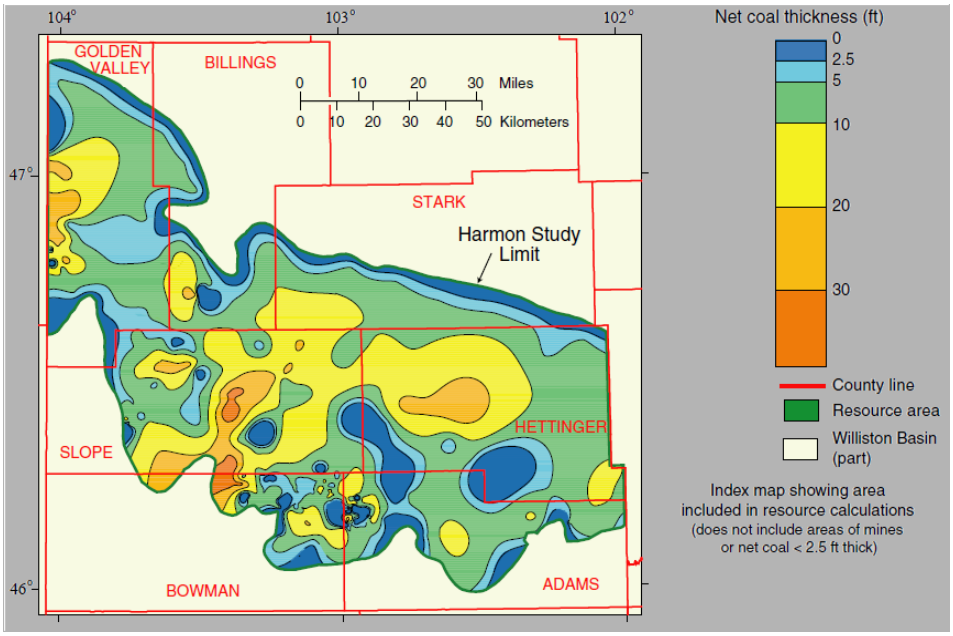

Figure 27. Harmon net coal isopach map and resource area [47].

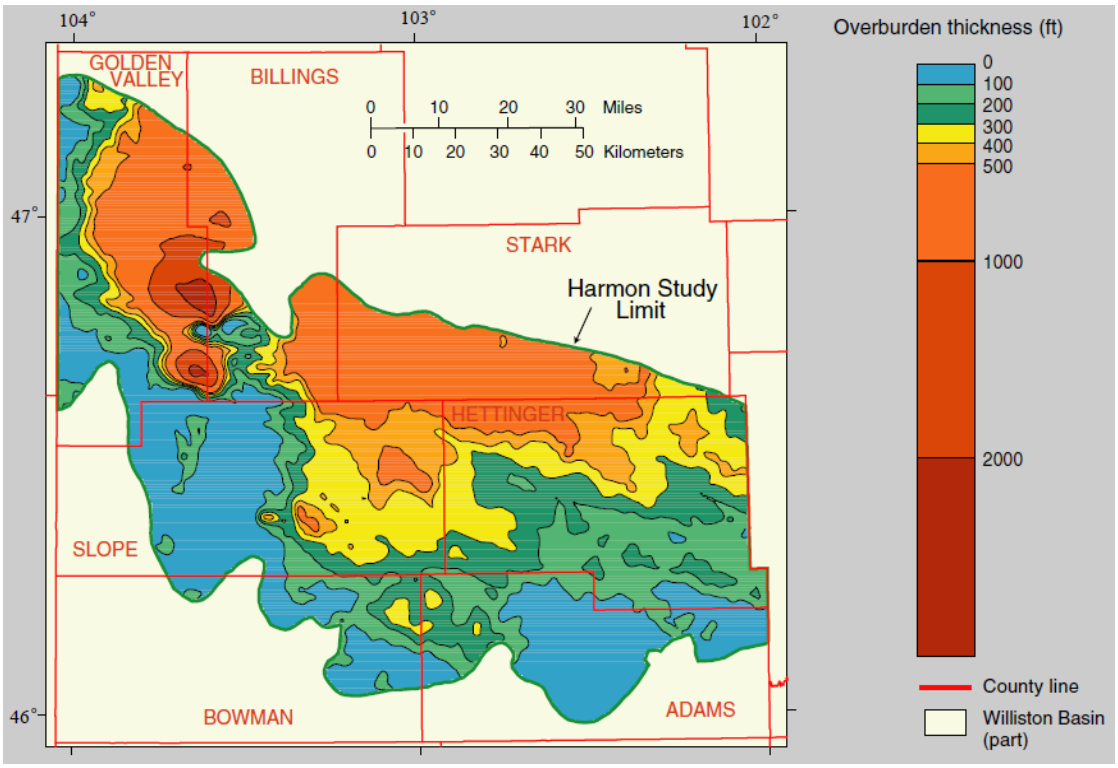

Figure 28. Harmon overburden isopach map [47].

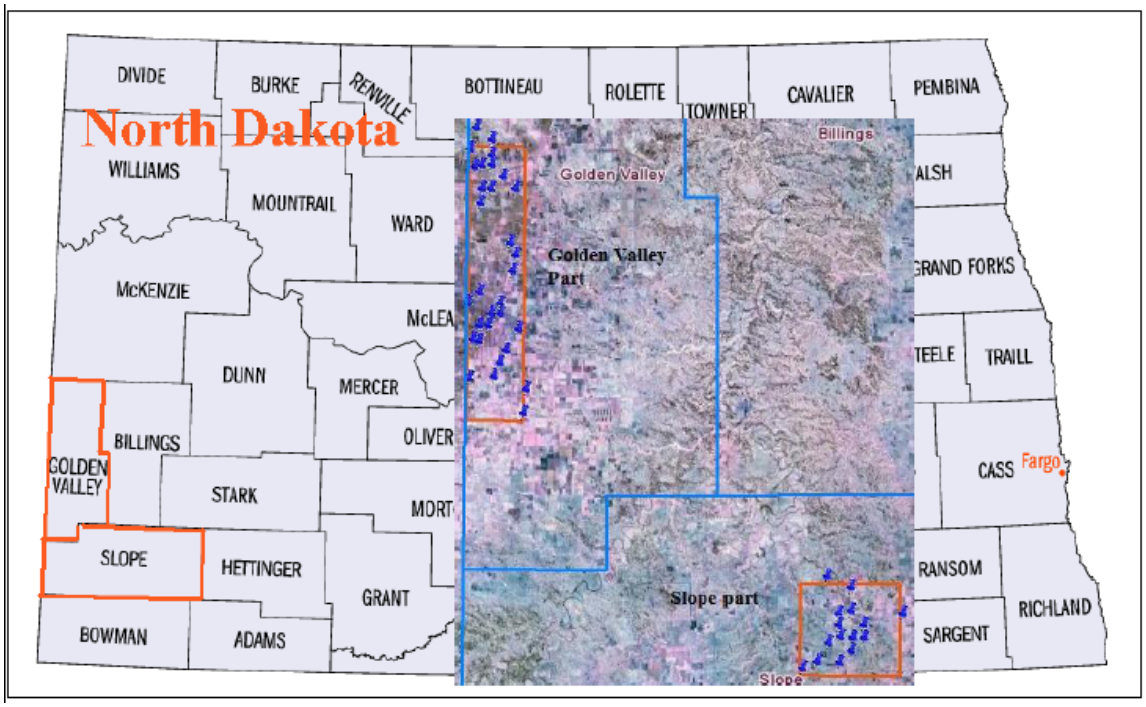

Figure 29. Locations of the Slope site and Golden Valley site.

From the isopach map of overburden thickness of the Harmon coal, it can be seen that in the west-central part of Golden Valley County, most coal seams are deeper than 30.5 m. In the central part of Slope County, most coal seams are shallower than 30.5 m. However, during primary selection, the depth of coal seams is not as important as coal seam thickness. In past UCG projects, the depth varied from 30 to 350 m in the former Soviet Union developments and U.S. experiments. Researchers in LLNL indicate that the minimum depth should be 12 m [8]. NDGS suggests 46 m as the maximum depth for surface mining.

In Murphy's detailed study about the lignite reserve in North Dakota [37], it presents thickness, number of seams, acre-feet, and tonnages of mineable lignite for every economic coal deposit in western and central North Dakota. Measured sections and electric logs through Fort Union strata reveal that 60 to 70% of this rock unit consists of claystone and mudstone. Sandstone constitutes approximately 25 to 30%, and lignite 5% of the Fort Union group. According to the information provided by Murphy, the Harmon coal bed beneath Dunn County is present as a thick, continuous bed (Figs 30, 31, and 32). Therefore, in addition to the sites in Golden Valley and Slope counties, a site of 4 townships (373 km^2) in Dunn County, North Dakota (Figure 33) is also chosen for this study. The selected site in Dunn County is right next to the Little Knife oil field.

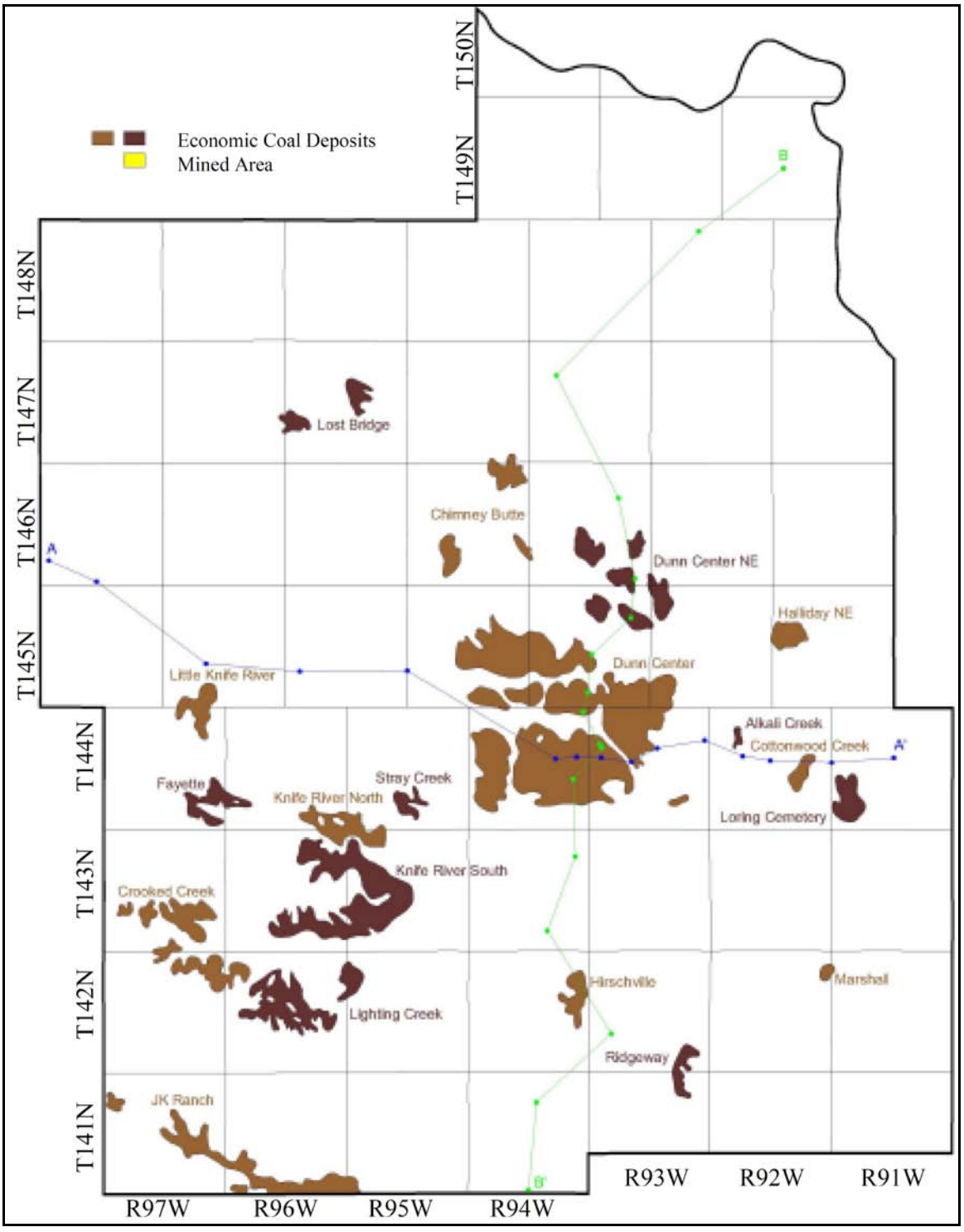

Figure 30. The mineable lignite deposits in Dunn County [37].

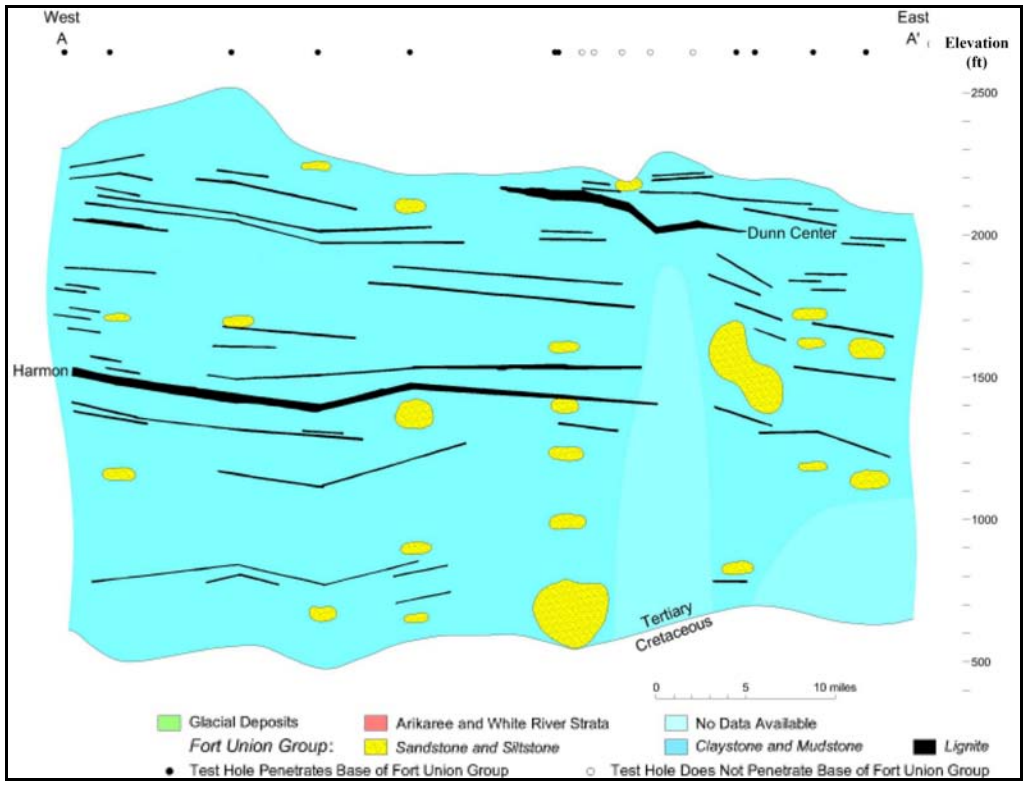

Figure 31. Cross-section A-A' through Dunn County. The trace of this cross section is in Figure 30 [37].

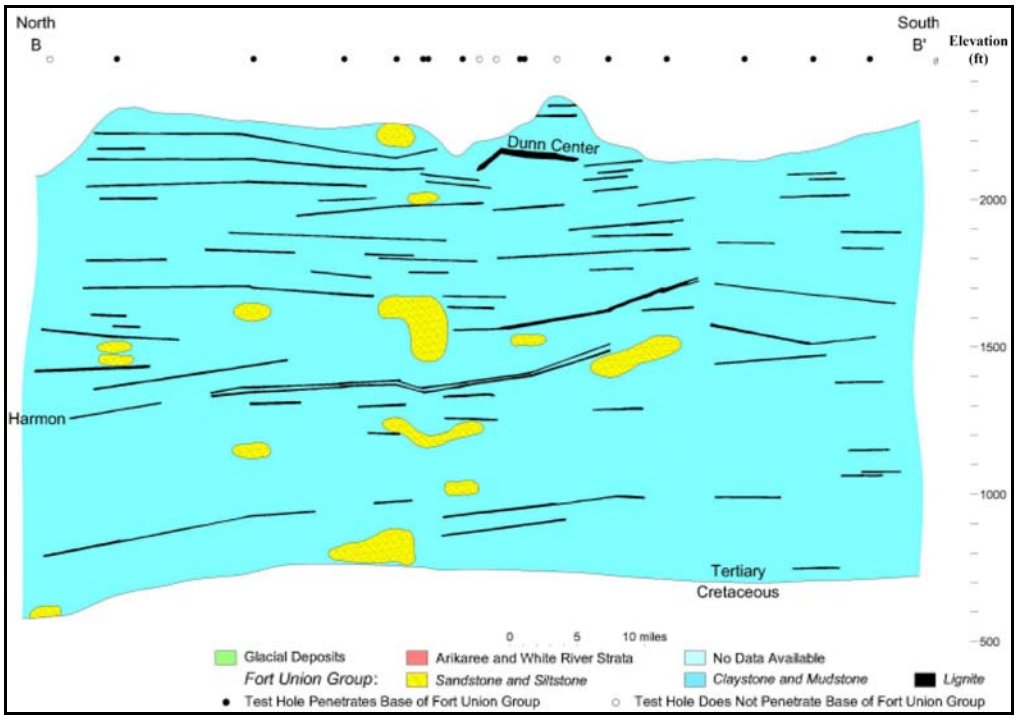

Figure 32. Cross-section B-B' through Dunn County. The trace of this cross section is in Figure 30 [37].

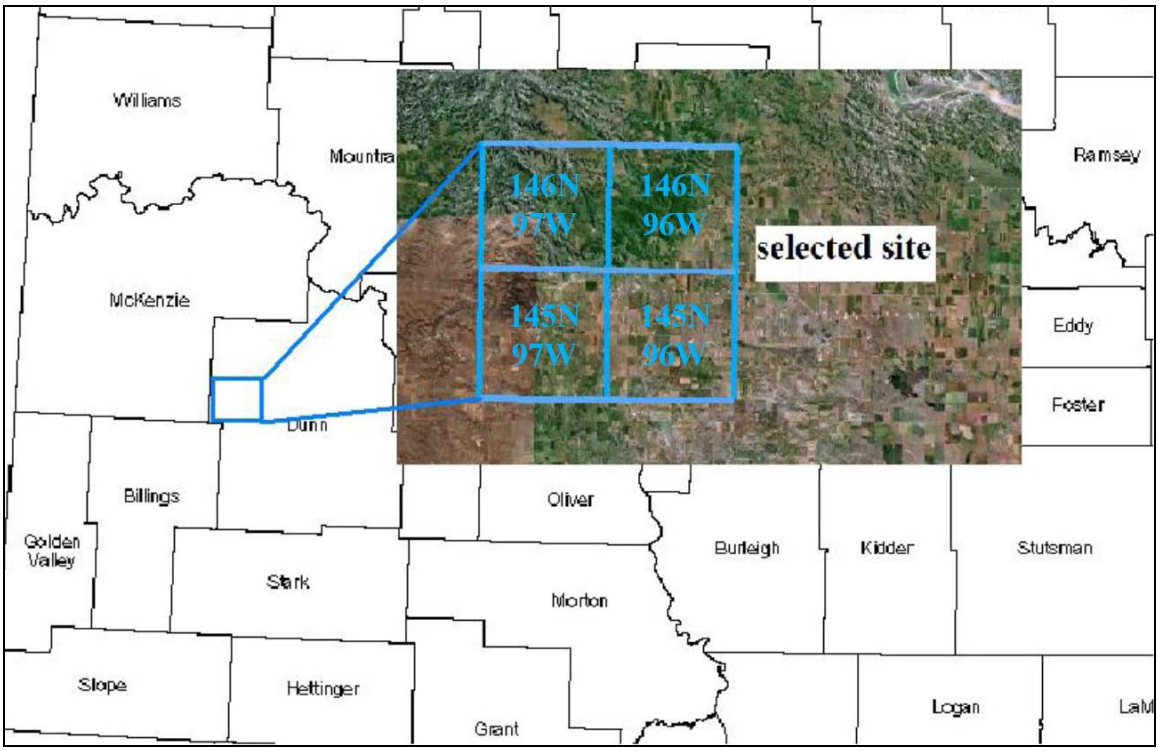

Figure 33. Location of the selected site in Dunn County.

3.3 Selected Sites in Golden Valley County and Slope County, North Dakota

There are 15 data points contained in the Slope assessment site, and 27 data points in the Golden Valley assessment site. After pre-processing, the data were loaded onto *Petrel*. Using the simulator, a three-dimensional lithologic model was generated, together with associated overburden up to the surface, and an underlying zone which extends downward 9.1 m (30 ft) from the bottom of the coal seam. Based on the coal deposits indicated in the three-dimensional model, and with reference to the isopach map of coal seam depth in Figures 27 and 28, a single, relatively continuous coal seam can be recognized, and is considered as a major coal seam. An isopach map of thickness, contour maps of depth and overburden-thickness ratio of the recognized coal seam were then generated.

3.3.1 The Slope Site

The three-dimensional lithological model of the major coal seam, associated overburden and the underlayer in the Slope site is shown in Figure 34. The boundary of the model was set arbitrarily to best enclose the input data points. In the model, purple represents coals, blue means claystone, yellow indicates sandstone, and red represents siltstone. The green arrow points to the north.

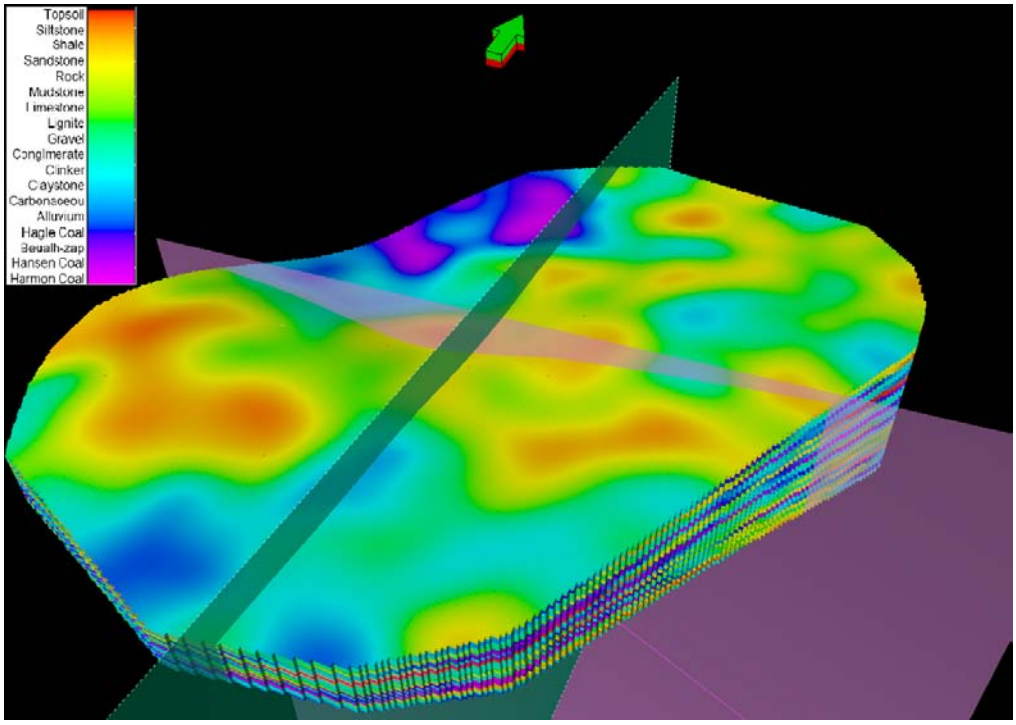

Figure 34. Three-dimensional the coal seam and overburden in Slope site. 20 times vertical exaggeration, green arrow points to the north.

The north-south cross sectional view and east-west cross sectional view are indicated in Figures 35 and 36, respectively. In general, the south portion of the major coal seam (the purple part) is thicker than the north portion, and the west portion is thicker than the east portion. Regarding its depth, the coal seam becomes deeper from north to south, and from

west to east. Most of the overburden and underlayer is claystone, dominantly interbedded with sandstone, shale, limestone, and siltstone. Within the overburden, there are isolated small coal deposits. The calculated volume of the major coal seam in this model is approximately 3.7×1010 ft3, or 850,253 acre-ft. Using a conversion factor of 1,750 short tons per acre-ft for lignite rank coal [47], coal resources in this coal seam are about 1,350 million tonnes (1,488 million short tons).

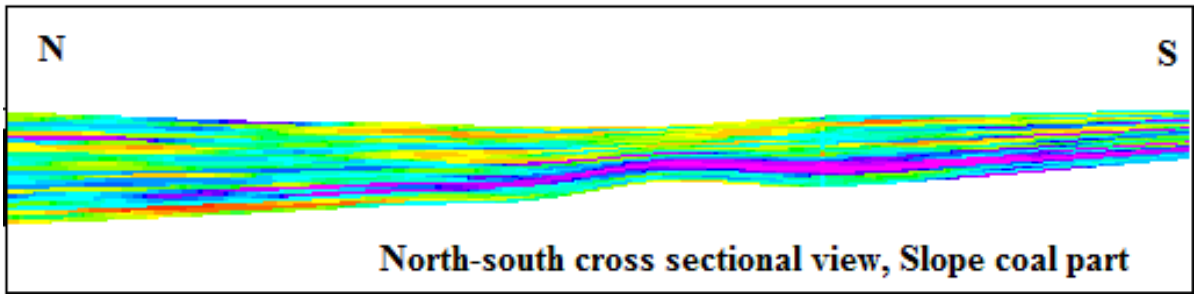

Figure 35. North-South cross-sectional view, Slope site.

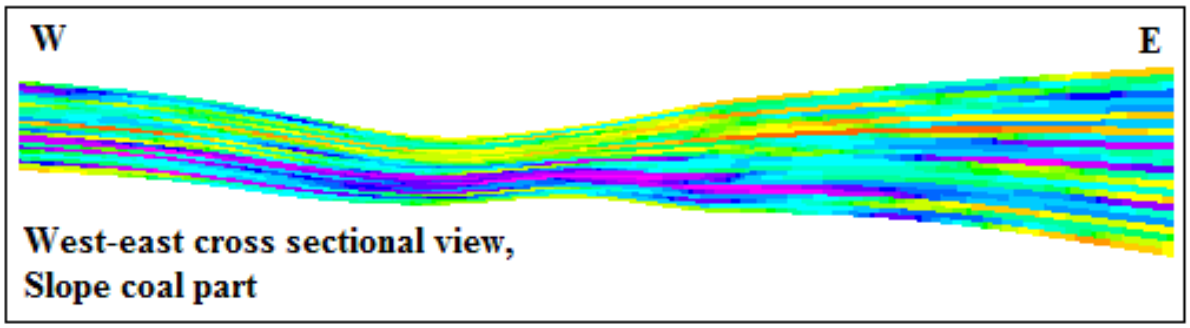

Figure 36. West-East cross-sectional view, Slope site.

After the major coal seam is recognized in *Petrel*, related isopach maps and contour maps of the coal seam can be generated. The boundary of these maps is shown in Figure 29. Figure 37 shows the thickness isopach map of the major coal seam. The solid lines represent location where coal seam thickness is more than 2 m. Assuming 2 meters is the minimum thickness for UCG projects, Figure 37 shows that a significant part of the coal

seam in this assessment site is suitable for UCG development with enough coal seam thickness, especially in the east part. The depth contour map of coal seam is shown in Figure 38, where the dashed lines indicate depths less than 50 m, close to the economic limit of surface mining suggested by NDGS. Comparing with Figure 37, we consider that the east part of the coal seam has good potential for UCG projects with both criteria satisfied: coal seam thickness and overburden thickness. Scattered coal deposits existing above the major coal seam may provide opportunities of injecting separated CO_2 as described above in the UCG-CCS concept. In general, coal seams used for CO_2 sequestration and enhanced coal bed methane recovery are considered as unmineable, and the definitions of unmineable coal seams vary, as discussed above. Detailed information of these scattered coal deposits needs to be investigated further. The contour map of depth-to-thickness ratio is given in Figure 39. Although the depth-to-thickness ratio of the west side is less than 10, it does not mean that the coal seam in this part is economical for surface mining. Instead, UCG projects might be a better option, because the depth is more than 50 m.

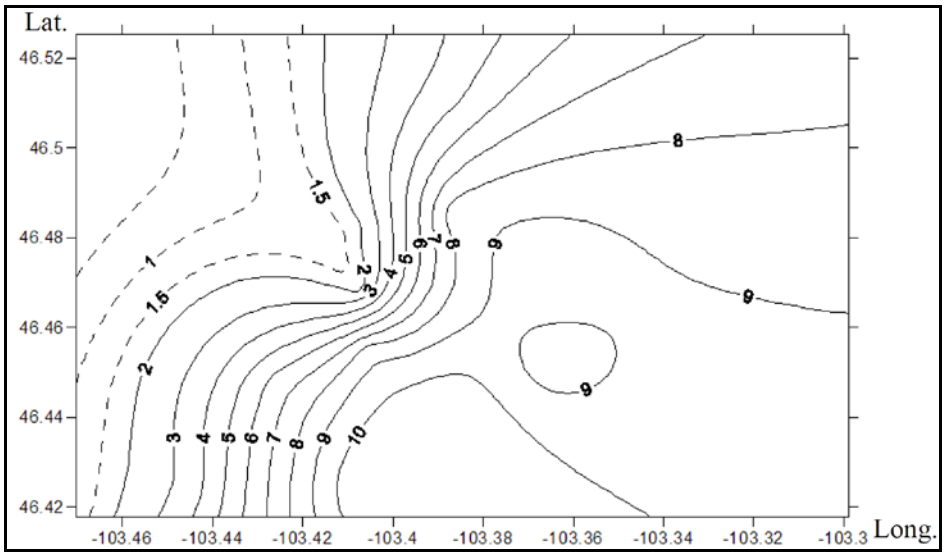

Figure 37. Isopach map of the major coal seam at Slope site, in meters.

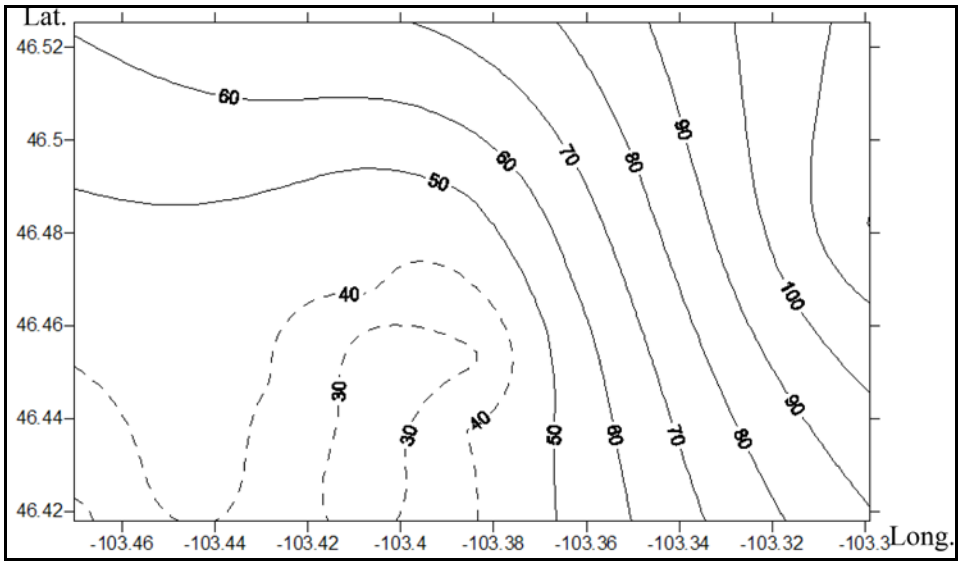

Figure 38. Depth contour map of the major coal seam depth at Slope site, in meters.

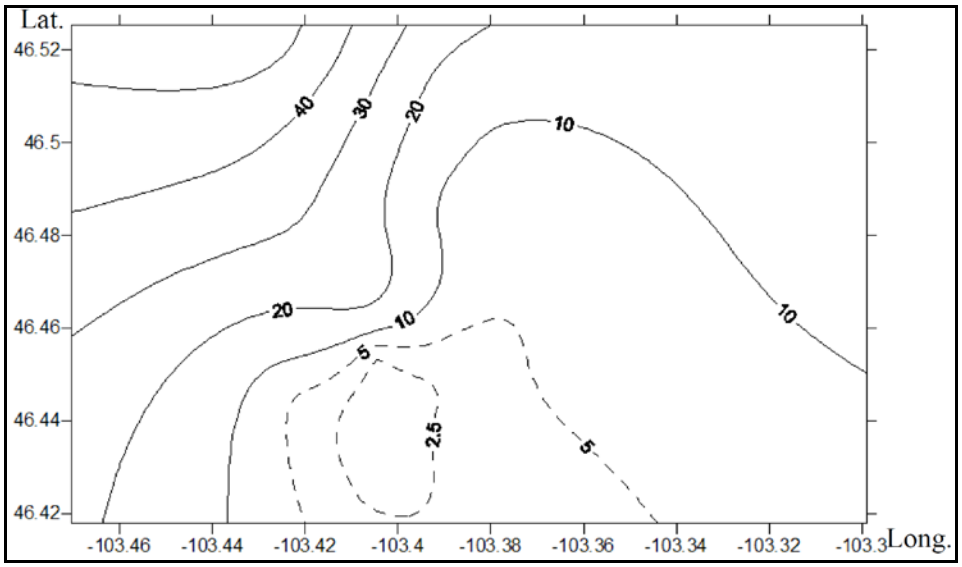

Figure 39. Contour map of the major coal seam depth/thickness ratio at Slope site.

3.3.2 The Golden Valley Site

Figure 40 shows the three-dimensional lithological model of the major coal seam, associated overburden and underlayer in the Golden Valley site. In the model, purple represents coals, blue means claystone, yellow indicates sandstone, and red represents

siltstone. The green arrow points to the north in the figure. The north-south cross sectional view and east-west cross sectional view are indicated in Figure 41. In general, the south portion of the major coal seam (the purple part) is shallower than the north portion; and the west portion is deeper than the east portion. In the figures, the thickest part of the major coal seam is in the south-central part. Claystone is the dominant rock in the overburden and the underlayer, interbedded with sandstone, shale, limestone, and siltstone. There are small isolated coal deposits within the overburden, which can be used as CO_2 storage sites. The calculated volume of the continuous major coal seam in this model is approximately $6.1 \times 10^{10}\,ft^3$, or 1,401,492 acre-ft. Using a conversion factor of 1,750 short tons per acre-ft for lignite rank coal [47], coal resources in this coal seam are about 2,225 million tonnes (2,453 million short tons).

The related isopach map and contour maps of the major coal seam in the Golden Valley site are shown in Figure 42. In the thickness isopach map, the solid lines represent where the coal seam is thicker than 2 m. The figure shows that most part of the coal seam in the Golden Valley site is suitable for UCG with the criterion for coal bed thickness. In the depth contour map of coal seam, the dashed lines indicate depths less than 50 m. In the figure, it can be seen that the coal seam in the central part of the zone is deeper where the coal seam is also thicker. This results in higher depth-to-thickness ratios (>10) in most part of the coal seam. The highest depth-thickness ratio occurs at the central part.

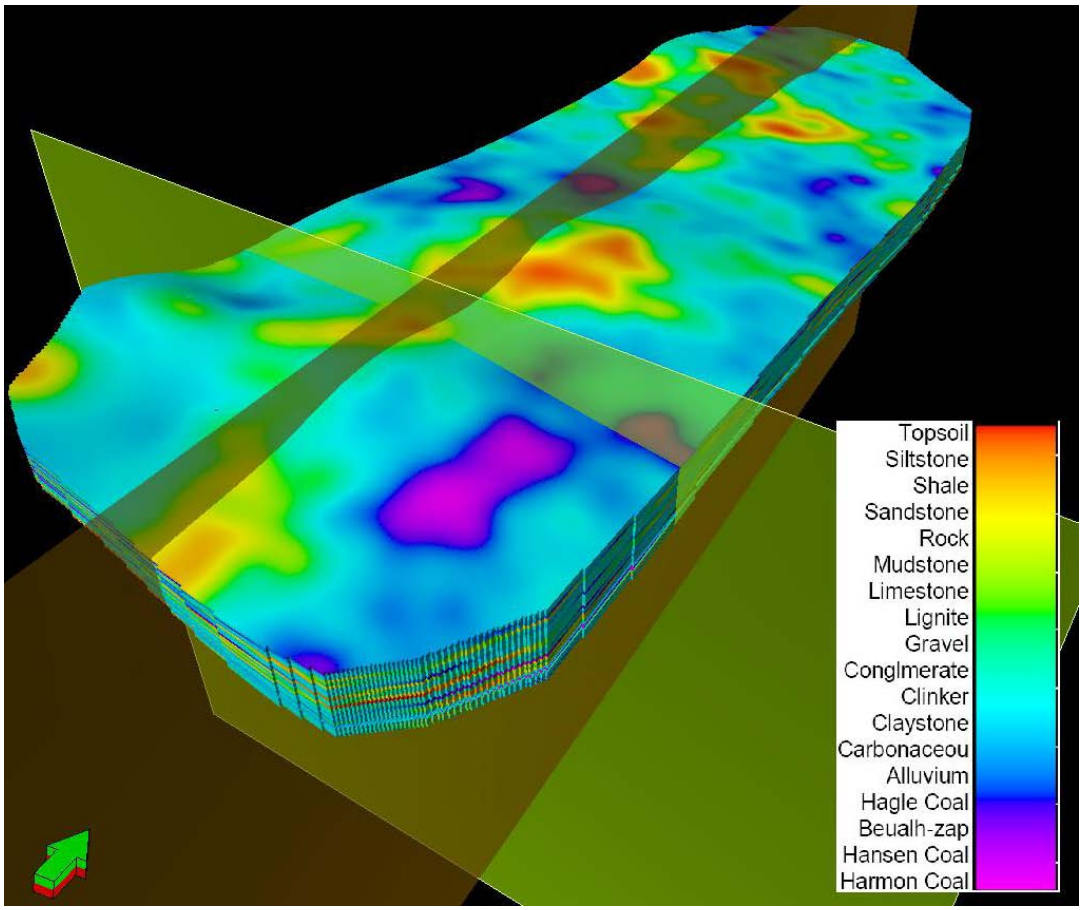

Figure 40. Three-dimensional lithological model of the coal seam and overburden at Golden Valley site. 25 times vertical exaggeration, the green arrow points to the north.

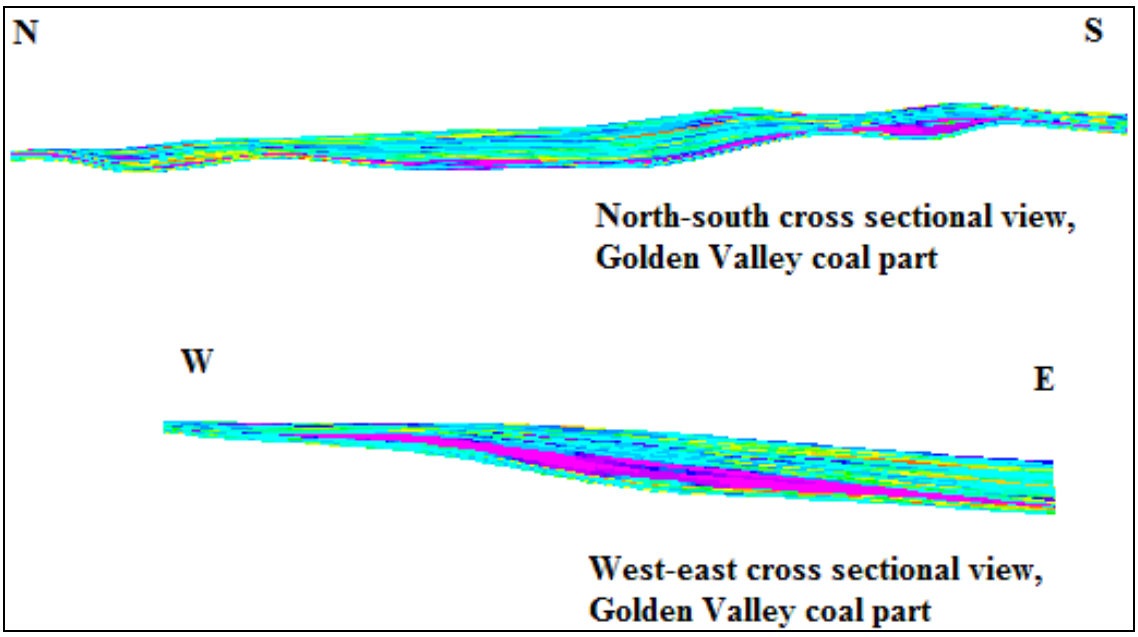

Figure 41. Cross sectional views, Golden Valley site.

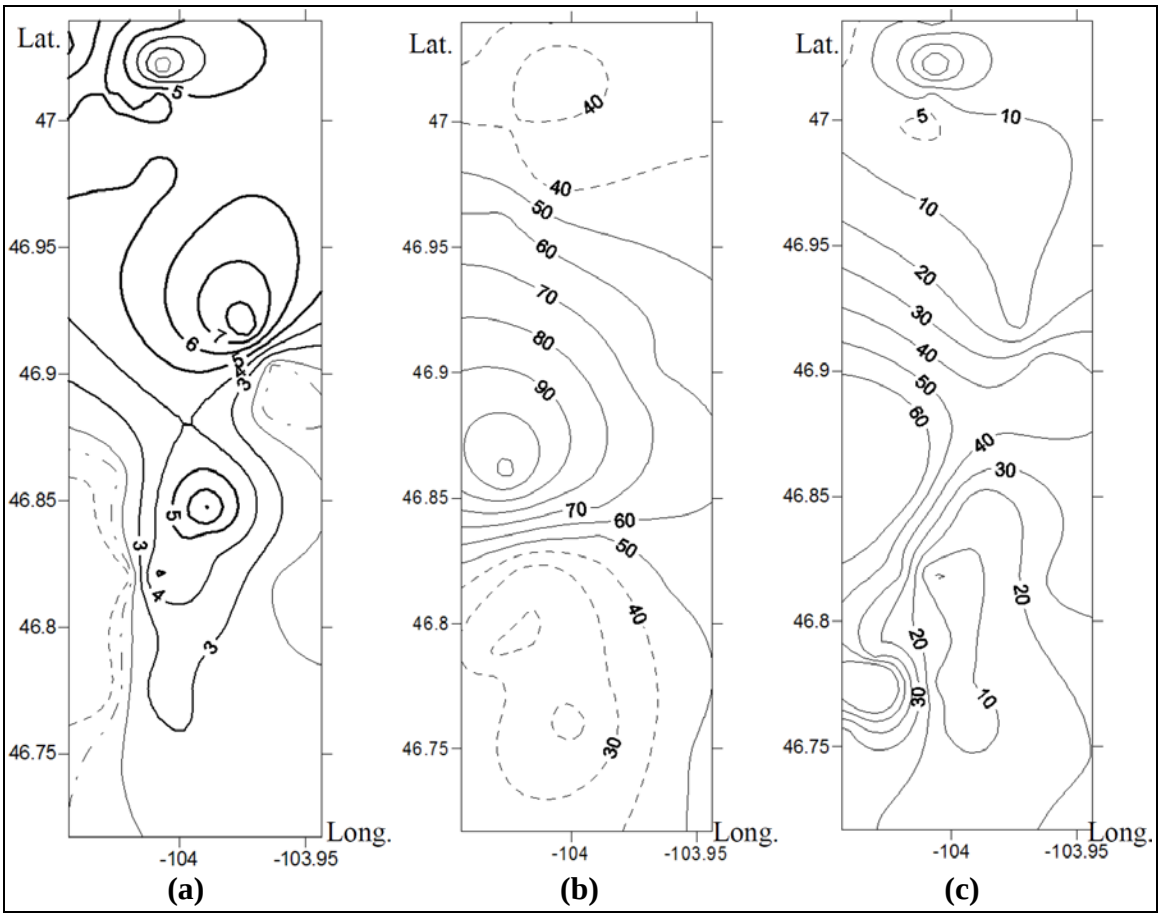

Figure 42. Isopach map (a) and contour maps of the major coal seam depth (b) and depth/thickness ratio (c) at the Golden Valley site, in meters.

3.4 Selected Site in Dunn County, North Dakota

Based on the reviewed literature and the primary selection criteria, a site with an area of 4 townships (373 km^2) in Dunn County, North Dakota (Figure 33) is chosen. Forty wells with gamma ray (GR) logs located within the selected site were used in model building. The three-dimensional model of this site provides a visualized structural demonstration to the coal seam and surrounding rocks, describes the lithology facies, clay content, presence of aquifers, and will serve as an input for further dynamic modeling of the gasification process.

3.4.1 Geological Properties of the Coal Seam and Surrounding Rocks

The measured depth and thickness of the coal seam is shown in Figures 43 and 44, respectively (Universal Transverse Mercator coordinate). As shown in the figures, most of the coal seam has a depth greater than 244 m (800 ft) below the surface, and a thickness greater than 6 m (20 ft). Based on the thickness and depth, the Harmon coal seam is an ideal candidate for UCG utilization. The topography of the selected site and the coal seam are shown in Figure 45. The north and northwest portion of the topography is hilly. The rest of the site is flat. The calculated bulk volume of the Harmon lignite of a single bed contained in this area is 2.67×10^{9} m^3 (9.44×10^{10} ft^3), which is about 3,793 million tonnes (4,181 million short tons) of lignite resource.

The thickness of the coal seam shown in Figure 44 gives a clue to the depositional environment of the Harmon bed in the modeled site. As described in Section 2.2, the Harmon bed was deposited in a mixed system of inter-channel fluvial system and lacustrine swamp. Peat accumulated in river channels usually is relatively thick, while peat formed in inter-channel swamps is relatively thin. In most part of the site, the coal seam has a thickness between 20 and 20 ft. This means that the depositional system was probably swamp. Compared with the paleo-flow direction of the Powder River system given in Figures 21 and 22, the river channel probably existed in the northwest port of North Dakota, such as McKenzie and Williams Counties. However, if there are more wells available, the model can be improved, so the paleostructure of the site would be more accurate with the better well control.

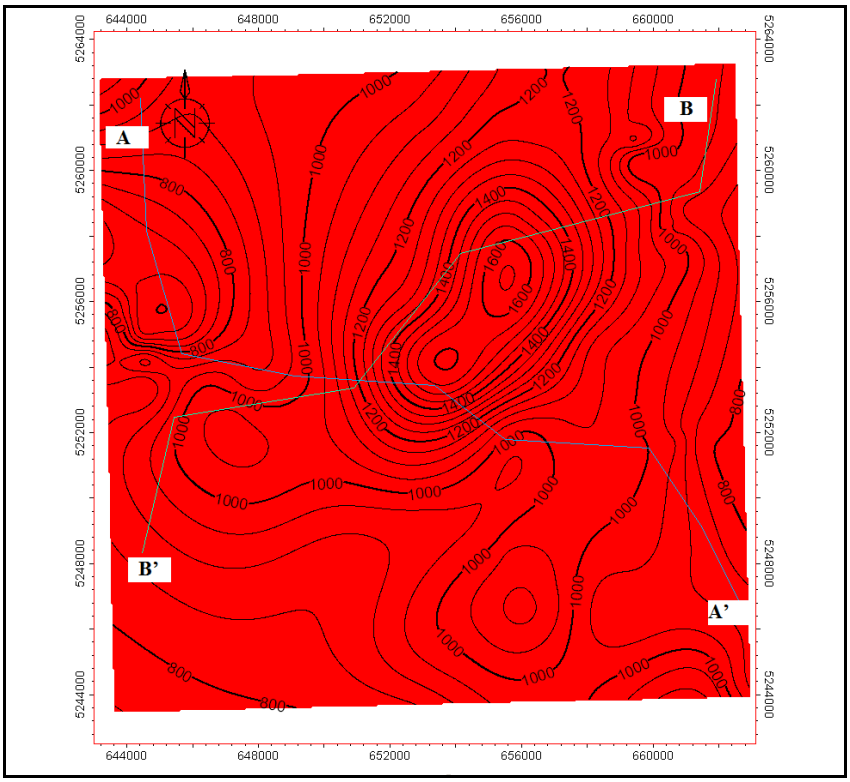

Figure 43. Contour map of the measured depth of the Harmon lignite bed at Dunn site, ft.

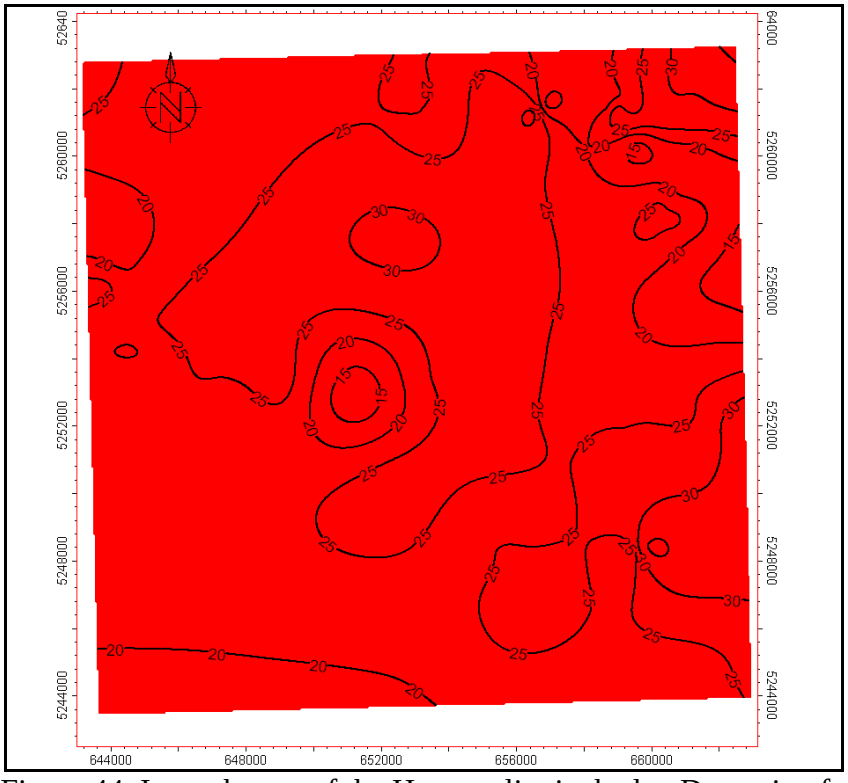

Figure 44. Isopach map of the Harmon lignite bed at Dunn site, ft.

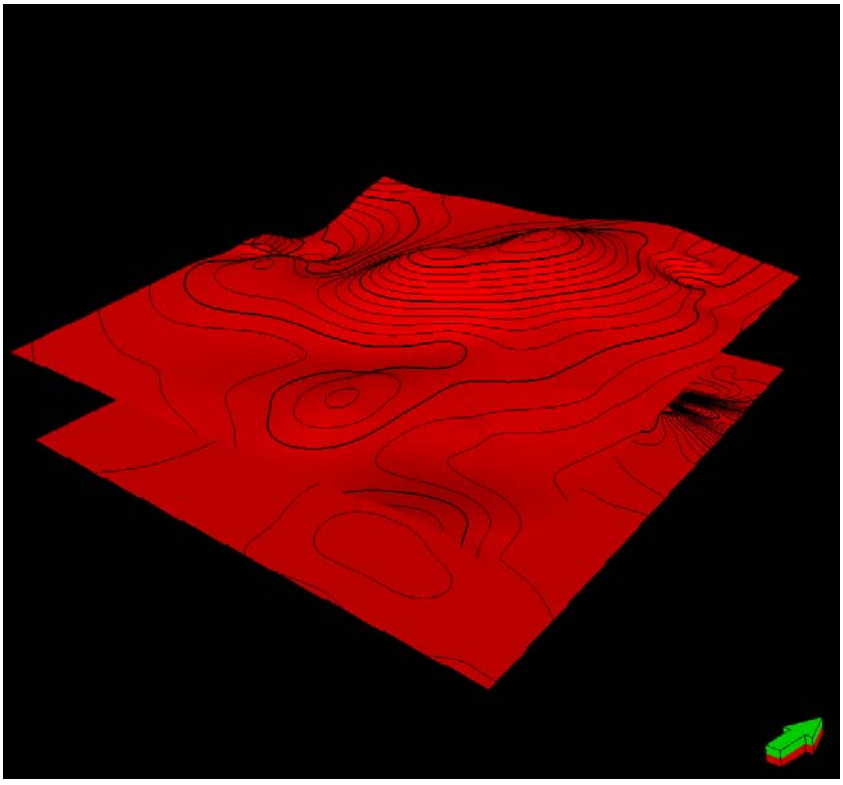

Figure 45. Topography and the Harmon coal seam, Dunn site (10 times vertical exaggeration, the green arrow to the north).

As discussed earlier, if coals were deposited in deltaic or fluvial successions, they are likely to be overlain by permeable layers. If coals were formed in a lacustrine system, they are likely to be covered by shales or high-clay content rocks, which provide good isolation for the contaminants generated during the UCG process. The clay contents in the strata below and above the coal seam of the site are shown in Figures 46 to 51. It can be seen that for the overlayer 9 m above the coal seam, the clay content is usually higher than 60% in most part; and the underlayer which is 9 m below the coal seam, the clay content is usually higher than 80% in most part of it. According to the simulation, about 88% of the overburden by volume is claystone. These maps of the clay distribution help locate the gasification zone to avoid the low-clay content rocks for the purpose of preventing contaminant leakage.

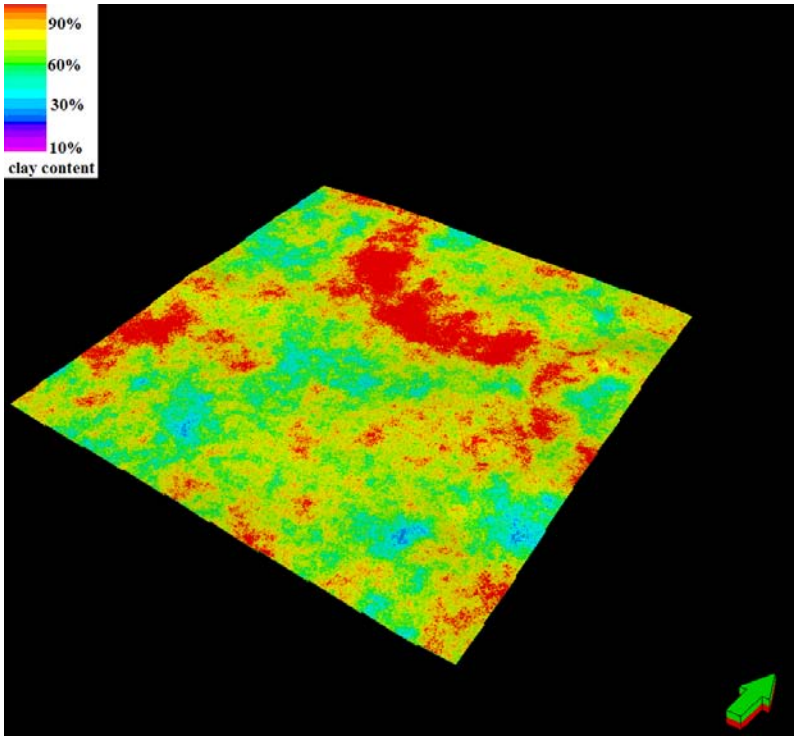

Figure 46. Clay contents of the underlayer, 9.1 m (30 ft) below the Harmon coal seam, Dunn site (10 times vertical exaggeration, the green arrow to the north).

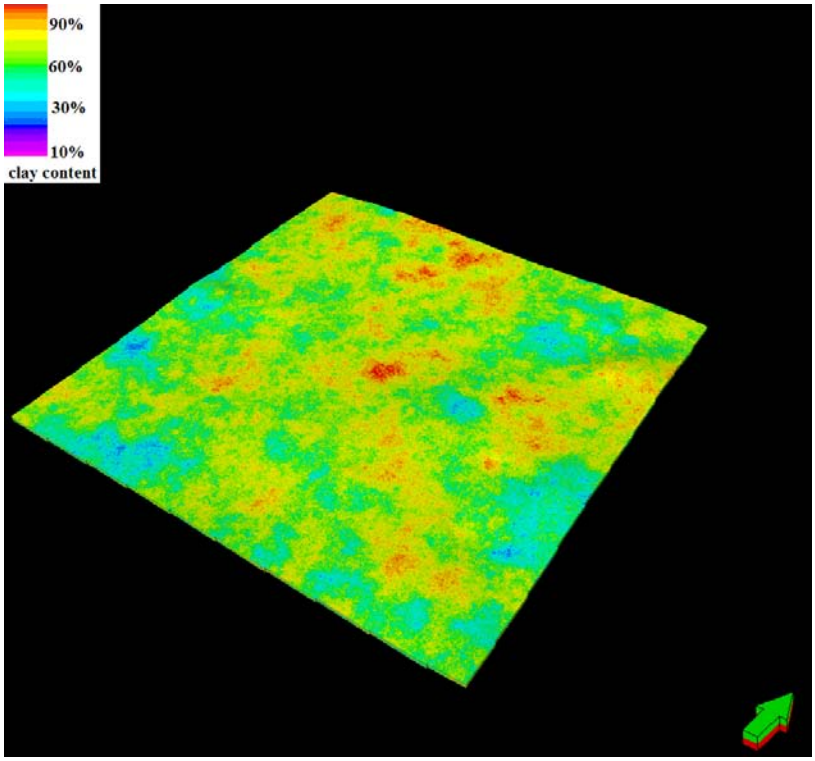

Figure 47. Clay contents of the underlayer, 18.3 m (60 ft) below the Harmon coal seam, Dunn site (10 times vertical exaggeration, the green arrow to the north).

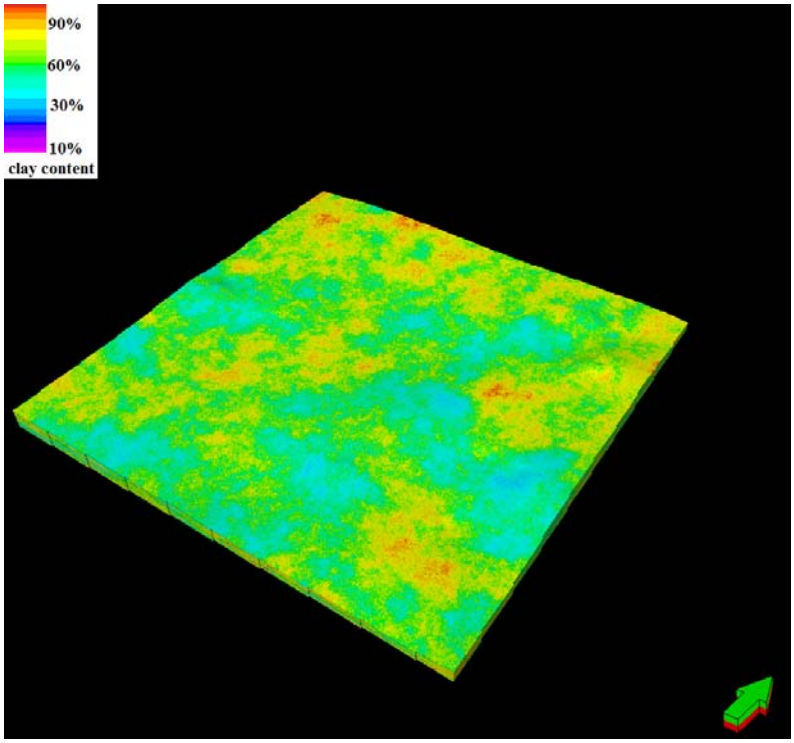

Figure 48. Clay contents of the underlayer, 30.5 m (100 ft) below the Harmon coal seam, Dunn site (10 times vertical exaggeration, the green arrow to the north).

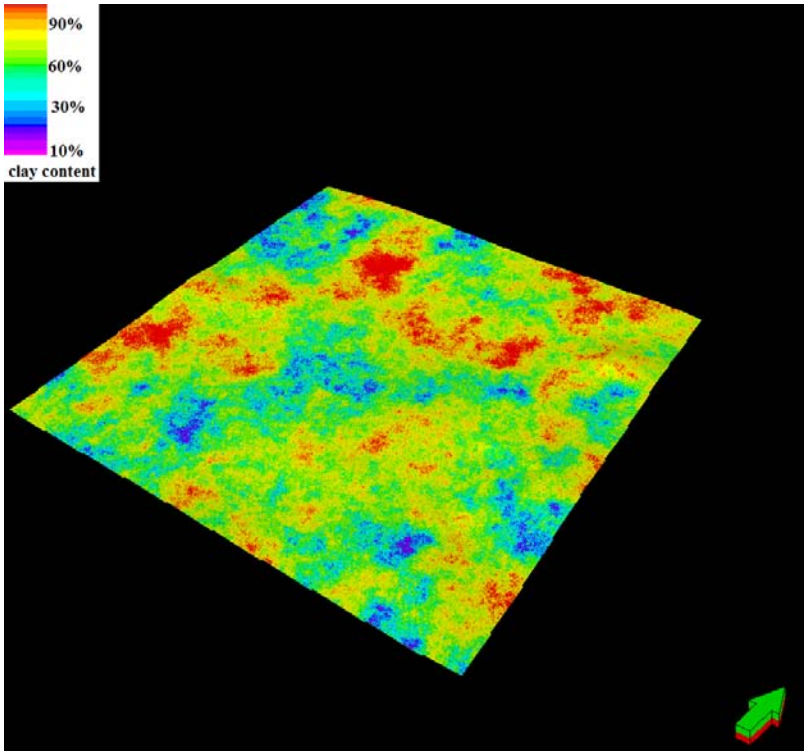

Figure 49. Clay contents of the overlayer, 9.1 m (30 ft) above the Harmon coal seam, Dunn site (10 times vertical exaggeration, the green arrow to the north).

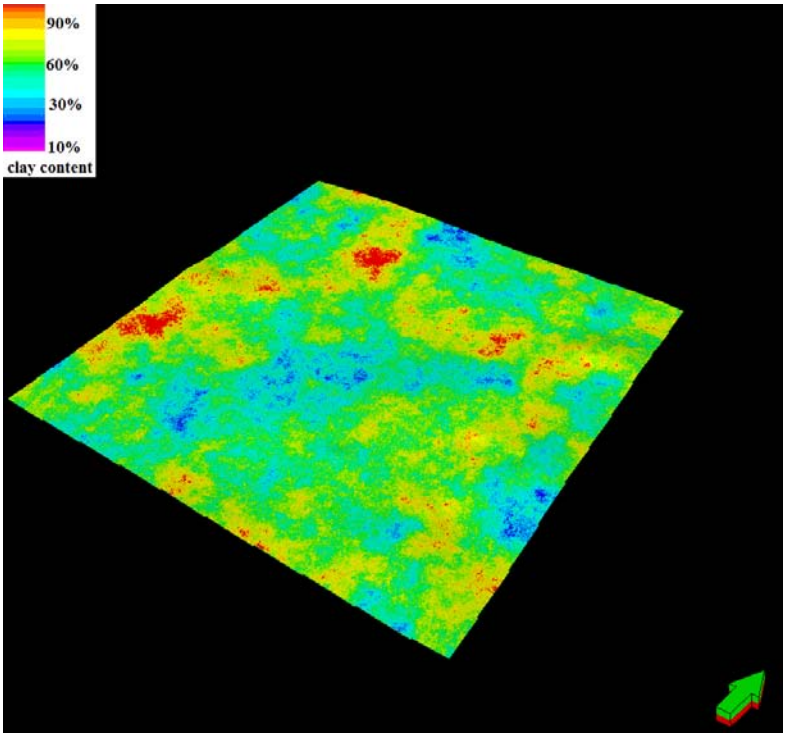

Figure 50. Clay contents of the overlayer, 18.3 m (60 ft) above the Harmon coal seam, Dunn site (10 times vertical exaggeration, the green arrow to the north).

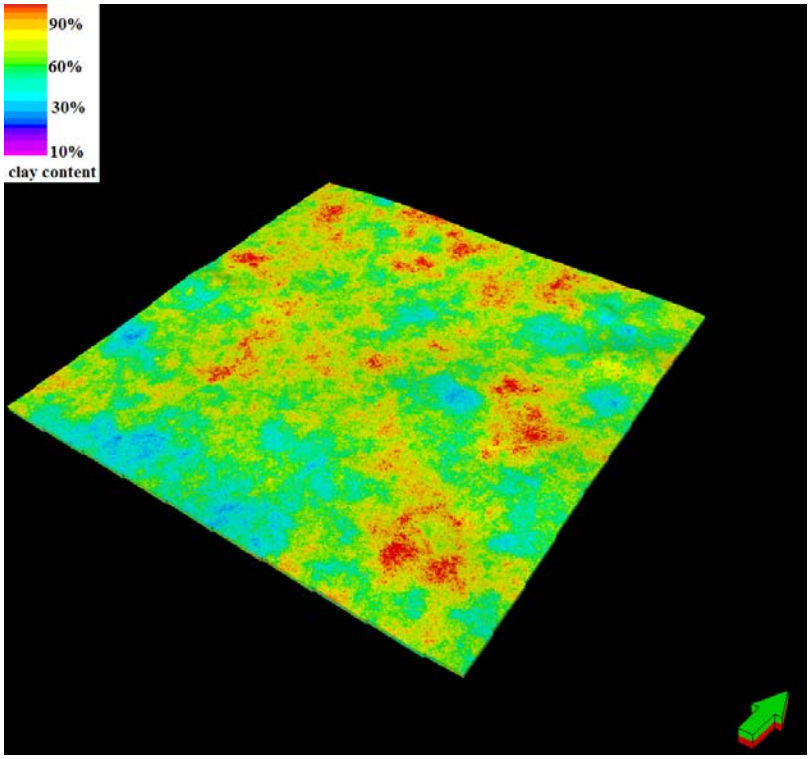

Figure 51. Clay contents of the overlayer, 30.5 m (100 ft) above the Harmon coal seam, Dunn site (10 times vertical exaggeration, the green arrow to the north).

3.4.2 Hydrogeological Conditions

The selected lignite-bearing formation in the Dunn site coincides with the Lower Tertiary Aquifer. This confined aquifer consists of sandstone beds, interbedded with shale, mudstone, siltstone, lignite, and limestone. It is one of the five major aquifers in the Northern Great Plains Aquifer System [52]. The Lower Tertiary Aquifer is not highly permeable, but is an important source for water supply due to its large quantity [52]. According to the description in a USGS report, water recharges into the aquifer from outcrops at high altitude, and discharges from the aquifer into major streams, such as the Missouri River. From the Ground-water Resource of Dunn County [53], aquifers in the Tongue River Member are also recharged by leakage from aquifers in the overlying Sentinel Butte Formation. Aquifers in the Tongue River Member include very fine- to fine-grained sandstone beds which range in thickness from about 3 m to 30 m, and frequently pinch out into siltstone or sandy clay. The water-head in the selected area is about 607 m above mean sea level, and the water general flow northeastward [53]. Available data are insufficient to determine if there is a hydraulic connection between the sandstone beds for this study; consequently each bed is considered as an isolated aquifer here.

Through interpretation and comparison of well logs (including lithology logs), five aquifers of relatively large size are recognized. One aquifer (AQ1) is located under the Harmon lignite bed, and some part of it is almost connected to the coal seam. The other four aquifers (AQ2, AQ3, AQ4 and AQ5) are above the coal seam at different distances. AQ2 is very close to the Harmon coal bed while others are separated by claystone layers.

Figure 52 shows the locations of the upper four aquifers related to the lignite bed. Figure 53 shows the cross-section view of A-A', and Figure 54 shows the cross-section view of B-B', both defined in Figure 43. There are some other aquifers within the overburden, but are either of small size and/or not close to the coal bed. So they are not considered as being important to the UCG operation. In general, considering the depth and thickness of the lignite seam (Figures 43 and 44), clay content of adjoining rocks (Figures 46 – 51), and locations of major aquifers (Figures 52 – 54), a suitable UCG site would be chosen in the central-north portion in the township 146N97W (Figure 33).

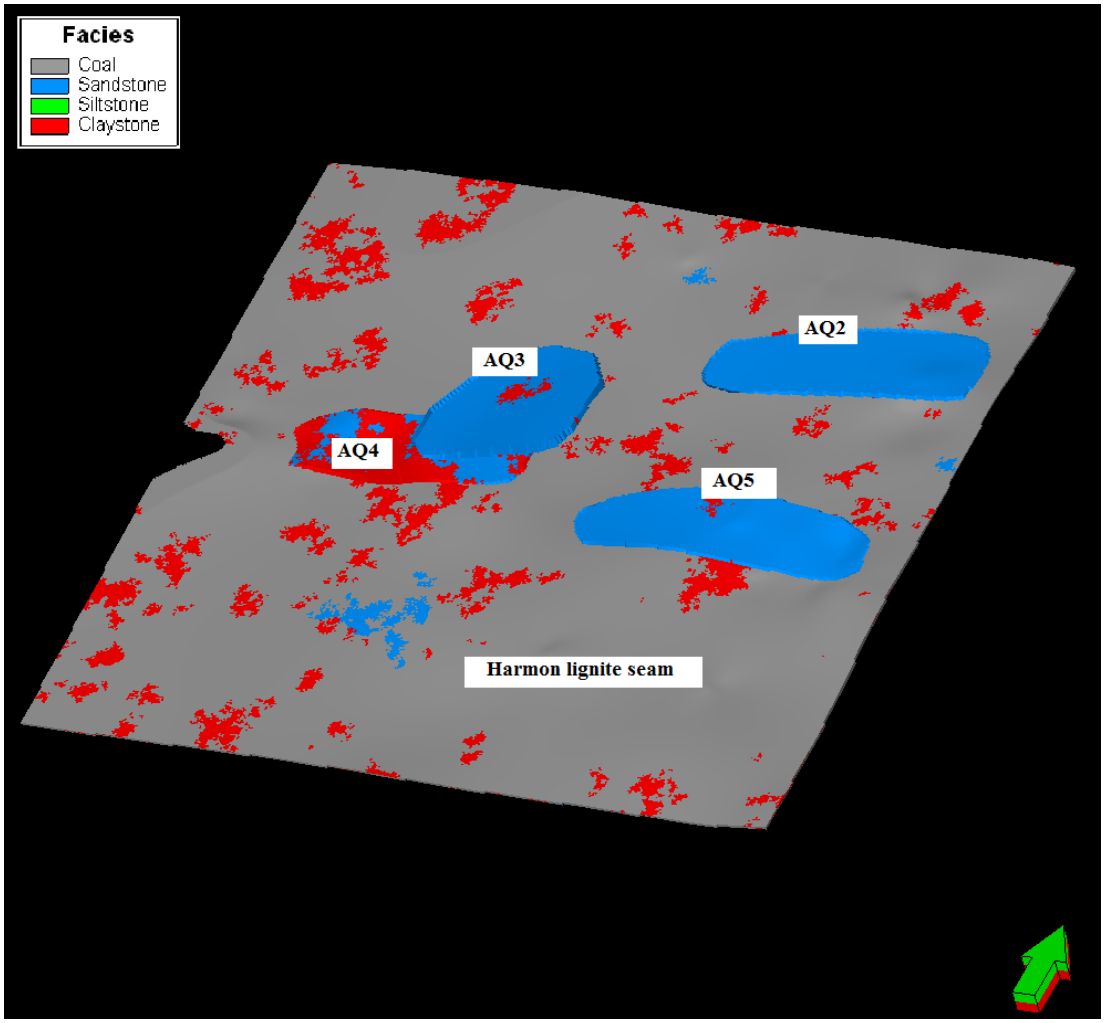

Figure 52. Aquifers above the Harmon lignite seam (10 times vertical exaggeration, the green arrow to the north).

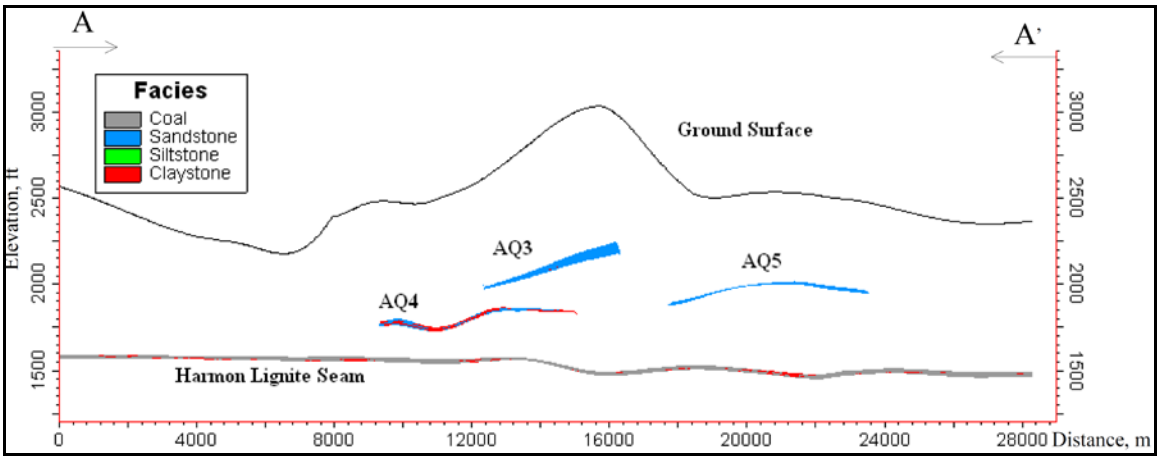

Figure 53. Cross-section view of A-A' defined in Figure 43 (10 times vertical exaggeration).

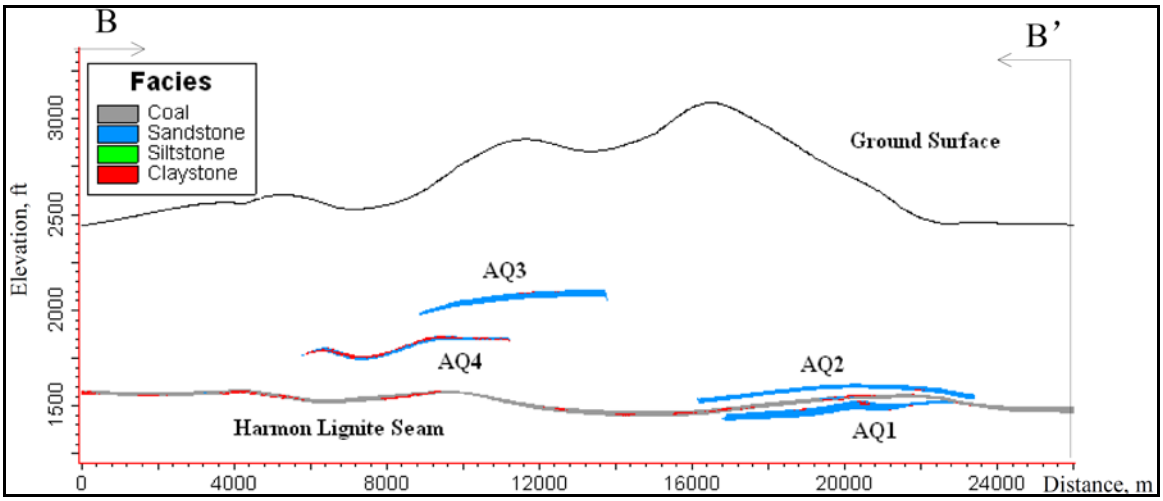

Figure 54. Cross-section view of B-B' defined in Figure 43 (10 times vertical exaggeration).

The North Dakota State Water Commission conducted laboratory tests and slug tests to measure the hydraulic conductivity of the sand bed aquifers in the Tongue River Formation. Results are shown in Table 3 [53]. Although none of the locations of these tests are inside the selected site, these values do provide a good reference. UCG sites need to avoid these aquifers, especially AQ1 and AQ2, which are very close to the lignite seam. However, it is possible that the claystone is naturally fractured, providing channels for the water to move through. This makes the Lower Tertiary a complex dual system.

More detailed site investigation is needed to find the right site.

Table 3. Hydraulic conductivity of the Tongue River Aquifer in Dunn County [53]

Sidewall-core analyses		
Location	Sampling depth (m)	Hydraulic conductivity (m/d)
141-096-29CCC	206	0.290
141-096-29CCC	272	0.027
142-092-09DAB	128	0.053
142-092-09DAB	184	0.003
148-097-33ABB	105	0.054
Slug tests		
Location	Screened interval (m)	Hydraulic conductivity (m/d)
143-091-19AAA1	199-204	0.122
144-097-26CBD1	213-219	0.274

3.5 CO_2 Market in the Selected Area

The North Dakota portion of the Williston basin holds significant resources for both petroleum and coal. Oil has been produced from Bakken, Red River, Lodgepole, Duperow, Three Forks, Madison group, and other formations. However, various challenges have blocked further exploration and production of these resources: some coal resources are too deep to be economically mined by conventional methods; the oil production rates are low in tight reservoirs like the Bakken; oil fields with low reservoir pressure after the primary phase of development need to be boosted by injecting fluids EOR process.

The research purpose aims here at combining the UCG with CO_2 EOR. Such a concept

enables the exploitation of deep coals, the utilization of generated CO_2 to boost oil production, and the sequestration of the CO_2.

The selected UCG site in Dunn County overlies the Little Knife Anticline, and is close to the Nesson Anticline and Billings Anticline, where thousands of oil and gas wells have been drilled. Some oil fields in this area are now at the secondary or tertiary production phase, which means a potentially big demand on CO_2 for EOR [54]. There are 604 oil wells in the selected 15 townships, 262 of which are currently producing oil. Major producing pools include Bakken, Duperow, Madison, and Red River (Table 4). So far, most of the cumulative production is contributed by the Madison Pool (Table 5).

Table 4. Oil wells in the proposed area, after [54]

Total	262	100%
Bakken wells	172	66%
Duperow wells	6	2%
Madison wells	79	30%
Red River wells	3	1%

Table 5. Cumulative oil production in the proposed area, after [54]

Total, bbl	54,510,254	100%
Bakken Pool, bbl	11,032,992	20%
Madison Pool, bbl	39,861,109	73%
other pools, bbl	3,616,153	7%

It can be concluded that the Bakken and Madison are the two main production pools. Although the Madison Pool shares about 73% of the cumulative production, most of its wells started in 1970s and 1980s, with total production time over 300 months (Figure 55).

On the other hand, most wells producing from the Bakken are fairly new and were drilled within the last 3 years, and are at the primary recovery stage (Figure 56).

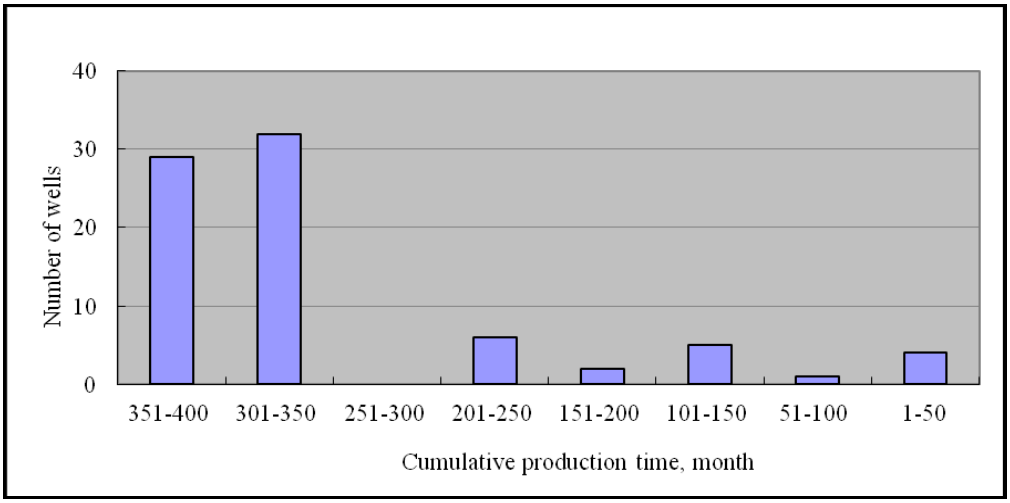

Figure 55. Cumulative production time of current oil wells in Madison Pool (data up to May 2010).

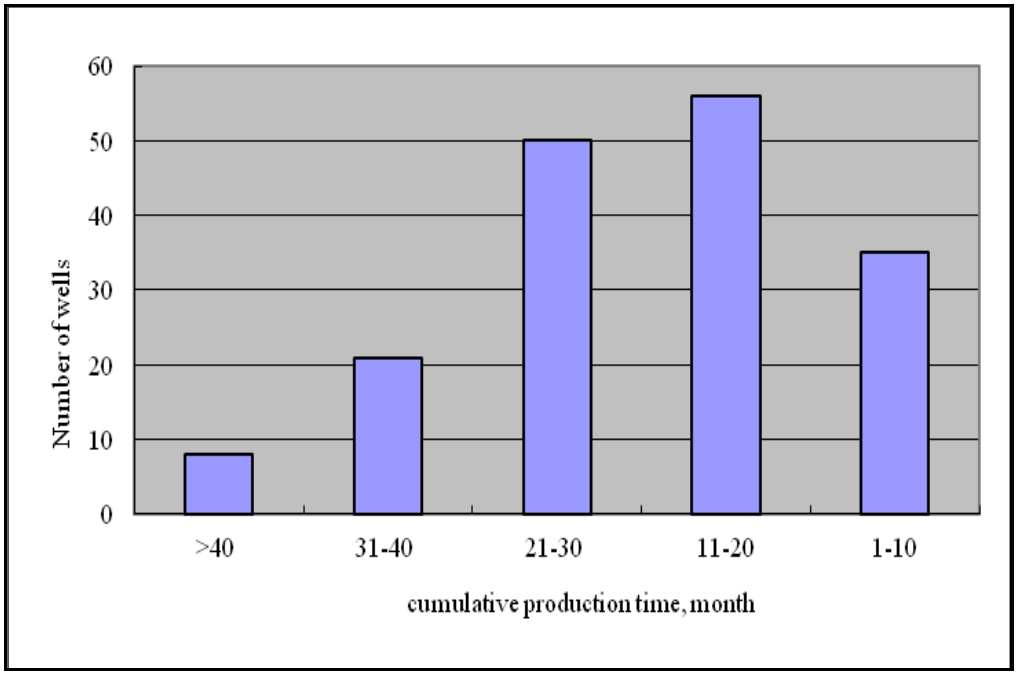

Figure 56. Cumulative production time of current oil wells in Bakken Pool (data up to May 2010).

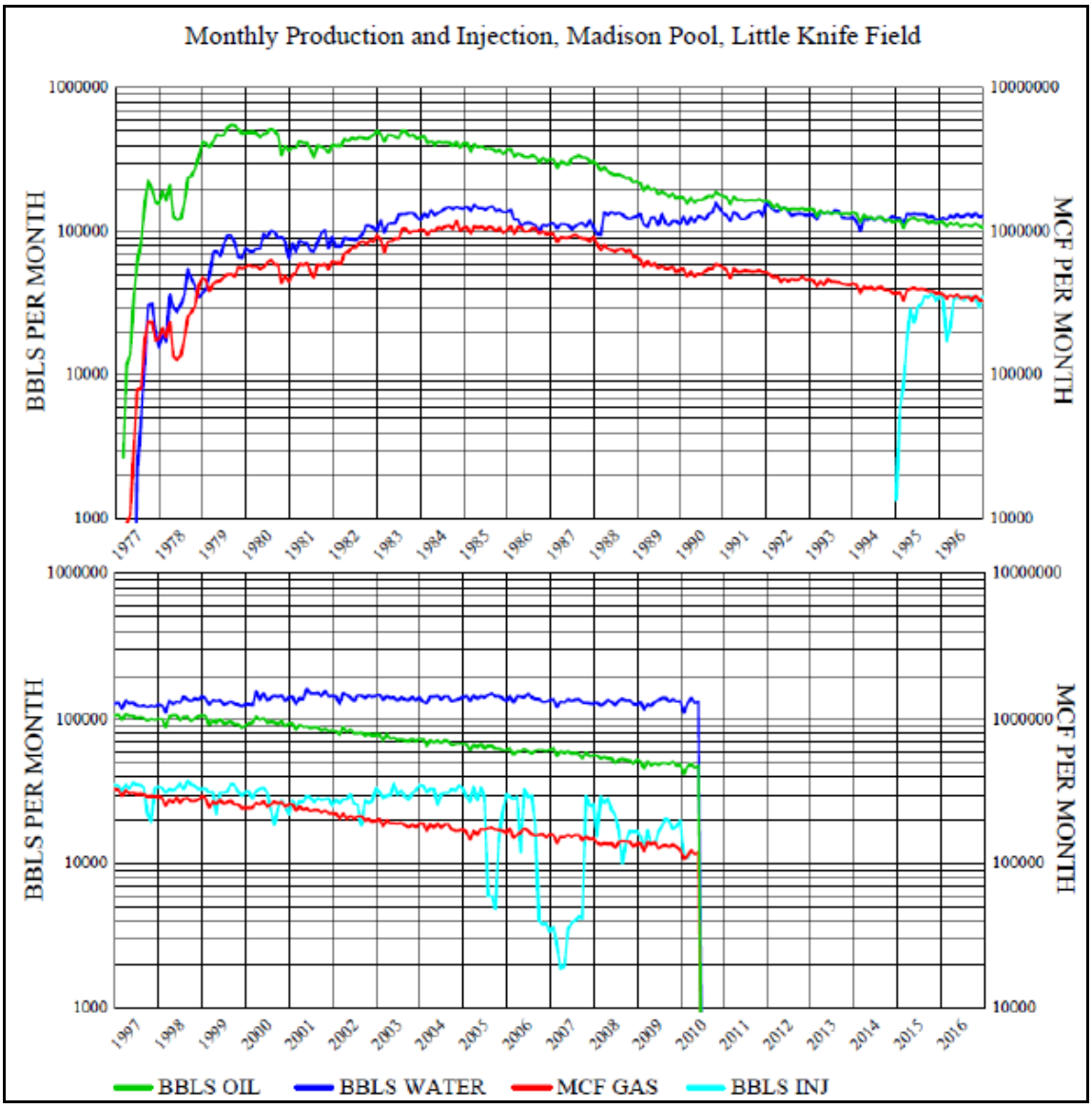

Figure 57. Monthly production and injection curves of the Madison Pool, Little Knife Field [54].

Within the 15 selected townships, Little Knife Field is the largest oil field, and is the only one that currently produces with water injection. This field has two water injection wells: Well #6205, and Well #12996. Well #6205 injected water from Dec-1994 to Jul-2008, with cumulative injected amount of 1,791,021 bbl, and is currently abandoned (shut-in > 12 months). Well #12996 injected water from Jan-1995 to Mar-2010, with cumulative injected amount of 2,908,138 bbl, and current is inactive (shut-in 3~12 months). Monthly

production and injection curves of the Little Knife Field are indicated in Figure 57. The Little Knife Field has an estimated original oil in place (OOIP) of 4,128,000 bbl, and its current cumulative production is 1, 336, 669 bbl.

Except the Little Knife field, there are some other fields in nearby townships which are in secondary and tertiary production stages (Table 6). More detailed information can be obtained at NDIC's website [54].

Table 6. Oil fields under fluid injection near to the proposed area

Oil field	Pool	Phases	Injected fluid	Estimated OOIP, bbl	Cumulative oil Production, bbl	Injection start date
Little Knife	Madison	2	water	4,128,000	1,336,669	12/7/1994
Blue Butte	Madison	3	water	92,700,000	34,569,042	11/1/1968
Big Stick	Madison	2	water	166,000,000	55,288,780	7/9/1988
Knutson	Madison	2	water	19,100,000	4,928,678	1/6/2001
Rough Rider	Madison	2	water	31,000,000	7,340,704	2/13/1997
T.R.	Madison	2	water	42,656,906	11,992,910	11/19/2004

The capacity of CO_2 sequestration through EOR in the Little Knife field can be estimated by using the equation provided by Smith et al. [41] as follows:

$$Q = OOIP \times 0.12 \times 8000 \quad (1)$$

where Q is the CO_2 remaining in the reservoir after the flooding process is complete, standard cubic feet (scf); OOIP is the original oil in place (bbl); 0.12 is the estimated

recovery factor of oil from CO_2 flood; and 8,000 is the amount of CO_2 required to produce 1 bbl of oil from CO_2 flooding, scf.

The estimated total OOIP of these oil fields listed in Table 6 is 355,584,906 bbl, under the standard oil and gas condition, one metric ton of CO_2 has a volume of 19,010 scf. Therefore, the CO_2 storage capacity is 17,956,944 tonnes.

CHAPTER IV

GEOMECHANICAL STUDY ON THE SURROUNDING ROCKS

4.1 Coupled Mechanisms in the UCG Process

During the gasification process, the coal-bearing formation is subject to a drastic alternation of its in situ stress field because of gasification-induced cavity excavation, high temperature (~1000^{o}C), and internal pressure. Stress concentration around gasification cavities can generate fractures, hence reducing the strength of the rock, and providing transport paths for contaminants. Alternation of stress and temperature would also lead to the change of transport and elastic properties of the coal-bearing formation.

UCG cavity evolution is a complex mechanism which involves a coupled thermal-hydrological-chemical-mechanical (THCM) process in the hosting coal and adjoining rock mass (caprock and bedrock). Conditions in the UCG cavity and combustion zone are strongly influenced by water influx. The total influx of water into the gasification zone determines the overall convective cooling effect on the cavity temperature. The water influx is dependent on the product permeability of coal and adjoining rock, and the difference between the hydrostatic pressure in the strata and the cavity pressure. In many cases, the coal-bearing formation is fractured, so permeability of

the coal seam and its adjoining rocks can be divided as matrix permeability and fracture (cleat for coal) permeability.

The modeling results of Buscheck et al. [55] showed that the gasification cavity temperature is relatively insensitive to coal matrix permeability, as well as coal matrix porosity. Thermal conductivity of the bedrock does not influence the cavity temperature either. The cavity temperature is moderately sensitive to the thermal conductivities of the caprock and coal. As expected, the cavity temperature is found to be strongly affected by fracture and cleat permeability. In general, the cavity temperature is most sensitive to the permeability of the coal cleat, followed by the fracture permeability of bedrock and caprock.

At elevated temperatures, coal and rocks demonstrate viscoelastic behavior [56], complicating the control of gasification process. Understanding formation properties that control these behaviors and being able to analyze these behaviors under different combinations of related parameters is vital. Behaviors of the rock and coal at high temperatures will be discussed in the last part of this chapter. Morris [57] listed several important factors of the natural conditions of the geological formations for UCG: thermal conductivity, coal chemistry, permeability, hydrostatic pressure, ratio of fracture surface area to bulk rock volume, geomechanical properties of fractures, and coal/rock matrix.

Based on an extensive literature review of the UCG process, a 5 by 5 interactive matrix is generated to represent the coupled THCM process in UCG (Figure 58). Five major

factors or effects are identified and put in the leading diagonal as primary variables: rock mass structure, in-situ stress, water flow, excavation, and thermal effects. These five main factors or effects would influence each other during the UCG process. The interactive mechanisms are interpreted in the off-diagonal terms. For example, the water flow (Term 33) will impact the rock mass structure (Term 11) by weathering processes caused by groundwater, which is represented by Term 31. The rock mass structure would also impact the water flow since the discontinuities in rock mass would dominate the transport behavior, as explained in Term 13. In some cases, two interactive mechanisms are involved. For example, the thermal effects (Term 55) would influence the water flow in two ways: the thermal stress may induce fractures, so the permeability is significantly increased; and the thermal-drive flow may also influence the amount and direction of the water flow. In general, this interactive matrix lists most of the coupled mechanisms involved in the UCG process, and is helpful in identifying needed work.

In a UCG plant of commercial scale, multiple gasification cavities are arrayed as a set of “parallel tunnels” with spacing between each other. The induced stress fields of these cavities interact with each other. Design of the cavity size and spacing (distance) is based on the physical properties of the rock and coal formations, and significantly influences the economics of the UCG plant. As mentioned above, the thermal and mechanical response of the rock formations during the UCG process is complex, presenting challenges in evaluating the site stability, recovery factors, contaminant propagation, product gas flow through the coal seam, and other issues. Therefore, detailed knowledge about the geomechanical, petrophysical, and hydrogeological characteristics of the

coal-bearing strata is necessary. Characterization of the coal-bearing formation is an important procedure in UCG site selection, and provides essential information for the gasification process design.

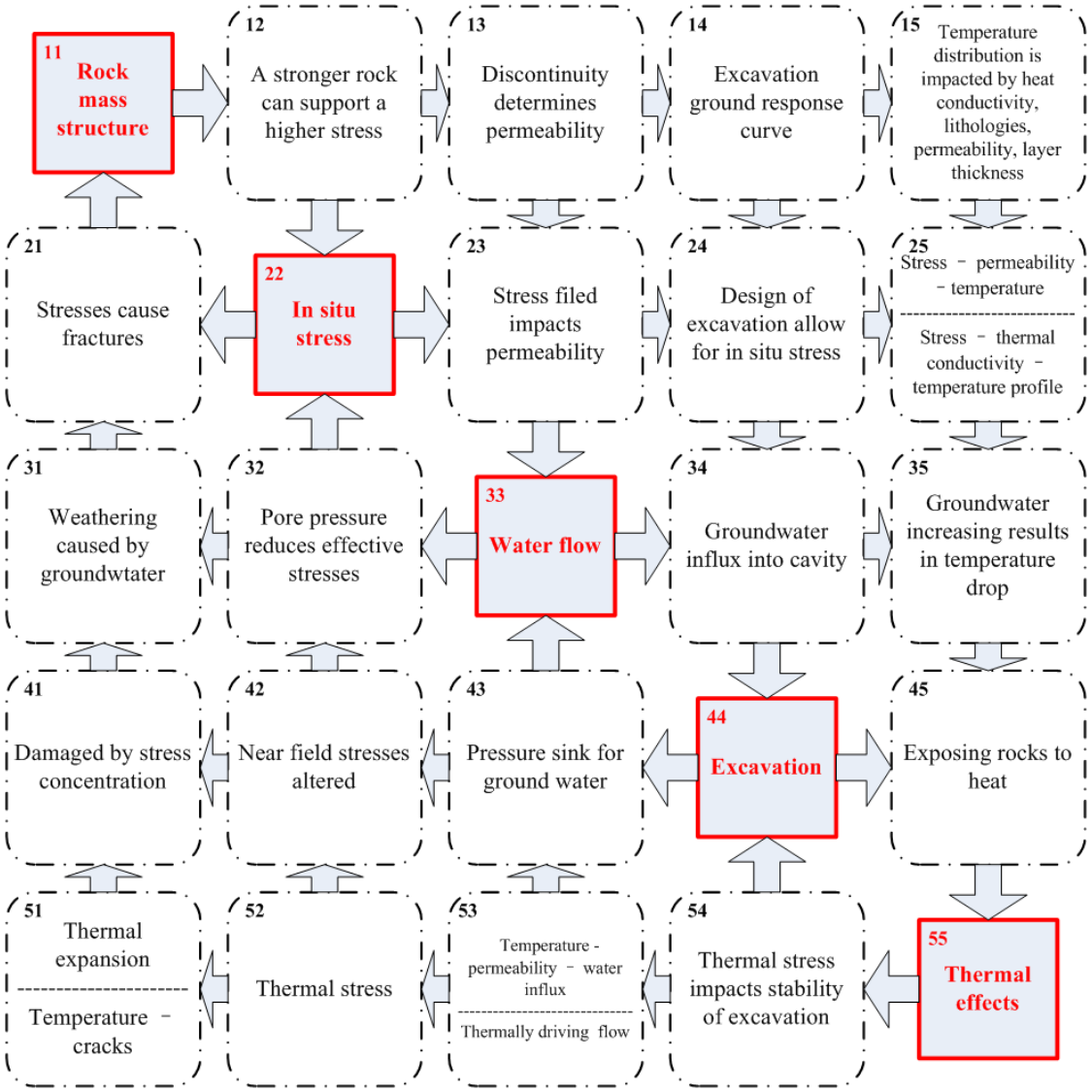

Figure 58. The coupled geomechanical, hydrological, thermal and engineering process.

The key properties of the coal-bearing formation which are needed to assess and model the UCG process are listed in Table 7. Functions of those properties are listed in Table 2 in Chapter III.

Table 7. Related properties in the coupled process

Parameters to be obtained	
Strength	Tensile, uni-axial, tri-axial, etc.
Elasticity	Young's modulus, Poisson's ratio
Thermoelasticity	Thermal expansion coefficient, heat conductivity, heat convection coefficient, heat capacity
Poroelasticity	Biot's coefficient
Petrophysics	Porosity, permeability (conductivity), rock density, fluid PVT
Formation	Hydrostatic pressure, facies distribution, clay content, in-situ stress, structure of formation

4.2 Analogue to Tunneling and Longwall Mining

The temperature in the gasification cavity can reach as high as 1000^{o}C during the gasification process [31]. The gasification process is usually conducted at a pressure slightly lower than the formation pressure of the groundwater to prevent escape of contaminants [46]. Therefore, the induced stresses during the UCG process can be attributed to three parts: the thermal stress induced by high temperature, the induced stress due to the internal pressure in the gasification cavity, and the induced stress due to opening of the burnt cavity. Related literature has provided estimates about stress distribution in the rock mass where UCG is operated [58-60].

The induced stress field in an UCG process can be analyzed by analogy to longwall mining and excavation of tunnels. By analogy to longwall mining, Younger [59] considered that in the strata overlying the voids (goaf) left by gasification, in the order

from bottom to top, there exist a “lower zone of net extension”, a “zone of net compression” (also termed “pressure arch”), and an “upper zone of net extension”, as shown in Figure 59. In the “pressure arch”, the beds are squeezed tighter together than was the case before gasification, and the compression usually reduces permeability. Therefore, the pressure arch functions like a hydraulic seal for the gasification to prevent contaminant transport, as well as to support the load from overburden. In the numerical modeling of Tan [60], similar conclusions are reached. Tan described that, in the burned-out region, the bottom of the roof rock and the top of the floor rock of the gasification zone suffer from tensile stresses; in contrast, the top of the roof rock and the bottom of the floor rock subject to compressive stresses. Comparing the results of Tan and Younger, it can be concluded that the tensile stress zone described by Tan corresponds to the zone of net extension defined by Younger, and the compressive stress zone corresponds to the “pressure arch”.

Applying the experience from tunneling engineering, a conclusion can be reached which is consistent to what has been described by Younger and Tan. After opening a tunnel, a plastic zone is formed around the opening due to stress redistribution and rock failure. The Mohr-Coulomb failure criterion is satisfied in this zone. Beyond the plastic zone, the rock mass remains in the elastic state, or in other words, the rock mass is in the elastic zone [61 – 63]. Rock mass in the plastic zone is loose and under poor constraint. The tangential stress reaches its peak value on the boundary of the plastic zone. In the elastic zone, the stresses gradually changes back to its original level, equal to stresses in undisturbed neighboring formations. If we consider the thermal effect, rocks in the plastic

zone would suffer tensile stress due to poor constraints of the neighboring rocks, and rocks in the elastic zone would suffer compressive stress because of constraints from neighboring rocks. As a comparison, the stress profile in the plastic zone is similar to that of Younger's "lower zone of net extension". The stress profile in the elastic zone is similar to that of the pressure arch.

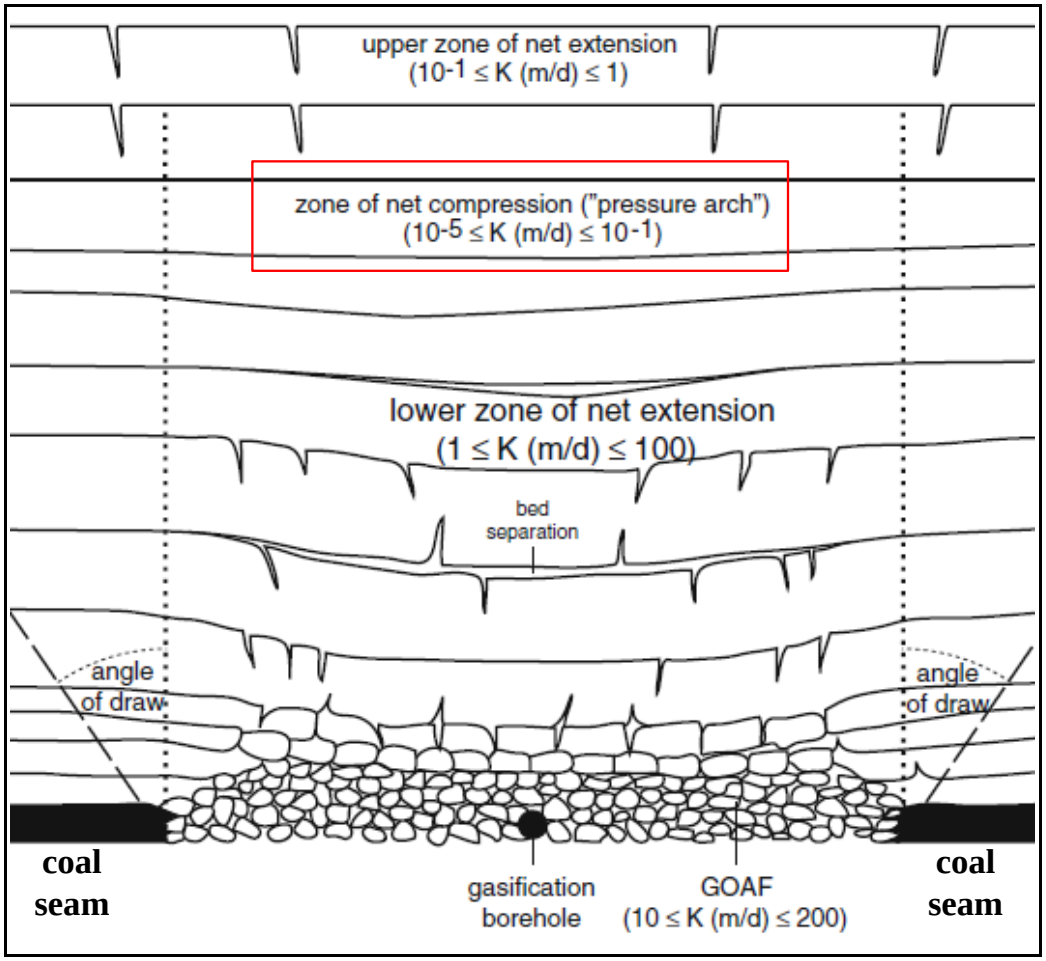

Figure 59. Schematic cross-section view of the strata over the void left by gasification, after [59].

Therefore, if it is assumed that the gasification cavity is a cylinder, and its cross section can be approximated as a circle, and the original in-situ stress is hydrostatic, the induced stress profile during UCG process would be axisymmetric. A failure zone (plastic zone)

would form immediately around the cavity. Out of the plastic boundary, the rock mass remains in elastic state, and a pressure arch forms just closely around the plastic zone. Due to the pressure difference inside and outside of the cavity, groundwater may be drawn into the cavity along the radial direction. A schematic stress profile in the overburden formation is shown in Figure 60. The transport property, such as permeability, is changed due to the alternation of the in-situ stress. Since the pressure arch plays an important role in the UCG process in terms of preventing contamination and sustaining the structural stability, it is very important to understand the behavior of rock masses under such stress conditions. The experiments presented in Section 4.3 describe the laboratory work simulating the stress conditions in the pressure arch, and measuring the elastic and transport properties.

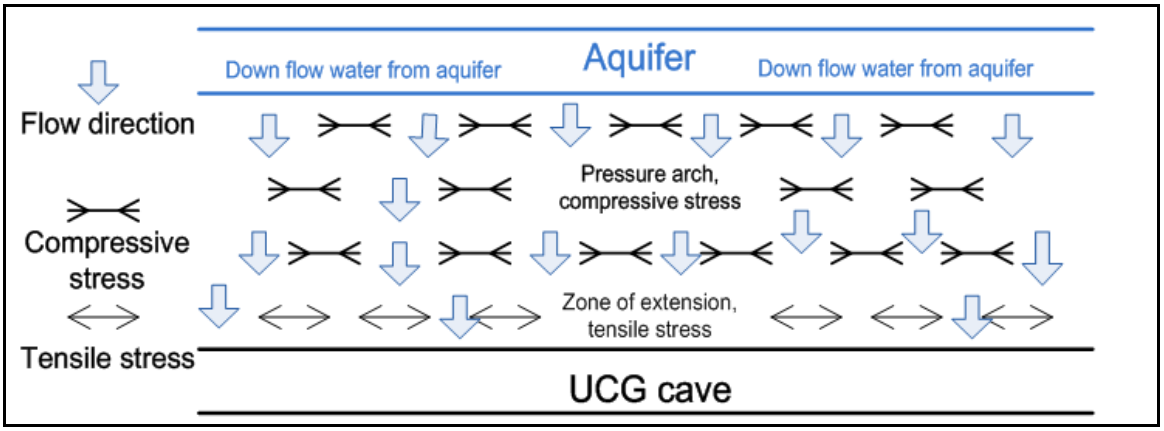

Figure 60. Stress and flow profile in the overburden of UCG cavity.

4.3 Geomechanical Testing

Rock samples from outcrops of the Harmon coal zone were collected and a laboratory geomechanical study was carried out to investigate the mechanical and fluid transport

properties of the surrounding rocks. Some interesting phenomena were observed. These results and observations can provide useful information on the assessment and design of UCG projects in the target coal-bearing formation.

4.3.1 Sample and Test Equipment

The rocks used in this study were collected from the outcrop of the Harmon bed, Fort Union formation located in the abandoned Gascoyne mine, Bowman County, North Dakota [36]. Measured properties include uniaxial compression strength, triaxial strength, permeability, porosity, Young's Modulus, and Poisson's ratio. An in-house developed triaxial fluid-rock interactive dynamics system and an MTS 816 uniaxial test system were used to measure these properties.

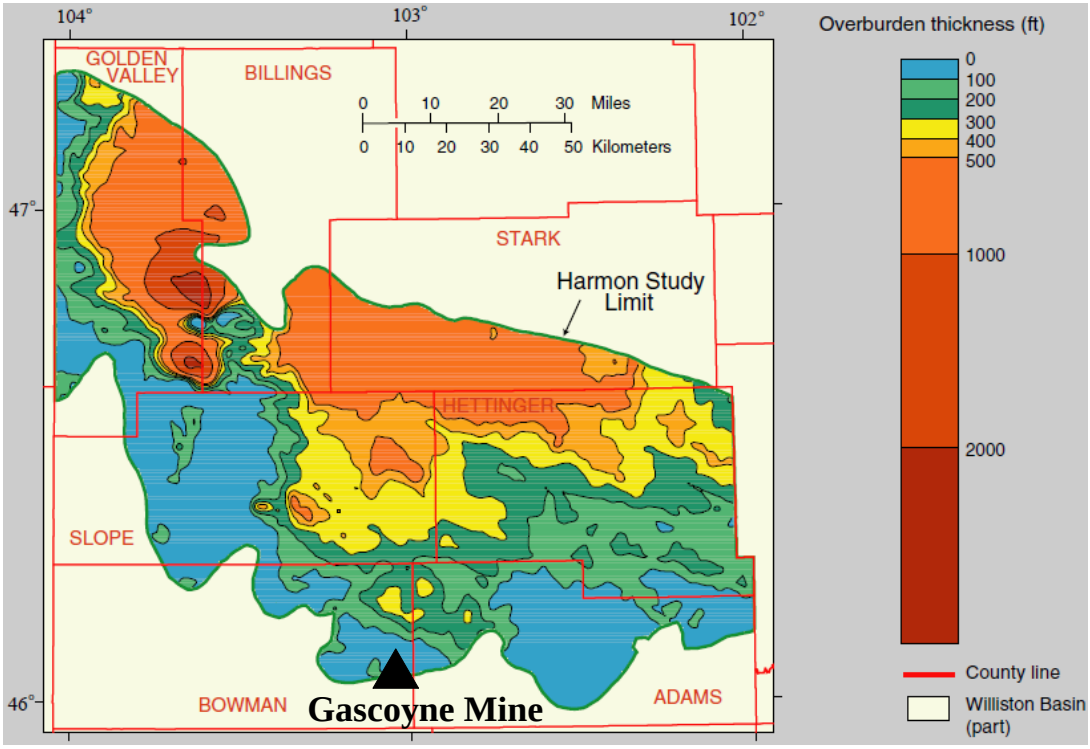

Figure 61. Location of the Gascoyne mine, after [36].

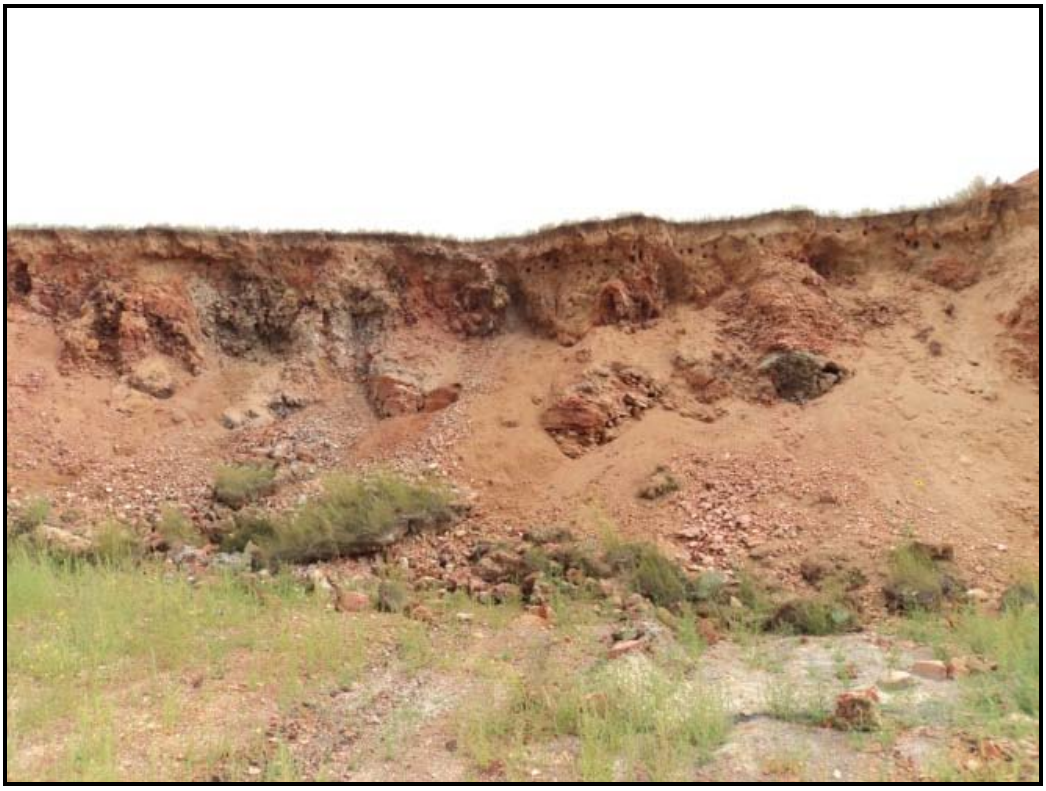

Figure 62. The outcrop where the rock samples were collected.

According to literature, the overburden of the coal seam is mainly claystone, interbedded with sandstone and mudstone [36, 37, and 64]. The only known Harmon coal outcrops are along the valley walls of the Little Missouri River, southwestern North Dakota. The Gascoyne mine was the only coal mine of the Harmon lignite, and it was active for much of the 20th century. The most active period for the mine occurred between 1975 and 1995, when about 2.3 million tonnes of lignite were produced per year, primarily for the Big Stone Power Plant. The mine began to reduce production in 1995, and was shut down completely in 1997. The rocks collected from the Gascoyne mine were identified as claystone. The rocks have a very fine-grained texture. Plug specimens were taken in the direction of vertical, parallel and 45^{o} to the beddings, respectively. Plugs were prepared that were 25.4 millimeter (mm) in diameter and 50.8 mm in length. Twenty two

specimens in total were used in the test. Before the test, the porosity of the specimens was measured by Boyle's law, using an UND in-house developed system. The measurement results show the average porosity was 33.7%. The average dry bulk density was 1730 kg/m^3. The porosity test system is shown in Figure 63.

The in-house developed triaxial fluid-rock interactive dynamics system was used to carry out the permeability and triaxial compression test [65]. Set up of this system is shown in Figure 64. The specimen was put in a high pressure steel core holder. Three independently-operated pumps were connected to the core holder to provide radial pressure, axial pressure, and pore pressure, respectively. Distillated water was used as the pressurizing media. During the test, the pressure and fluid volume changes in the pump cylinder were recorded by the monitoring system.

Figure. 63. The UND-in-house developed porosity test system.

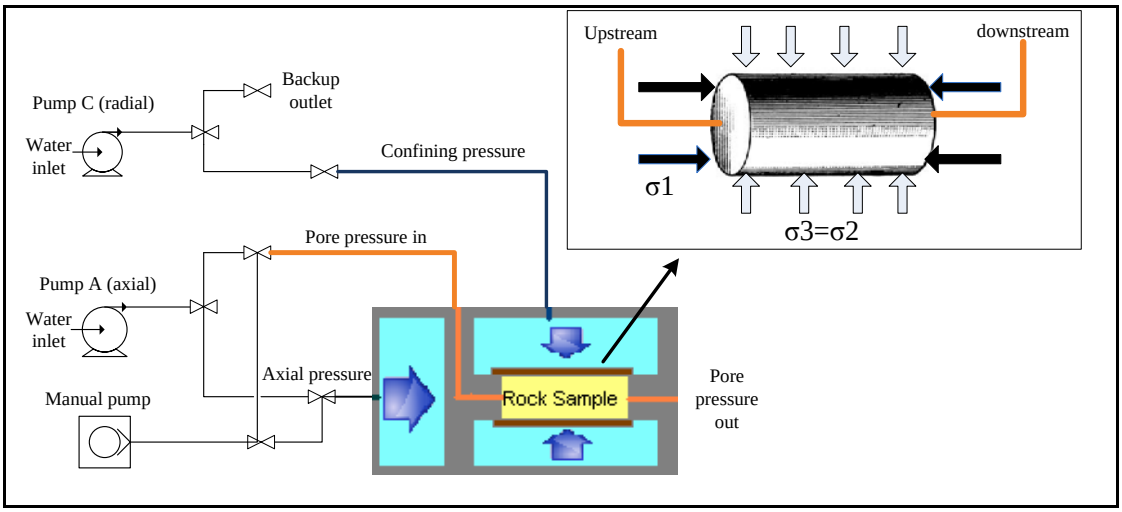

Figure 64. Set up of triaxial fluid-rock interactive dynamics system.

The 816 system, Figure 65, is a uniaxial compression test system developed by the MTS Company [66]. The system consists of a load frame assembly of high-stiffness, a servo-hydraulic performance package, digital control and monitoring packages. The system can perform laboratory experiments on materials ranging from soft sandstone to high strength reinforced concrete and high strength brittle rock. Young's Modulus and Poisson's' ratio can be measured during the uniaxial compression.

Figure 65. The MTS 816 test system [66].

4.3.2 Permeability Test

In the permeability test, the inlet pore pressure was kept constant, and the outlet pore pressure was kept at one atmospheric pressure. Thus the pressure difference along the specimen was kept constant. As the confining pressure and axial pressure were changed, alternation of the injection flow rate was recorded. The permeability was calculated using Darcy's law [67]; and results under different stress conditions were compared:

$$K = -\frac{QL}{A\Delta h} \tag{2}$$

$$k_i = \frac{K\mu}{\rho g} \tag{3}$$

where K is the hydraulic conductivity, Q is the flow rate, L is the length of the specimen, A is the cross-sectional area of the specimen, Δh is the hydraulic head drop along the specimen, k_i is the intrinsic permeability, ρ is the fluid density, μ is the viscosity, and g is the acceleration of gravity.

The measured values of the permeability under different stress conditions are summarized in Table 8. To present the data in a better form, the measured data were averaged for the value of each combination of axial stress and confining stress. Three groups of data are listed. It can be seen that the claystone has a low permeability, at the range of 0.4 to 3.1 mD. The average permeability of sandstones in the aquifers can be estimated by averaging the values listed in Table 3, Chapter III. From the table, the average hydraulic conductivity is 0.118 m/d, which means an intrinsic permeability of 124.5 mD. Therefore, the tested specimens have relatively low permeabilities and should limit contaminant propagation for the cavity.

Table 8. Measured permeability of claystone specimens

Axial stress, (MPa)	Confining stress, MPa	Permeability, mD
1.4	0.7	1.6
3.6	0.7	1.1
5.7	0.7	1.0
2.0	1.0	1.8
4.3	1.0	0.4
6.6	1.0	0.6
5.2	0.3	3.1
5.2	0.7	1.0
5.2	1.4	0.6

These averaged permeability values are also plotted in Figures 66 and 67 to indicate the trend how the permeability changes when the confining stress or axial stress is altered. In Figure 66, it can be seen that when the confining stress, which is perpendicular to the flow direction, increases, the permeability decreases. This observation is consistent with previous work of others [68, 69]. The explanation is that applying the confining pressure results in grain crushing and pore collapse, therefore leading to permanent loss of permeability. In Figure 66, the permeability dropped relatively fast when the confining pressure was first applied, and then dropped at a slower rate as the confining pressure reached a higher level.

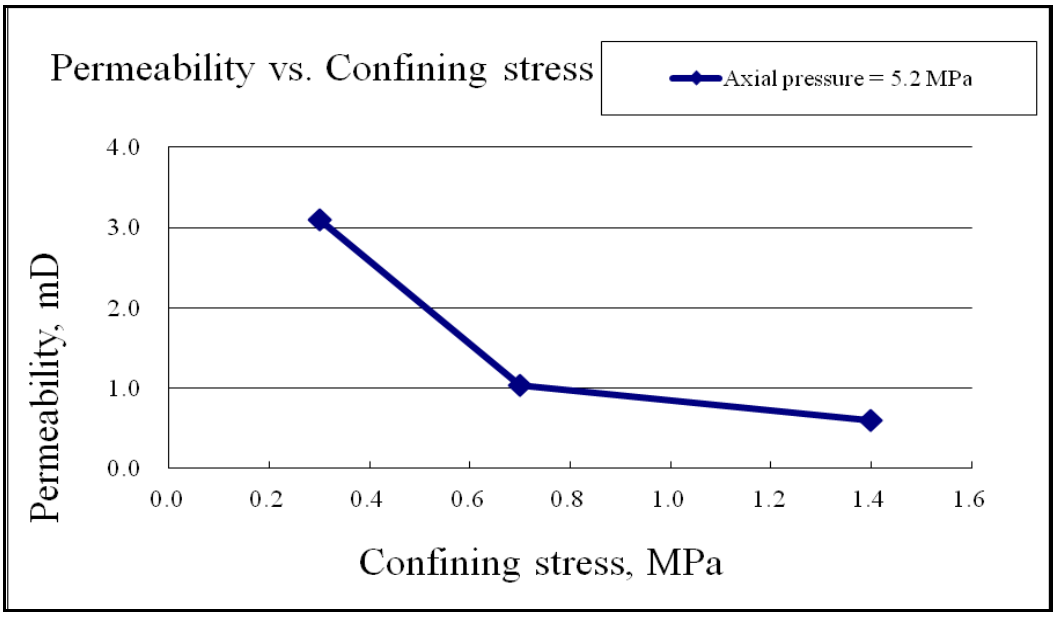

Figure. 66. Permeability changes with confining stress.

Figure 67 shows the change of permeability when the axial stress was changed. In the case that the confining pressure was kept at 0.7 MPa, the permeability decreased as the axial stress was applied. In the case that the confining pressure was kept at 1 MPa, the permeability dropped first, but increased later as the axial stress was raised. Observation of a permeability drop with increasing axial stress somewhat contradicts others' observations. For example, in Zhu's experiment [68], the permeability increased with the axial stress, and Zhu attributed this to the anisotropy in microcracking. Zhu mentioned that the microcracks in the specimen tend to be aligned parallel to the maximum principal stress (axial stress), and the preferentially aligned microcracks probably provided additional conduits for flow along this direction, hence increasing the permeability. However, in the test, the rock samples used are very soft claystone with relatively high porosities. At the initial stage, applying the axial stress could have significantly compressed the saturated specimen before any microcracks were generated. Compression would collapse the pore spaces, and reduce the permeability in all directions. After the

specimen was well compressed, microcracking may occur along the axial direction and increase the permeability, as in the case a confining pressure of 1.0 MPa. This may also explain that in the case of confining pressure at 0.7 MPa, the permeability dropped quickly at the initial stage of increasing axial stress, but dropped more slowly in the next stage.

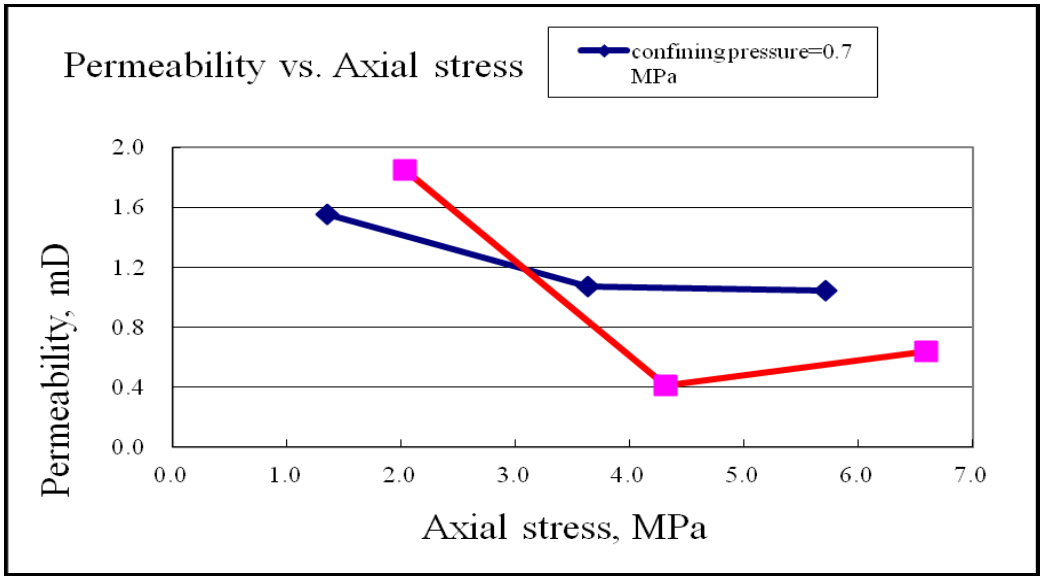

Figure 67. Permeability changes with axial stress

4.3.3 Strength Test

After the permeability test, the specimen was kept in the core holder for a triaxial compression test. The outlet valve of the pore fluid was shut off, so the pore pressure in the specimen was kept constant. The test started from the hydrostatic state. The radial stress was kept constant while the axial stress was increased by Pump A using a constant flow rate until the specimen failed. In this case, the effective stress, σ', applied on the specimen is defined by [70]:

$$\sigma' = \sigma - bp \tag{4}$$

where σ is the total stress, p is the pore pressure, and b is the Biot's poroelastic coefficient, and equal to 1 in this study, due to the high porosity and permeability.

In the uniaxial compression tests using the MTS 816 system, the axial stress was loaded at a constant strain rate, controlled by the servo motor. The axial stress, axial strain and circumferential strain were recorded by sensors and strain gauges. Therefore the Young's Modulus and Poisson's ratio can be calculated.

The maximum effective principal stress (σ_1') value obtained for different effective minimal principal stress (σ_3') values are summarized in Table 9. Due to the heterogeneity of the rock mass, the test results tend to be scattered. To present the data in a better form, the test results are averaged to give the value of each combination of σ_1' and σ_3', as shown in Figure 68.

Through regression analysis, the linear relationship between the effective principal stresses is:

$$\sigma_1' = 10.1\sigma_3' + 10.7 \tag{5}$$

As the Mohr-Coulomb criterion can be expressed in the (σ_1', σ_3'') plane as [61]:

$$\sigma_1' = \sigma_3' \frac{1+\sin\phi}{1-\sin\phi} + \frac{2c\cos\phi}{1-\sin\phi} \tag{6}$$

where c is the cohesion of the rock, and ϕ is the angle of internal friction of the rock.

Table 9. Measured strength of specimens

ID	σ_3' MPa	Average σ_1' MPa	Orientation to the beddings
11H015	0.0	9.4	horizontal
11H016	0.0	7.2	horizontal
11H017	0.0	13.5	horizontal
11H018	0.0	12.3	horizontal
11H019	0.0	11.1	horizontal
11H012	0.1	10.4	horizontal
11H002	0.2	8.0	horizontal
11H013	0.2	22.3	horizontal
11V004	0.5	30.6	vertical
11H008	0.5	15.0	horizontal
11H001	0.7	9.5	horizontal
11V003	0.8	15.4	vertical
11H003	0.8	9.6	horizontal
11H014	0.8	25.0	horizontal
11T001	0.8	15.8	45^o
11H004	1.2	15.0	horizontal
11T002	1.2	30.1	45^o
11H011	1.4	30.2	horizontal
11V002	1.5	20.9	vertical
11H005	1.5	18.7	horizontal
11T003	1.5	33.6	45^o

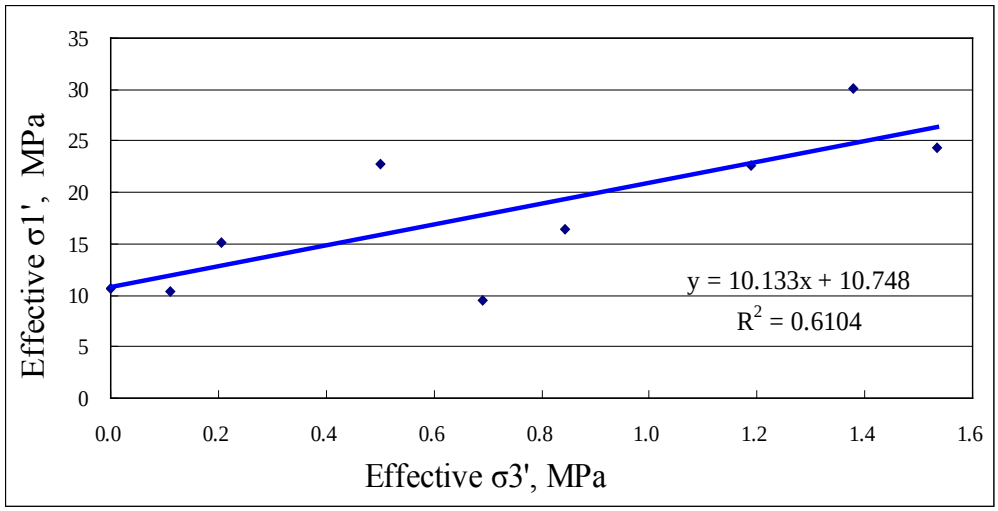

Figure 68. Effective σ_1' at failure and corresponding σ_3'.

Submitting Eq. (5) into Eq. (6), the angle of internal friction of the tested rock, ϕ, is 55.1^o. The cohesion, c, is 1.69 MPa. The results indicate the rock is relatively incompetent.

A behavior of the rock specimens observed during the test is worthy of mention. Since the specimens were used to conduct the permeability test first, specimens were already saturated with water in the triaxial compression test. In the test procedure, as the axial piston was loaded with external force, the axial pressure was observed to increase at an unusually slow rate, and the piston was able to move along the axial direction at a relatively fast rate, meaning the specimen was easy to compress like saturated soil. As mentioned above, the rocks have a high porosity (33.7%); this phenomenon indicates that, after being saturated with water, the rock became even softer, and demonstrated a quasi-creeping behavior. The relatively high compressibility of the specimen also buffered the applied load.

Figure 69 shows some typical cracks on the specimens after failure. Some cracks are about 30^o ~ 40^o to the maximum principal stress, similar to most other types of rock. However, some cracks are almost parallel to the maximum principal stress. This is probably because some micro-fractures exist in the rock, and these micro-fractures behave like weakness planes. So the specimen broke along these weakness planes.

Figure 69. Typical cracks on the specimens.

4.3.4 Elastic Properties

Four specimens were used in the uniaxial test. The rocks were tested dry. Figure 70 shows the stress-strain curves of Specimen 11H019 obtained from the uniaxial test. The

uniaxial strengths are listed in first five rows in Table 9. The measured Young's Modulus and Poisson's ratios are listed in Table 10.

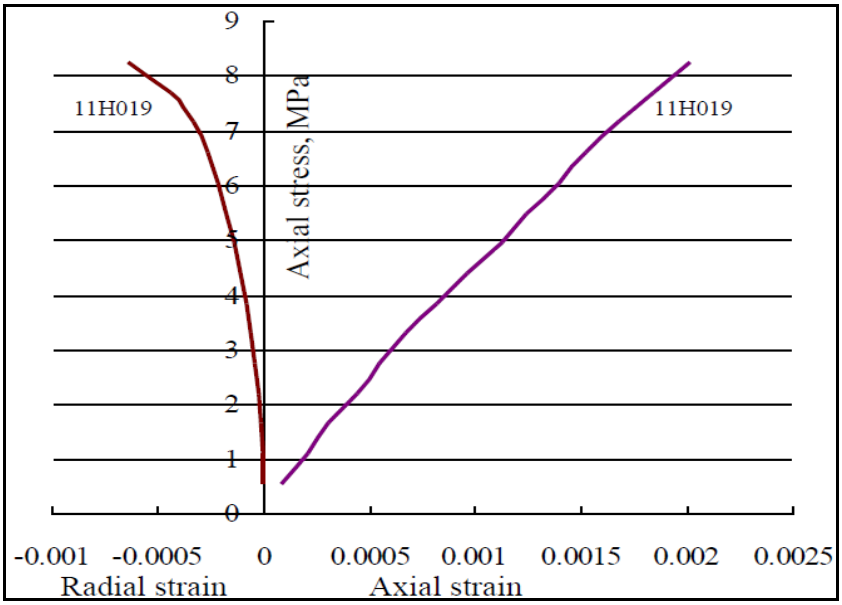

Figure 70. Stress and strain curve of Specimen 11H019.

Table 10. Young's Modulus and Poisson's ratio of tested specimens

ID	Young's modulus, GPa	Poisson's ratio
11H015	5.72	0.26
11H016	5.68	0.33
11H017	3.69	0.15
11H018	5.34	0.26
11H019	4.03	0.25

4.4 Interpretation of Test Results

The test results indicate that the rocks have a low strength, which would be considered as a disadvantage for the stability of the gasification cavities. During the UCG process,

significant induced stresses will be present around the cavity. The formation may easily fail due to the low cohesion value of the rock. Some of the rock samples are so soft that they behave like soil at failure; and this can be risky during the gasification process.

On the other hand, the rock specimens had low permeabilities during the tests. The measured permeability of the adjoining rocks is much lower than the sandstone in aquifers mentioned in the literature [53]. The permeability tends to reduce with both increasing stresses perpendicular and parallel to the flow direction. This means that the overburden rocks may function well as a hydraulic seal to the gasification zone, and prevent the escape of contaminants during gasification process.

During the UCG process, groundwater may be drawn into the gasification zone from adjacent aquifers. Therefore, dry rocks around the gasification zone may become saturated with water as the gasification process continues. In the tests, we observed the rocks showing compressibility and a quasi-creeping behavior after being saturated with water; and the specimens were able to buffer the load. How such phenomena would affect the gasification process needs further investigation.

During the gasification process, properties of remaining fresh coal and surrounding rocks can change due to the effects of high temperature. Change of strength, permeability and other elastic properties of the coal and rocks would impact the response of the formation during UCG process. Due to the limitation of the laboratory equipment at this moment, the specimens were not tested at elevated temperatures. A literature review about

behaviors of coals and rock at high temperatures is presented at the following section.

The overburden of the Harmon coal zone is described as mainly claystone, interbedded with sandstone and mudstone [36]. Only claystone samples were collected from the outcrop and used in this study. These samples are weathered at different degrees, and the properties would be somewhat different to those underground. While this study obtained the preliminary results and developed experimental methods, it is strongly suggested tests on claystone and other type of rocks from underground formations be conducted to compare the results, as well as to provide more reliable information to future UCG assessment work.

4.5 Rock Behavior at High Temperatures

Due to the limitations of our laboratory facility, geomechanical tests of the rock specimen at high temperatures have not been conducted. Instead, a literature study was conducted to investigate the rock and coal behavior at elevated temperatures, and its impact to UCG structural stability.

According to Shoemaker et al. [56], there is evidence that, at elevated temperatures, coal and rock are viscoelastic materials. Brewer [71] confirmed that, when bituminous coal is heated under appropriate conditions, it may exhibit plastic, viscous, or elastic flow, and often combinations of all three. Macrae and Mitchell [72] reported that the ultimate failure stress and deformation of coal were notably time dependent. At room temperature, failure occurred after a high stress had been maintained on the specimen for an extended

period of time. Sanda and Honda [73] have demonstrated the compressive creep characteristics of coal in a limited temperature range (200 to 370^{o}C).

In examining structural property effects on subsidence, roof collapse, and various modes of failure, specific types of data are required. The basic properties required are directional (for coal) and temperature-dependent stress-strain relations and failure stresses in compression and shear.

Through the viscoelastic experiments, it was found that the orientation of the constant applied load (normal or parallel to the bedding plane) has an influence on the creep compliance in coal. This directional effect is apparently due to increased resistance to deformation in the face and butt cleat directions caused by the interlayering of the organic and inorganic materials when the loading is parallel to the bedding planes. The test data represent a large variety of linear and nonlinear rheological properties, including plasticity and creep, depending upon temperature.

Tian et al. [60] concluded that, in general, permeability of rock increases, and strength decreases, as temperature rises. In Tian's experiment [60], sandstone, claystone, clayey sandstone, and sandy claystone were heated up to 1000^{o}C. It was observed that cracks were produced on the rock samples, especially claystone, due to the difference in thermal expansion properties of the rock, resulting an increase of permeability and a decrease of mechanical strength.

During the 1970s, the LLNL and Morgan Town Energy Center conducted a series of laboratory experiments and numerical modeling studies to investigate the behavior of coal and rocks at high temperatures during the UCG process. The basic research approach was to obtain the related properties of coal and rock at high temperatures through experiments, and the measured thermo-viscoelastic properties were applied in numerical modeling to solve the thermo-viscoelastic stress response problems.

Advani et al. [58] and Lin [74] described that the thermoviscoelastic characteristics of Pittsburgh coal demonstrate softening at about 340^{o}C, the material properties near the cavity will show sharp boundary layer-type transitions resulting from the coke, softened layer and coal states near the surface. The effective permeability of the coal and coke with the intervening softened layer will be affected by the stress distribution around the cavity surface.

The coal specimen used in Lin's report [74] was Pittsburgh coal. Through experiments, the elastic moduli and shear moduli as functions of temperature were obtained. The creep compliance curves and temperature shift functions in compression and shear for corresponding normal and parallel planes were obtained by use of the time-temperature superposition principle. The creep compliance curve can be expressed by the four-parameter fluid model (Burger's model), in which the spring constants and dashpot coefficients are expressed as functions of temperature. By using the rock specimen from the adjoining rocks, an experimental study of the effect of temperature and stress on the creep of rocks was conducted. The creep equations of sandstone and shale for different

temperatures were obtained. The Young's moduli for temperatures ranging from room temperature to 370^{o}C were also obtained. These thermo-mechanical properties were then employed in a finite element model.

In the finite element (FE) model, the effects of layering, coke/softened layered regimes, and roof collapse were investigated. Both elastic and elasto-plastic FE models were employed to compute the stress profile around the cavity, fracture development, cavity length, roof convergence, surface displacements, and surface strains [74].

At elevated temperatures, the visco-elastic moduli of coal and the immediate rock overburden are considerably lower than that of room temperature. Computations of the associated thermo-viscoelastic boundary value problems indicated that the thermal stress, which depends on Young's modulus, is several orders smaller. The magnitudes of induced visco-elastic cavity hoop stresses are one order lower than the corresponding elastic value. However, the stress profiles have the same shape.

Compressive fracturing may occur not only around the cavity coke surface, but also around the coal surface, even with a softened layer existing between the coke layer and the coal. The corresponding magnitudes of the stresses in the softened coal layer are of the order of 200 kilopascal (kPa).

Along the axis of the gasification cavity, when the burning front moves to a critical distance from the injection borehole, partial closure of the cavity occurs. The

thermal-softening effect on the mechanical properties of the rock and coal near the cavity can largely increase the roof convergence so that an early roof collapse can be achieved, and the critical length of the cavity is shortened. With a shorter critical length, the volume of the gasified zone is reduced.

Heating of the cavity surface during gasification causes creep and drying of the immediate roof and induces extra compressive stresses around the cavity. The surface horizontal strain (subsidence profile) derived by a elasto-plastic model is less steep compared to that derived by the classical elastic model. The thermo-viscoelastic response of the shale overburden at elevated temperatures will increase the roof convergence and the corresponding surface subsidence and horizontal strains. Both computed roof convergence and surface subsidence from the elastic model were increased as the elasto-plastic model was employed in the finite element modeling.

CHAPTER V

CAVITY STABILITY AND MINING RECOVERY FACTOR

5.1 Concept of UCG Plant of Commercial Scale

UCG technology has been developed for several decades; however, there is currently no commercial scale UCG plant in operation anywhere in the world [9, 10]. Environmental concerns such as groundwater pollution and stability of the cavity (subsidence due to excavation) are the major obstacles to popularizing the UCG technology. Researchers and the industry have proposed the concept of a UCG plant at a large commercial scale, where coals are gasified in multiple underground gasification panels as shown in Figure 71 [58, 59]. These multiple gasification panels (cavities) are arrayed as a set of “parallel tunnels” in the coal seam. During the operation of a UCG plant, these gasification panels will be developed one after another, to ensure continuous production of the syngas. Each gasification cavity can have its own injection and production wells, or shares common wells, as shown in Figure 71. The gas transmission pipelines and other maintenance facilities on the surface are shared by the cavities. The size of these gasification cavities, spacing, in-situ stress and properties of the coal-bearing formation together determine the stability of the altered formation structure, as well as how much coal can be recovered by the plant.

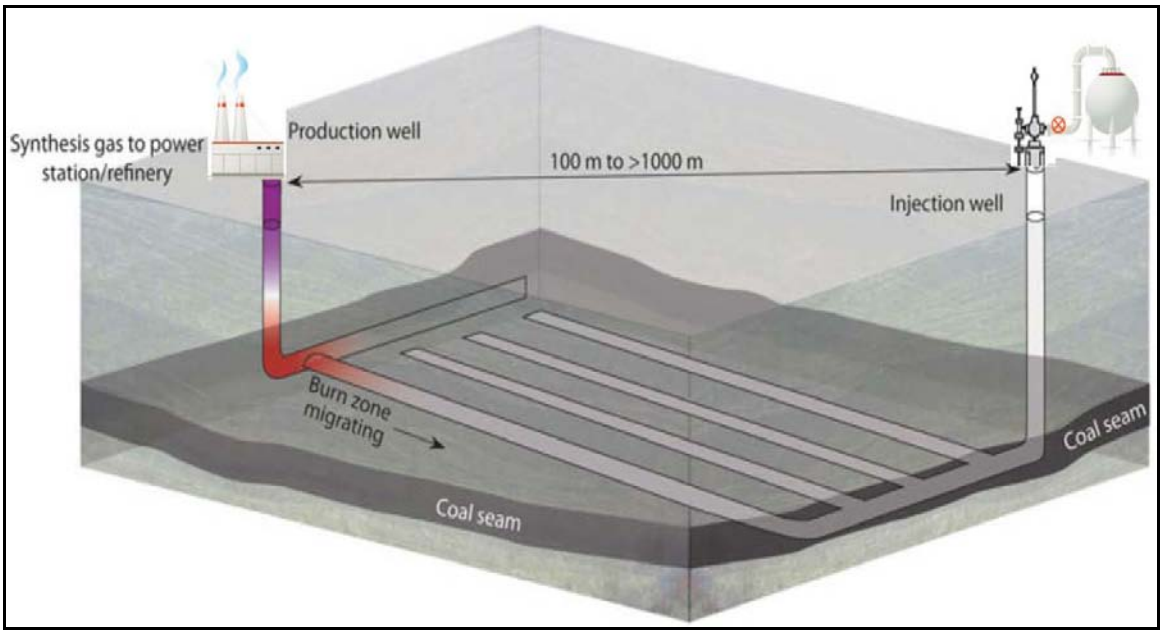

Figure 71. Concept of a commercial scale UCG plant with multiple gasification cavities, after [58, 59].

Since the UCG technology can be applied to coal seams which are too deep and/or too thin to be reached by conventional mining methods, it is estimated that UCG could increase recoverable coal reserves in the USA by three times [75].

The recovery efficiency of a UCG plant is defined as the ratio of the energy contained in the produced syngas to the energy contained in the in-situ target coal seam. The recovery efficiency is a product of two parts: the mining recovery factor and the chemical conversion efficiency. The mining recovery factor refers to the volumetric percentage of the target coal seam that can be recovered. The chemical conversion efficiency is the efficiency of converting the “mined” coal to syngas. The chemical conversion efficiency is equivalent to the cold gas efficiency of the surface gasifiers, which is between 70% and 90% in most cases. On the other hand, the actual mining recovery factor to the coal seam by a commercial UCG plant is determined by the allowable size of the gasification

cavities and reasonable spacing between the cavities. These parameters have to be determined by the in-situ conditions of the coal-bearing formation.

In light of the concerns of rock failure, this chapter presents an analytical study to estimate the cavity size and mining recovery factor in a conceptual UCG plant based on the analysis to the induced stresses. Experiences from tunneling in civil engineering and wellbore stability in petroleum engineering are cited. Although some simplifications and assumptions are made in this study, the methodology and results provide a convenient and fast approach to assess the recovery efficiency and the economics of a UCG plant once the fundamental properties of the target coal seam are known.

5.2 Assumptions of the Gasification Cavities

An imaginary commercial scale UCG plant is developed on a coal seam as shown in Figure 71. In the commercial production process, coals are gasified in a series of panels one by one. In this study, the following simplifications and assumptions are made to the cavities:

a) A cavity is a long cylinder lying horizontally and all the cavities have the same geometry;
b) The cross-section of the cavity can be approximated as a circle;
c) The length of the cylinder is much larger than its diameter, so plain strain is assumed;
d) The coal seam is horizontal;
e) All the cavities in the coal seam are at the same level, with the same spacing. Therefore, the centers of all the circles are on the horizontal axis; and

f) We assume a steady state gasification process.

During the gasification process, the temperature in the cavity can increase to 1000^{o}C. Due to the constraint of neighboring formations, the rock-mass will subjected to thermal stress. The gasification pressure is usually kept slightly below the hydrostatic head of the groundwater so as to keep the groundwater influx to the gasifier and prevent the escape of contaminants [46]. Therefore, during the gasification process, we consider the induced stresses consist of three parts:

a) The thermal stress induced by high temperature;

b) The induced stress due to the internal pressure in the gasification cavity; and

c) The induced stress due to opening of the cavity.

As mentioned above, the gasification cavities will be developed one by one during the production process. The remaining part of the coal seam between two cavities functions as a “pillar” to support the load from the overburden.

As the gasification cavities are developed one after another, different stress fields will be formed at different development stages. To simplify the development stages for an UCG plant, we classify the entire developmental procedure into three main phases. Figures 72 to 74 show the cross sections and description of the gasification area in these three different phases.

Phase 1 is the development of the first cavity. In this phase, there is only one cavity (Cavity A, Figure 72) in the coal seam. Stresses are altered based on the natural in-situ stress field. Induced stresses only result from Cavity A. After Cavity A is finished with gasification in this phase, it cools down and is filled with groundwater, and the stress field in the formation is disturbed from the original state.

Phase 2 is the development of the next cavity (Cavity B in Figure 73) based on the disturbed stress field. The stress field in which Cavity B is developed is determined by the last phase but the induced stresses result from Cavity B. Phase 2 also applies to the development of other subsequent cavities after Cavity B.

Phase 3 is post gasification (Figure 74). At this phase, all the cavities have been gasified and cool down. Groundwater fills the cavities, and it is assumed that there is no induced thermal stress in the formation.

The induced stress field and the plastic zone around the cavity are different in each of the above phases. Since the thermal stress is released in the post gasification phase, we assume that if the rock mass is stable in Phases 1 and 2, it will not fail in Phase 3. Thus, in the analytical study, we only calculate the stress field and radius of the plastic zone in Phases 1 and 2 in the following sections.

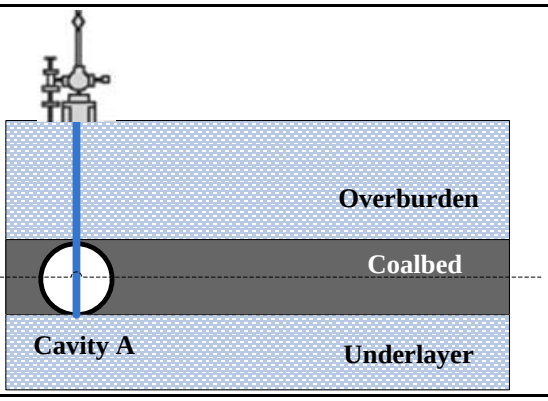

PHASE 1	First cavity under gasification
Description	Cavity A is in the gasification process
Induced Stress	Thermal stress
	Induced stress due to internal pressure in the cavity
	Induced stress due to evolution of the opening

Figure 72. Phase I of the UCG plant development.

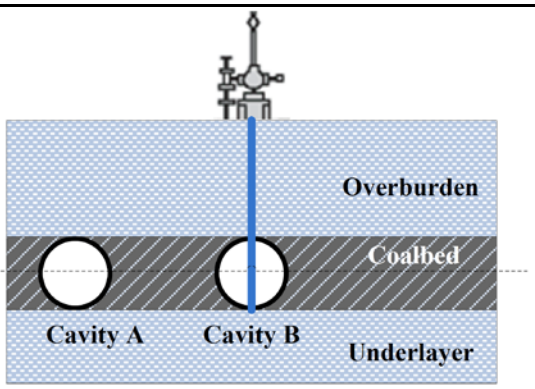

PHASE 2	Next cavity under gasification
Description	Cavity A is finished with gasification and Cavity B is under gasification
	Cavity A is cooled down and filled with groundwater equal to hydrostatic head
	In situ stress field is altered by Cavity A before gasifying Cavity B
Induced Stress	Thermal stress due to Cavity B
	Induced stress due to internal pressure in Cavity B
	Induced stress due to evolution of Cavities A and B

Figure 73. Phase II of the UCG plant development.

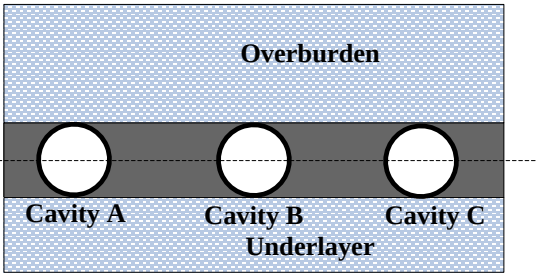

PHASE 3	Post gasification
Description	Cavities are finished with gasification
	Cavities are cooled down and filled with groundwater equal to hydrostatic head
Induced stress	Induced stress due to internal pressure in the cavities
	In situ stress field is altered due to opening of the cavities

Figure 74. Phase III of the UCG plant development.

5.3 Governing Equations

The surrounding rocks and coals are both assumed to be elastic material and follow the Mohr-Coulomb failure criterion.

5.3.1 Thermal Stress

Assuming the gasification is a steady state process, the temperature in the underground gasifier is kept as T_i, and at infinite distance, the temperature in the formation drops back to the original formation temperature, T_∞. The temperature profile, $T_{(r)}$, around the reactor is axisymmetric, and is given by [76]:

$$T_{(r)} = C_1 + \frac{C_2}{r} \tag{7}$$

where r is the radius from the center of the cavity, C_1 and C_2 are constants.

If the radius of the cavity is R_a, applying the boundary conditions on the wall of the cavity and at infinite distance:

$$T_{(Ra)} = T_i \tag{8}$$

$$T_{(\infty)} = T_\infty \tag{9}$$

The temperature profile is given as:

$$T = T_\infty + \frac{(T_i - T_\infty)R_a}{r} \tag{10}$$

Since the temperature profile is axisymmetric around the cavity, the induced thermal stress is also axisymmetric. The radial term, σ_{rt}, and the tangential term, $\sigma_{\theta t}$, are given as [58, 77]:

$$\sigma_{rt} = \frac{aE}{r^2}\frac{1}{(1-\nu)}\left(\int_{R_a}^{r} rTdr\right) \tag{11}$$

$$\sigma_{\theta t} = -\frac{aE}{r^2}\frac{1}{(1-\nu)}\left(-Tr^2 + \int_{R_a}^{r} rTdr\right) \tag{12}$$

where α is the linear thermal expansion coefficient, E is the Young's modulus, and ν is the Poisson's ratio.

Submitting the temperature profile given by Eq. (10), and integrating the equation, the thermal stresses are presented as Eq. (13) and Eq. (14):

$$\sigma_{rt} = -\frac{aE}{r^2}\frac{1}{(1-\nu)}\left[\begin{array}{l}\frac{1}{2}T_\infty\left(r^2 - R_a^2\right)+ \\ (T_i - T_\infty)R_a(r - R_a)\end{array}\right] \tag{13}$$

$$\sigma_{\theta t} = \frac{aE}{r^2}\frac{1}{(1-\nu)}\left\{\begin{array}{l}-r^2\left[T_\infty + (T_i - T_\infty)R_a\frac{1}{r}\right]+ \\ \frac{1}{2}T_\infty\left(r^2 - R_a^2\right) \\ +(T_i - T_\infty)R_a(r - R_a)\end{array}\right\} \tag{14}$$

5.3.2 Stress Induced by Internal Pressure

During the gasification process, the internal pressure of the gasifier usually is kept slightly below the pressure of groundwater in the formation. There are two benefits in

applying such a gasification pressure: to control water influx to the gasification zone and to prevent contaminants escaping from the gasifier to aquifers. The induced stresses (σ_{ri} and $\sigma_{\theta i}$) due to internal pressure are also axisymmetric, and are already defined in petroleum wellbore stability studies [61, 77]:

$$\sigma_{r\,i} = p_w \frac{r^2}{R_a^2} \tag{15}$$

$$\sigma_{\theta\,i} = -p_w \frac{r^2}{R_a^2} \tag{16}$$

where p_w is the internal pressure of the gasification reactor.

5.3.3 Stresses Induced by Opening in Intact Rocks

After opening the cavity, a plastic zone is formed around the opening due to stress concentration and rock failure. Mohr-Coulomb failure criterion for intact rock is satisfied in this zone. Beyond the plastic zone, the rock-mass remains in the elastic state, or in other words, the rock-mass is in the elastic zone. If we only consider the induced stress due to excavation, the altered stress field (σ_{re}, $\sigma_{\theta e}$ and $\tau_{r\theta e}$) in the elastic zone is given by Kirsch's equation [61, 62]:

$$\sigma_{re} = \frac{1}{2} p_0 \left[(1+k)\left(1-\frac{R_a^2}{r^2}\right) - (1-k)\left(1-4\frac{R_a^2}{r^2}+3\frac{R_a^4}{r^4}\right)\cos 2\theta \right] \quad (17)$$

$$\sigma_{\theta e} = \frac{1}{2} p_0 \left[(1+k)\left(1+\frac{R_a^2}{r^2}\right) + (1-k)\left(1+3\frac{R_a^4}{r^4}\right)\cos 2\theta \right] \quad (18)$$

$$\tau_{r\theta e} = \frac{1}{2} p_0 \left[(1-k)\left(1+2\frac{R_a^2}{r^2}-3\frac{R_a^4}{r^4}\right)\sin 2\theta \right] \quad (19)$$

where θ is defined positive counterclockwise from the horizontal axis in the opening cross section, P_0 is the original in-situ stress in the vertical direction, and k is the ratio of original in situ horizontal stress to its vertical counterpart.

In this study, the induced stresses are calculated by summing the perturbation due to excavation, thermal effects and internal pressures. The rock mass in the plastic zone has already failed, so the plastic zone is considered unstable. In the design of a UCG plant, we are interested in knowing the radius of the plastic zone and the stress profile in the elastic zone. So we will be able to estimate the reasonable spacing between two cavities. On the boundary between the elastic and plastic zones, the stresses induced by excavation satisfy Kirsch's equation; and the total tangential stress and radial stress satisfy the Mohr-Coulomb criterion. Assuming R_p is the outer boundary of the plastic zone, then the stresses on the boundary are expressed as:

$$r = R_p \tag{20}$$

$$\sigma_\theta = \sigma_{\theta e} + \sigma_{\theta t} + \sigma_{\theta i} \tag{21}$$

$$\sigma_r = \sigma_{re} + \sigma_{rt} + \sigma_{ri} \tag{22}$$

$$\sigma_1 = \frac{\sigma_r + \sigma_\theta}{2} + \sqrt{\left(\frac{\sigma_r - \sigma_\theta}{2}\right)^2 + \tau_{r\theta}^2} \tag{23}$$

$$\sigma_3 = \frac{\sigma_r + \sigma_\theta}{2} - \sqrt{\left(\frac{\sigma_r - \sigma_\theta}{2}\right)^2 + \tau_{r\theta}^2} \tag{24}$$

$$\tau_{r\theta} = \tau_{r\theta e} \tag{25}$$

$$\sigma_1 = \sigma_3 \frac{1+\sin\phi}{1-\sin\phi} + \frac{2c\cos\phi}{1-\sin\phi} \tag{26}$$

where σ_θ is the total tangential stress, σ_r is the total radial stress, σ_1 is the maximum principal stress, σ_3 is the minimum principal stress, c is the cohesion of the rock, and ϕ is the angle of internal friction.

On the horizontal axis between two cavities, θ is zero. In the elastic zone, the stresses can be calculated by using Eqs. (21) and (22), where r is any value larger than R_p.

5.3.4 Stress Induced by Opening in Rock Mass with Discontinuities

Most coal seams are fractured and the strength is affected by the presence of discontinuities. Discontinuities behave as planes of weakness, and slippage is likely to

happen along the discontinuities. Figure 75 shows a specimen with a single discontinuity, and the principal stresses applied on it.

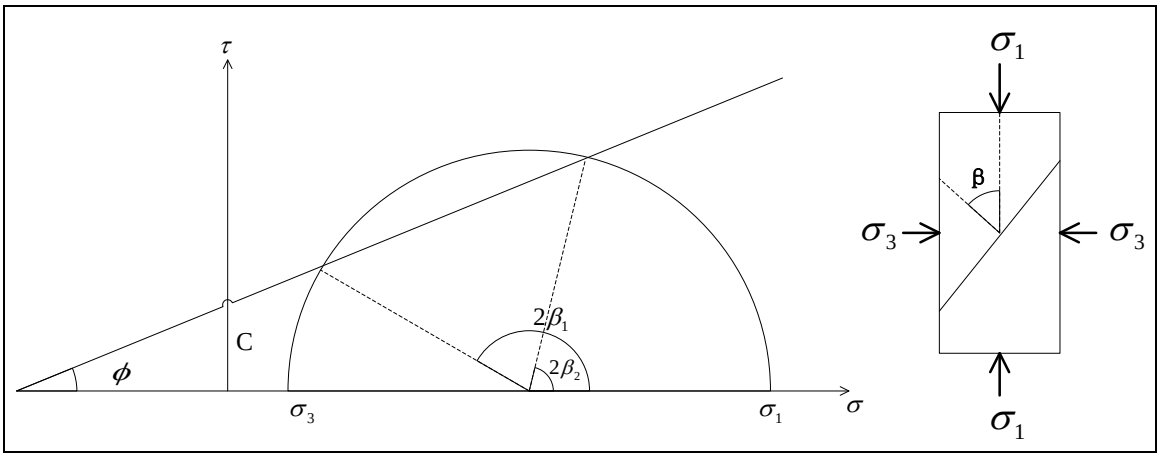

Figure 75. Failure along the discontinuity on a specimen.

It also shows the Mohr-Coulomb failure loci for the discontinuity. If β is defined as the angle between σ_1 and the normal of discontinuity plane, failure will happen when β reaches any value between β_1 and β_2.

Through geometric analysis on the failure loci, it can be proven that when the failure occurs along the discontinuity, σ_1 and σ_3 on the specimen satisfy the following relationship [62, 63]:

$$\sigma_1 = \sigma_3 + \frac{2c + 2\sigma_3 \tan\phi}{(1 - \tan\phi \cot\beta)\sin 2\beta} \tag{27}$$

where c is the cohesion of the discontinuity, ϕ is the angle of internal friction of the discontinuity. The longest radius of the plastic zone will occur at β equal to $45^o+(\phi/2)$ [63].

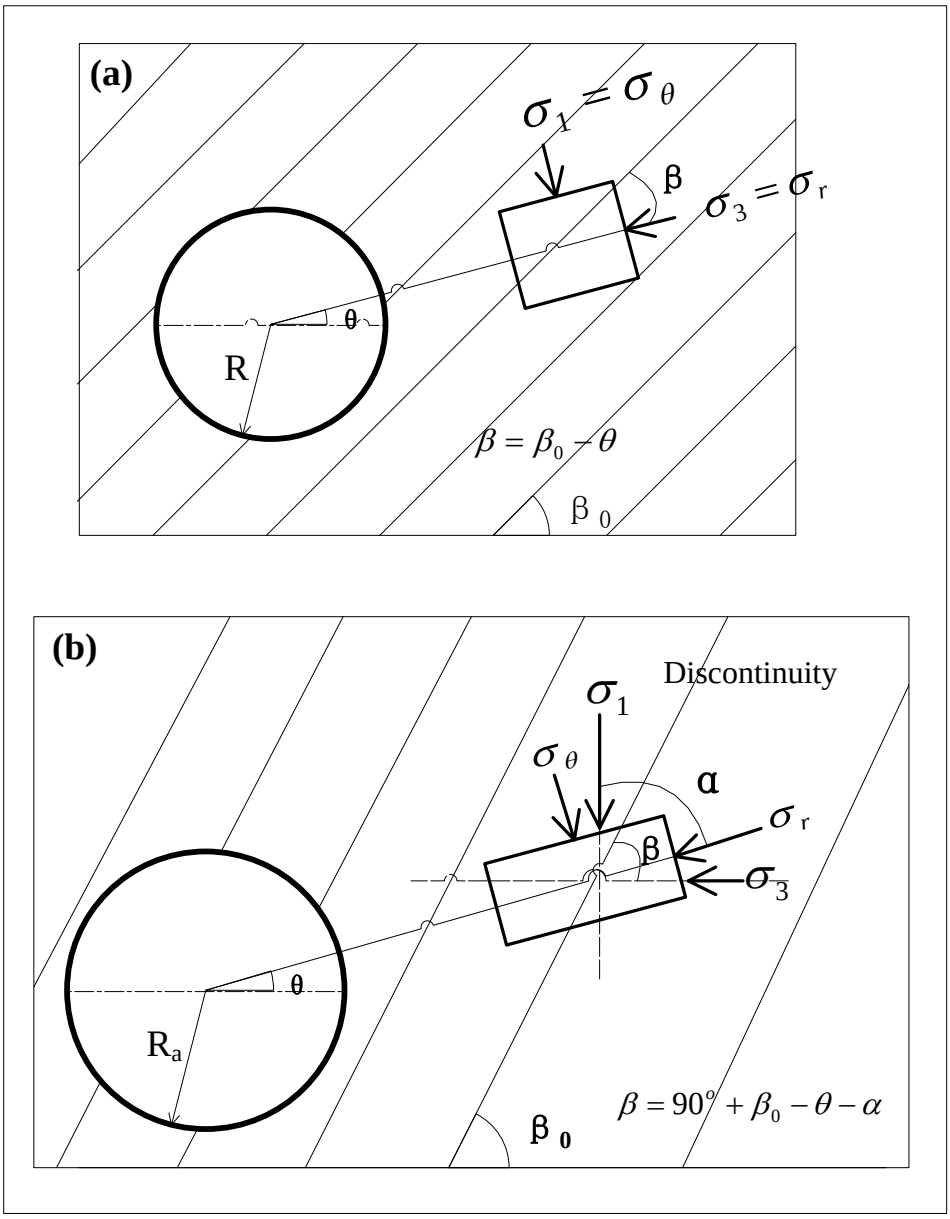

Figure 76. Relationship between β and θ under conditions of hydrostatic in situ stress (a) and non-hydrostatic in situ stress (b).

If the original in-situ stress is hydrostatic ($\sigma_h = \sigma_v$), σ_1 and σ_3 will be σ_θ and σ_r, respectively. Since β is also equal to the angle between σ_3 and the discontinuity, as shown in Figure 76A, the relationship between β and θ is given as:

$$\beta = \beta_0 - \theta \tag{28}$$

where β_0 is the angle of the discontinuity from the horizontal axis.

If the original in situ stress is non-hydrostatic, σ_1 and σ_3 can be calculated using Eqs. (23) and (24). Through geometric analysis in Figure 76B, the relationship between β, β_0, and θ can be expressed as Eq. (29) and Eq. (30):

$$\beta = 90^o + \beta_0 - \theta - \alpha \tag{29}$$

$$\tan 2\alpha = \frac{2\tau_{r\theta}}{\sigma_r - \sigma_\theta} \tag{30}$$

Similar to the situation of the intact rock, on the boundary of the elastic zone and plastic zone where r is equal to R_p, the stresses induced by excavation satisfy Kirsch's equation and the maximum and minimum principal stresses satisfy Eq. (27). With Eqs. (13) - (24), and Eqs. (27) - (30), R_p can be expressed as a function of θ, so the radius of the plastic zone can be obtained.

5.4 Safety Concerns and Mining Recovery

Considering a block of coal-bearing formation as shown in Figure 77, the width of the coal seam is W, its thickness is H, and its length is L. If the cavities have a radius of R_a, and the spacing, S, is defined as the distance between the centers of two neighboring cavities, the mining recovery factor, M.R.F., would be the volume ratio of the cavities to the coal seam:

$$M.R.F. = \frac{\left(\frac{W}{S}\right) \cdot \left(\pi R_a^2\right) \cdot L}{W \cdot H \cdot L} = \frac{\pi R_a^2}{SH} \tag{31}$$

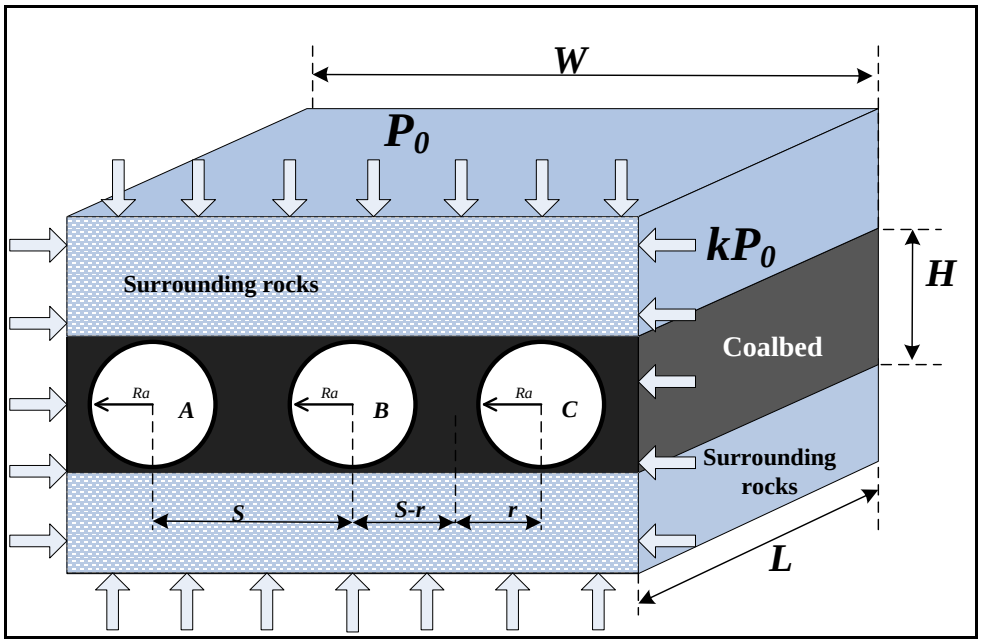

Figure 77. Gasification cavities in a coal-bearing block.

5.4.1 Intact Rock Formation

If the coal seam and surrounding rocks are assumed as intact rock, solving Eqs. (11) - (26) presented in the last section will yield the R_p and stresses on the horizontal axis.

As mentioned in Section 5.2, there are three phases for the induced stress conditions corresponding to the development of first gasification cavity, gasification of subsequential cavities, and post gasification. Plastic boundary for these phases can be calculated by following equations presented in Section 5.3. The largest value in any of the cases is supposed to be the final radius.

As mentioned above, the remaining part between two cavities functions as a “pillar”. In the design stage of a UCG plant, in order to ensure the structural stability, the “pillar” left

between two cavities must be in the elastic state. For safety reasons, we introduce the safety factor (S.F.), and assume that the stress in the pillar must satisfy the following relationship to guarantee stability of the cavities:

$$\sigma_{1,elastic} \leq \frac{\sigma_{1,Mohr}}{S.F.} \tag{32}$$

where $\sigma_{1,elastic}$ is the maximum principal stress in the elastic zone ("pillar"), $\sigma_{1,\,Mohr}$ is the maximum principal stress at failure corresponding to the minimum principal stress, given by the Mohr-Coulomb criterion. In this study, we assume an S.F. of 1.5.

For pillar design in underground mining, Zipf [78] described the stability-criterion-based, containment design approach. Both barrier and panel pillars are used (Figure 78). The barriers pillars limit potential failure to just one panel. Barrier pillars have a high width-to-height ratio, typically greater than 10. The panel pillars among the barrier pillars typically have a width-to-height ratio in the range of 0.5 to 2.

For a UCG plant of commercial scale, the similar arrangement of barrier pillars and panel pillars can be also applied. In this study, the pillar between two UCG cavities is treated as a panel pillar. Therefore, we assume that the width of the "pillar", where the stress condition satisfying Eq. (32), must be not less than three times of the cavity radius. The concept of "pillar" safety is presented in Figure 79.

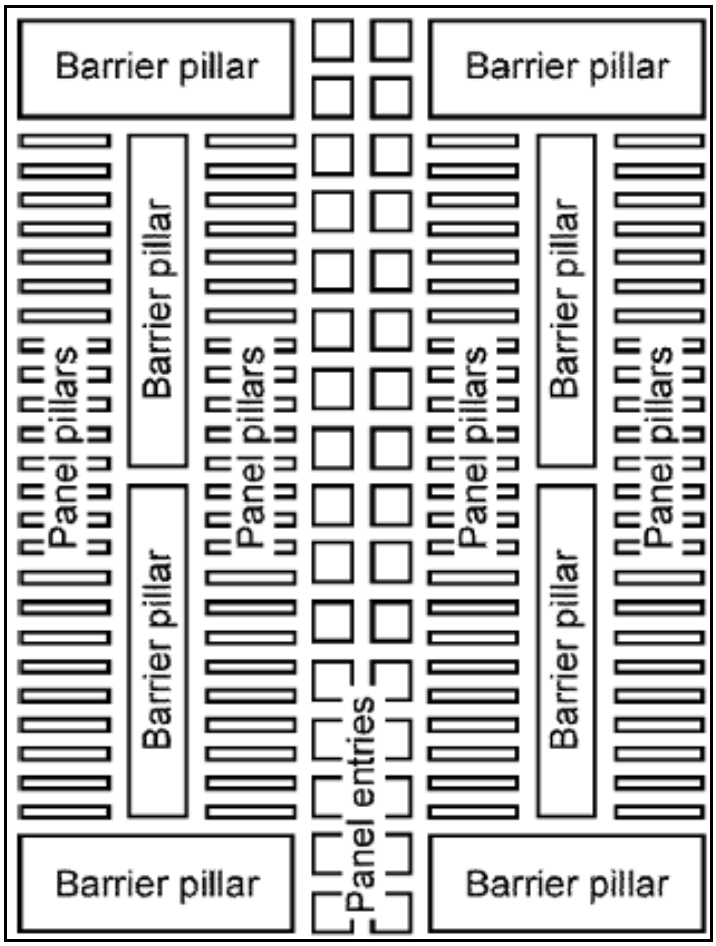

Figure 78. Room-and-pillar layout in underground coal mining [78].

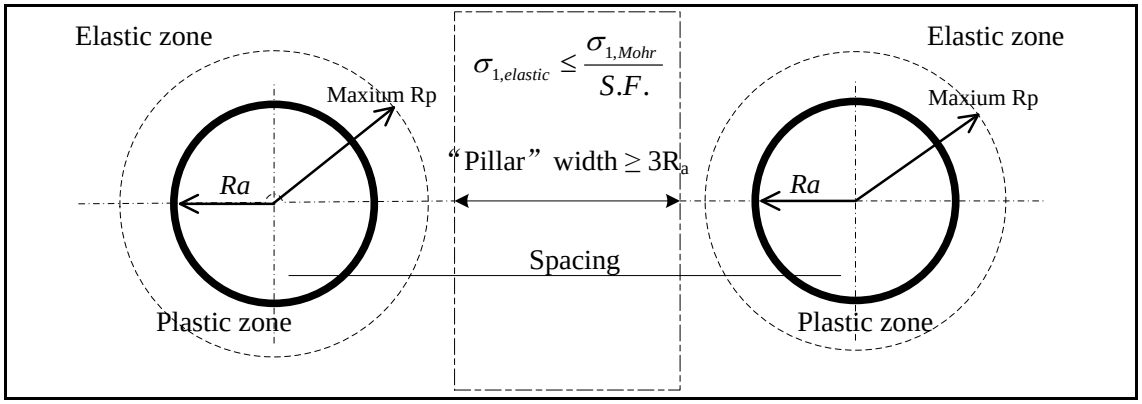

Figure 79. Safety requirement for the "pillar" between two cavities.

To satisfy the above requirement, the spacing between cavities, S, must be greater than a certain value for a corresponding cavity radius R_a. Therefore, the recovery factor can be

estimated based on the R_a. The calculation procedure based on the methods discussed above is shown in Figure 80. The concept and calculation can be illustrated using an example. In this example, a UCG plant is developed on an intact coal-bearing formation. The input data are listed in Table 12.

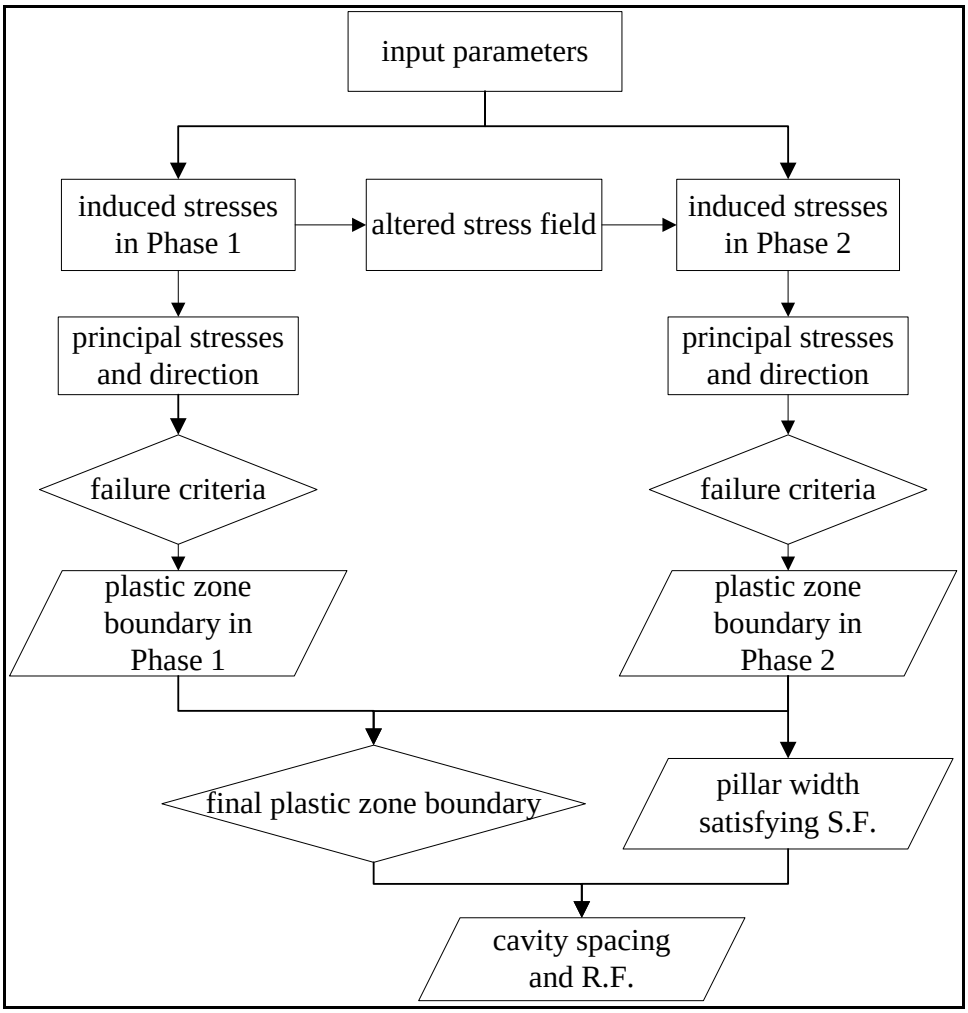

Figure 80. The calculation flow diagram.

Following the procedure in Figure 80, the results based on the parameters in Table 11 are listed in Table 12. As expected, the spacing increases with the cavity radius. The recovery factor reaches a maximum as the radius is equal to half of the coal seam

thickness. Using the cavity with a diameter of 2 m as an example, the stress profiles of Phase I and Phase II are shown in Figures 81 and 82, respectively.

Table 11. Parameters of a UCG plant in intact formation

Parameter	Value	Unit
Coalbed thickness, H	6	m
Cavity radius, R_a	1~3	m
Cohesion, c	3	MPa
Angle of internal friction, ϕ	30	degree
Original vertical in situ stress, P_0	8	MPa
Ratio of horizontal to vertical stresses, k	1.5	–
Young's Modulus, E	3790	MPa
Poisson's ratio, ν	0.44	–
Linear thermal expansion coefficient, α	6.0E-6	1/K
Gasification temperature, T_i	1273	K
Formation initial temperature, T_{inf}	293	K
Gasification pressure, p_w	2.67	MPa

Table 12. Calculated results for a UCG plant in an intact formation

R_a, m	R_p satisfying Eq. (32) on horizontal axis, m	S, m	M.R.F.
1.0	1.5	≥ 5.7	≤ 9%
1.5	2.2	≥ 8.5	≤ 14%
2.0	2.8	≥ 11.6	≤ 18%
2.5	3.6	≥ 14.1	≤ 23%
3.0	4.3	≥ 17	≤ 29%

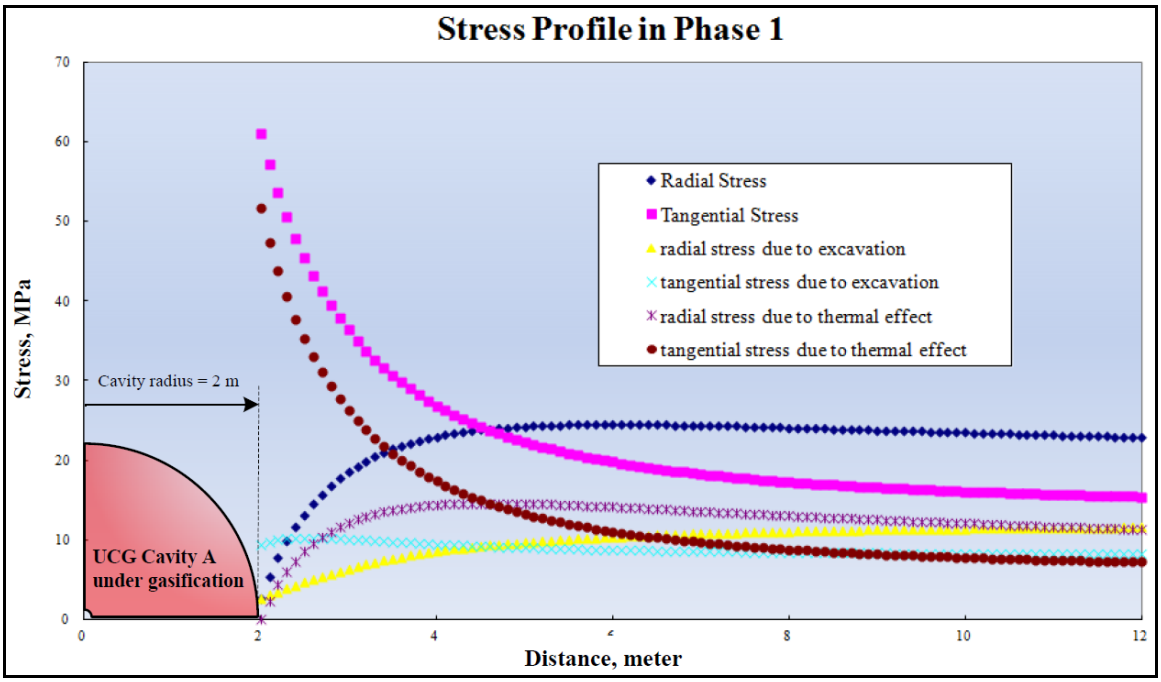

Figure 81. Stress profile of Phase 1 in intact rock, cavity radius is 2 m

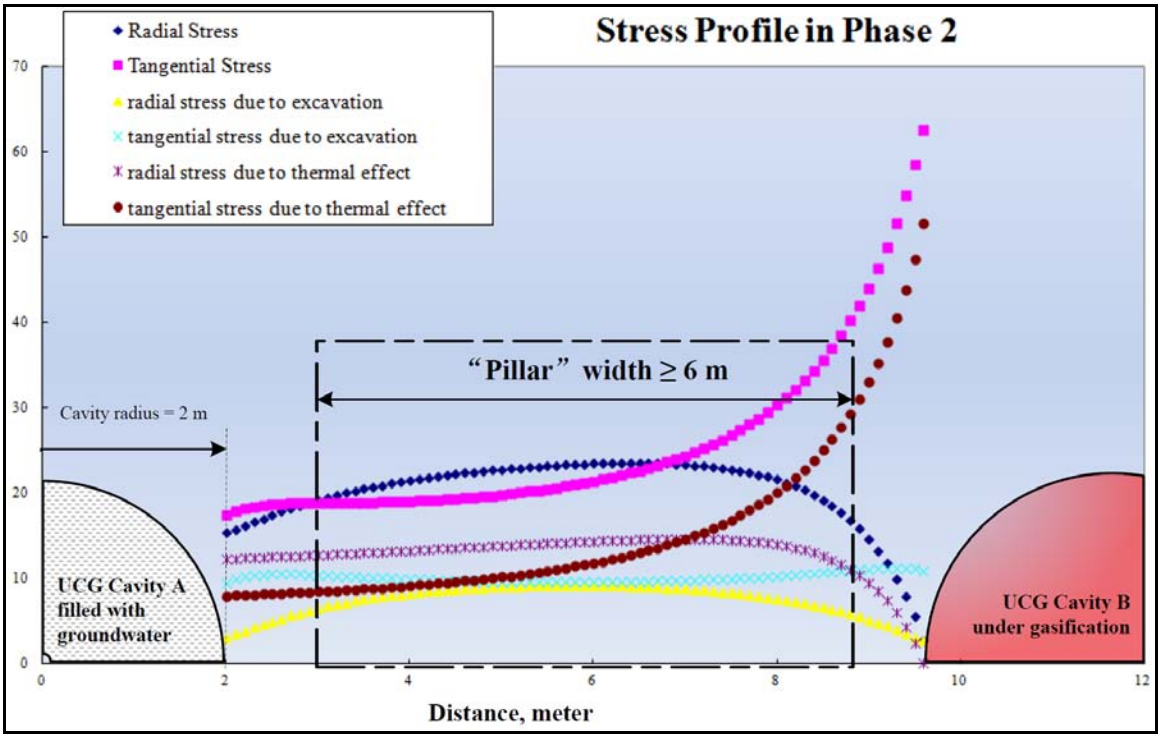

Figure 82. Stress profile of Phase 2 in intact rock, cavity radius is 2 m

5.4.2 Formation with Discontinuities

Due to the effect of the discontinuities, slippage along the plane of weakness occurs when β reaches a range of values (Figure 75). For a fractured formation, even if the original in-situ stress is hydrostatic, the plastic zone around the opening is not axisymmetric, different from the case in Figure 79. The value of the radius of the plastic zone changes with directions. The longest radius occurs at β equal to $45^{o}+(\phi/2)$, as discussed in previous sections. When the original in situ stress is non-hydrostatic, the stress field and the plastic zone boundary are difficult to present in an analytic solution. In the following example, we discuss the recovery factor to a coal-bearing formation with a single set of discontinuities, subjected to a hydrostatic in situ stress field. UCG parameters for this coal-bearing formation are listed in Table 13.

Table. 13. Parameters of a UCG plant in a fractured formation

Parameter	Value	Unit
Coalbed thickness, H	6	m
Cavity radius, R_a	1~3	m
Cohesion, c	0.7	MPa
Angle of internal friction, ϕ	15	degree
Angle of the discontinuity, β_0	70	degree
Original vertical in situ stress, P_0	8	MPa
Ratio of horizontal to vertical stresses, k	1	–
Young's Modulus, E	3790	MPa
Poisson's ratio, ν	0.44	–
Gasification temperature, T_i	1273	kelvin (K)
Linear thermal expansion coefficient, α	6.0E-6	1/K
Formation initial temperature, T_{inf}	293	K
Gasification pressure, p_w	2.67	MPa

The longest radius of the plastic zone in this example is obtained when β is equal to 60^o, or θ is equal to 10^o (Figure 83). Because of the symmetry of the stress field related to the discontinuities, the longest radius of the plastic zone also occurs when θ is equal to 190^o. Applying the same approach and the concept of safety in Section 5.4.1, the calculated results of spacing and the recovery factor are listed in Table 14. It can be seen that due to the presence of discontinuities, the spacing between cavities has to be increased to ensure safety, and the recovery factor drops. Similar to the case in intact formation, the recovery factor increases with the radius of the cavities (Table 14).

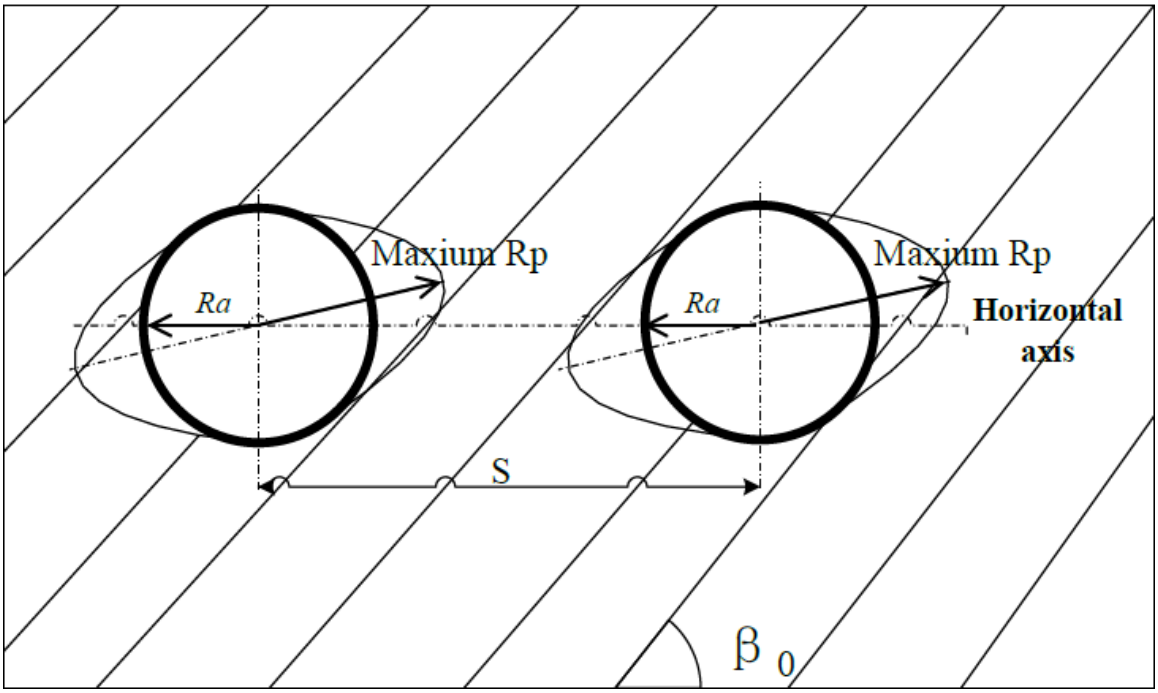

Figure 83. Plastic zone around the cavity in a formation with discontinuities.

Table 14. Calculated results for a UCG plant in a formation with discontinuities

R_a, m	R_p satisfying Eq. (32) on horizontal axis, m	S, m	M.R.F.
1.0	2.6	≥ 8.2	$\leq 6\%$
1.5	3.9	≥ 12.5	$\leq 9\%$
2.0	5.2	≥ 16.5	$\leq 13\%$
2.5	6.4	≥ 20.3	$\leq 16\%$
3.0	7.7	≥ 24.5	$\leq 19\%$

For a conceptual UCG plant at a commercial scale, we have classified its developmental procedure into three major phases, and examined the stress profiles, the recovery factor and structural stability. It can be seen that the properties of the coal seam and the presence of the discontinuities have a significant effect on the recovery factor, and hence on the economics of the plant. It is also worth noting that the width of the "safe pillar" discussed in Section 5.4.1 can affect the calculated results, and impact the recovery factor significantly. To guarantee safety, a conservative value may be assigned to the sacrifice of the recovery factor. In general, as demonstrated in the examples, by understanding the properties of the formation, and designing reasonable cavity radius and spacing, the stability of the cavities can be guaranteed, with an optimized recovery factor.

The methodologies and results presented in the above parts provide a convenient and fast way to estimate the economics of a UCG plant, while further improvements can make the estimation more accurate. For example, other failure criteria which are more suitable for fractured formations, such as the Hoek-Brown criterion, can be used. Instead of considering a process of steady state, a transient process and coupled mechanisms can be considered. Particular attention should be paid to consider influences from the change of

the elastic, thermoelastic and poroelastic properties due to the change of temperature and water saturation during the gasification process. However, such studies would require a better understanding to the fundamentals of the coupling mechanisms and advanced modeling numerical tools.

5.5 Numerical Modeling

A numerical modeling study was carried out to investigate the displacement profiles during the UCG process and to compare the induced stress profiles obtained from the analytical approach. The FE modeling work was processed using ANSYS [79]. Stress and displacement profiles with two different gasification cavity diameters (2 m and 3 m) were obtained for each of the three development phases of a commercial UCG plant. Detailed descriptions about these three phases are shown in Figures 72 to 74. As mentioned in Section 5.2, the length of the UCG cavities is much larger than its diameter, so plain strain is assumed. Properties and behavior of the modeled strata are assumed to follow the elastic assumptions. The model is two-dimensional based on the plain strain assumption. The numerical model contains a coalbed, with an underlayer and an overburden. The depth of the target coalbed is assumed to be 300 m, the same as the selected site in Dunn County, North Dakota. Based on the depth, the overburden pressure is assumed to be 7 MPa, and the gasification pressure is set as 2.67 MPa, which is equal to the estimated hydrostatic pressure of groundwater. The coalbed and the surrounding rocks are represented by different materials. Parameters of the modeled geologic formation are from the literature [58] and laboratory test results listed in a previous chapter. The parameters of material are listed in Table 15.

Table 15. Parameters used in the numerical modeling

Parameters	Value	Unit
Formation temperature	20	^{o}C
Gasification temperature	1000	^{o}C
Gasification pressure	2.67	MPa
Original in-situ stress in vertical direction	8	MPa
Hydraulic head of ground water	2.67	MPa
Thermal expansion coefficient of coal	6.0E-6	1/^{o}C
Young's Modulus of coal	3.79	GPa
Poisson's ratio of coal	0.44	-
Thermal expansion coefficient of rock	9.0E-6	1/^{o}C
Young's Modulus of rock	15.0	GPa
Poisson's ratio of rock	0.25	-

5.5.1 Case 1: Cavity Radius Equal to 2 m

The structure of the UCG model with a cavity radius equal to 2 m is shown in Figure 84. The thickness of the coalbed is 6 m. Both the overlayer and underlayer thicknesses are 10 m. The width of the model is 60 m to offset the impact of boundary conditions to the modeling results. Gasification cavities with a radius equal to 2 m are arranged in the coalbed with a spacing of 12 m, as suggested by the analytical solution. In the model, a pressure in the vertical (Y) direction is applied on the top boundary to simulate the overburden load. The bottom boundary of the model is fixed in the Y direction, and the two vertical sides are fixed in the horizontal (X) direction. The origin of the coordinate is set at the center of the model, as in Figure 84. In ANSYS, the sign of the displacement agrees with the direction of the coordinate axis. For example, expansion along the X axis to left will be assigned a negative value; expansion along the X axis to right will be

assigned a positive value. The materials used to represent the coalbed and adjoining rocks are assigned different attributes as listed in Table 15.

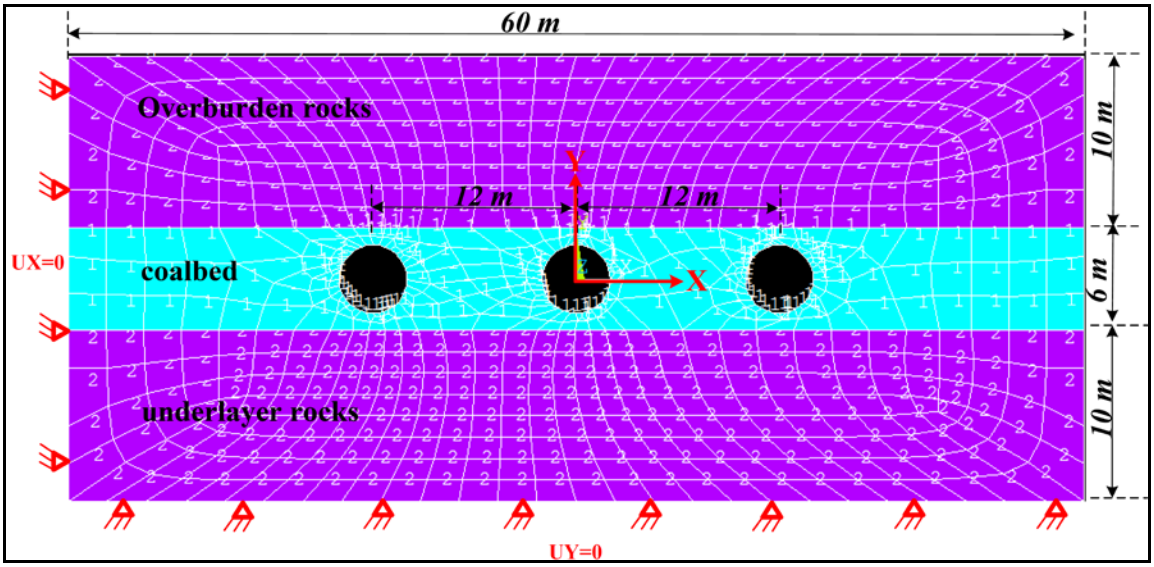

Figure 84. Structure of the UCG model, cavity radius of 2 m: cyan (Material 1) – coal, purple (Material 2) – surrounding rocks.

In Phase 1, gasification is undergoing in the first cavity, so thermal stresses and internal-pressure induced stresses exist around the cavity. Contour maps of the displacement are shown in Figures 85 and 86. In general, the stresses induce expansion in the X direction and subsidence in the Y direction. The maximum expansion in X direction is about 0.002 m, and the maximum subsidence in Y direction is about 0.02 m. The displacement induced by the gasification process in Phase 1 is very small. Contour maps of the maximum and minimum principal stresses are shown in Figures 87 and 88. The maximum magnitude of the principal stresses appear on the zone immediately around the cavity, then the stresses reduce to a value slightly lower than the original in situ stress, and finally increase back to the original value. The effect of different layer attributes on the distribution of the stresses is obvious from Figures 87 and 88. The vector map of the maximum principal stresses is shown in Figure 89.

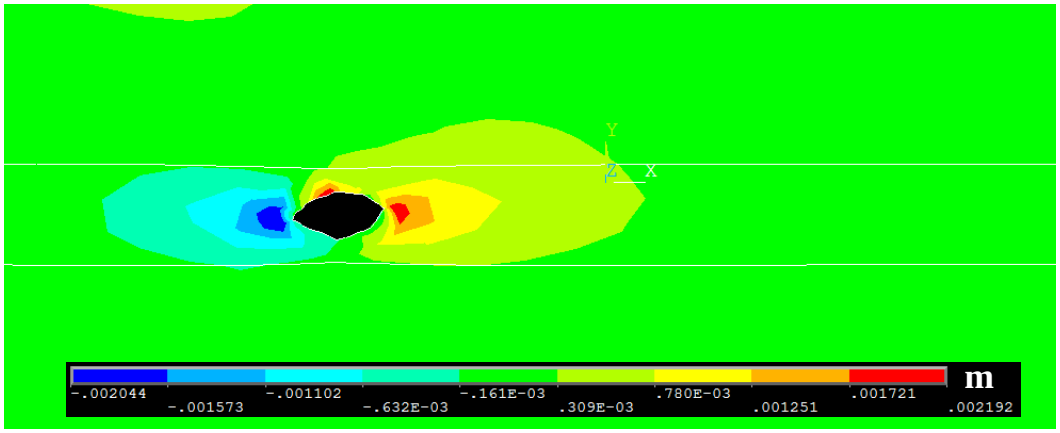

Figure 85. Contour map of displacement in X (horizontal) direction, Phase 1, cavity radius = 2 m.

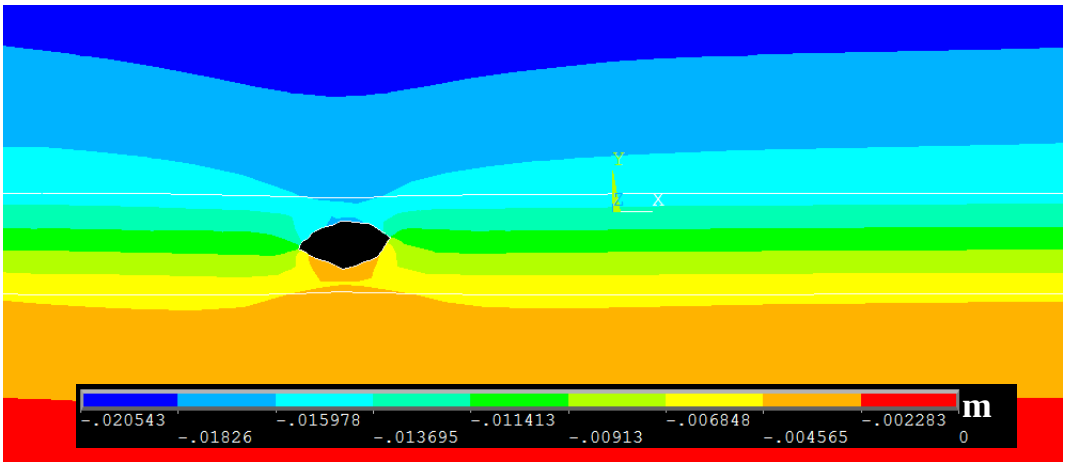

Figure 86. Contour map of displacement in Y (vertical) direction, Phase 1, cavity radius = 2 m.

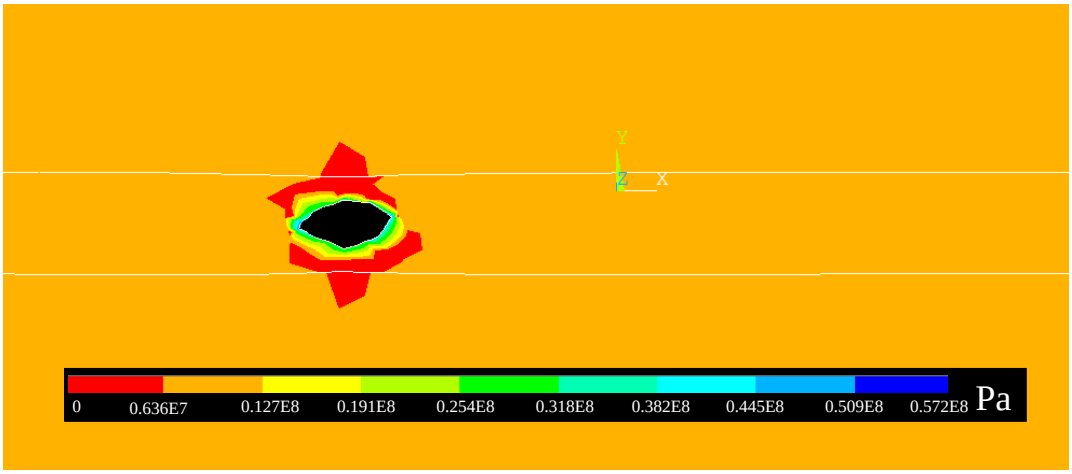

Figure 87. Contour map of maximum principal stress Phase 1, cavity radius = 2 m.

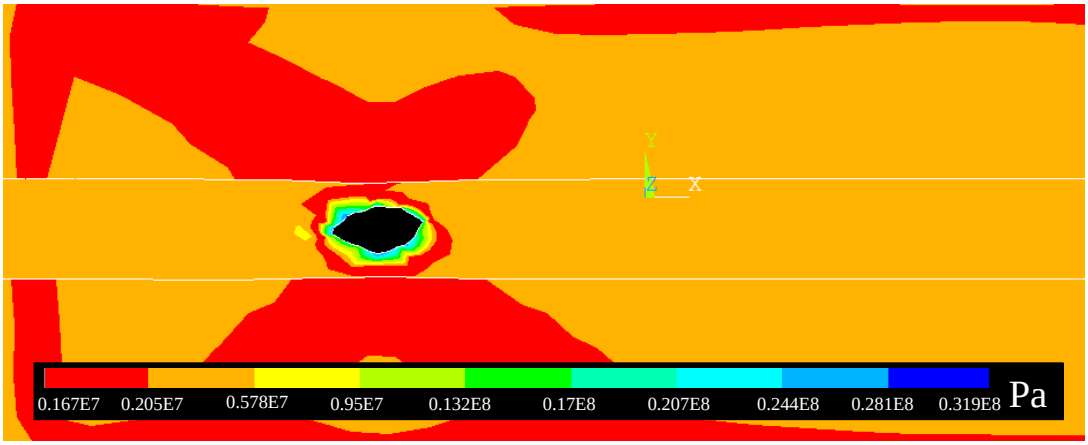

Figure 88. Contour map of minimum principal stress, Phase 1, cavity radius = 2 m.

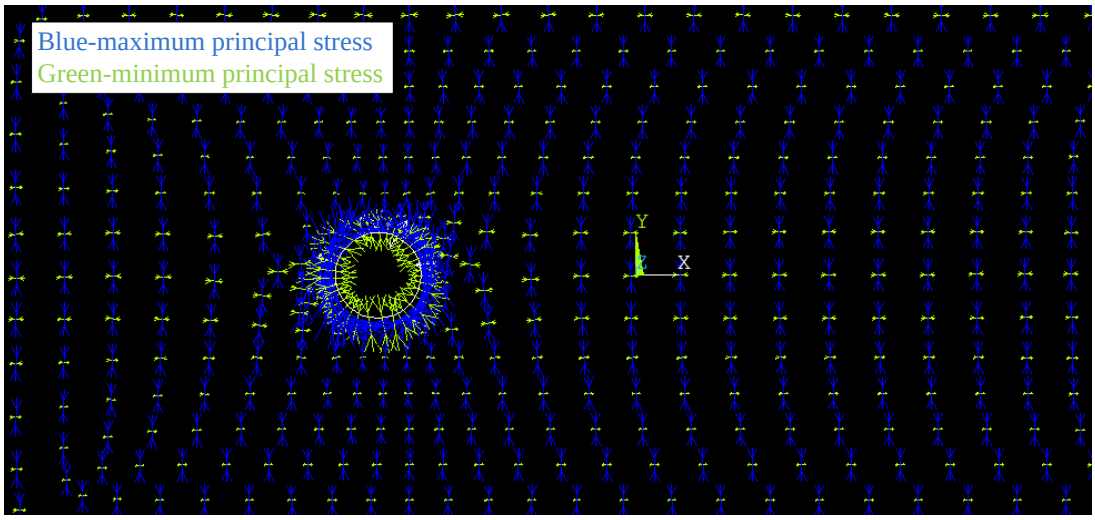

Figure 89. Vector map of principal stresses, Phase 1, cavity radius = 2 m.

In Phase 2, the first cavity is finished with the gasification process and filled with groundwater and the second cavity is being gasified, so the high temperature boundary condition is only applied on the wall of the second cavity. Contour maps of the displacement are shown in Figures 90 and 91, the maximum expansion in X direction is about 0.0024 m, and the maximum subsidence in Y direction is about 0.0216 m. Compared to Phase 1, the displacement is almost the same. Contour maps of the maximum and minimum principal stresses are shown in Figures 92 and 93. Due to the absence of thermal stresses, the magnitude of principal stresses around the first cavity is much lower than that around the second cavity. The maximum magnitudes of the principal stresses appear on the zone immediately around the second cavity. However, the highest value of maximum principal stress is very close to that in the Phase 1. It can be seen that between the cavities, the stresses are of low magnitude, and pillar is in the safe status. The vector map of the maximum principal stresses is shown in Figure 94.

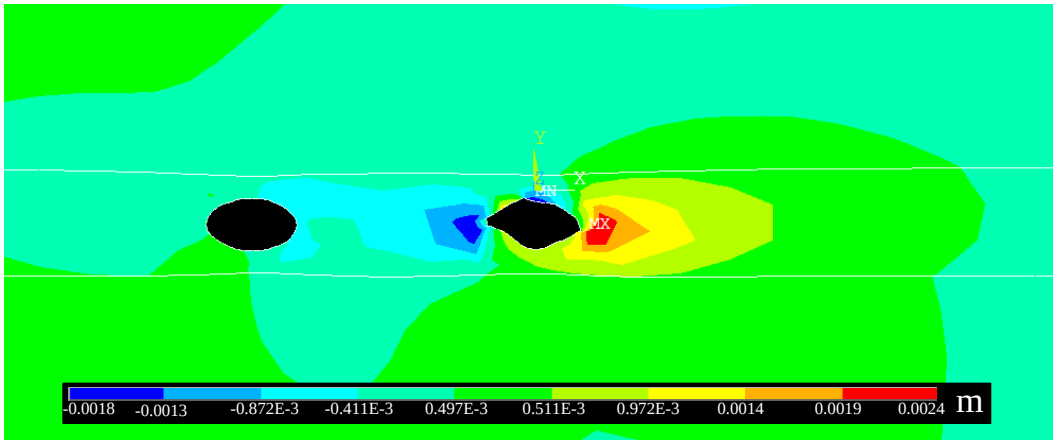

Figure 90. Contour map of displacement in X (horizontal) direction, Phase 2, cavity radius = 2 m.

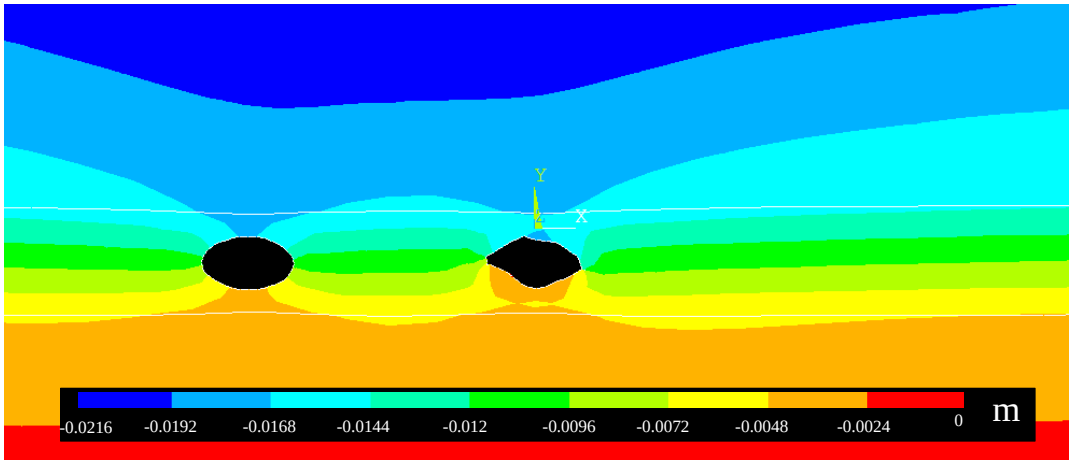

Figure 91. Contour map of displacement in Y (vertical) direction, Phase 2, cavity radius = 2 m.

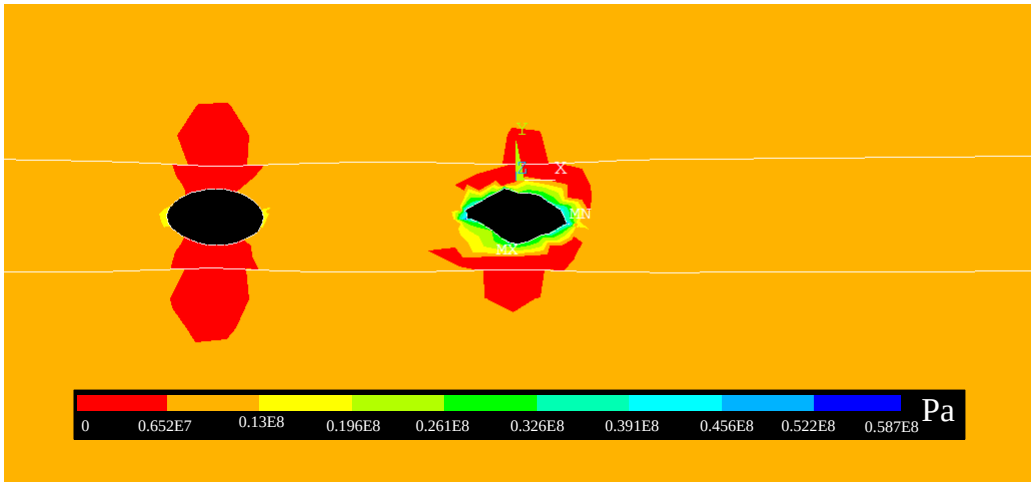

Figure 92. Contour map of maximum principal stress Phase 2, cavity radius = 2 m.

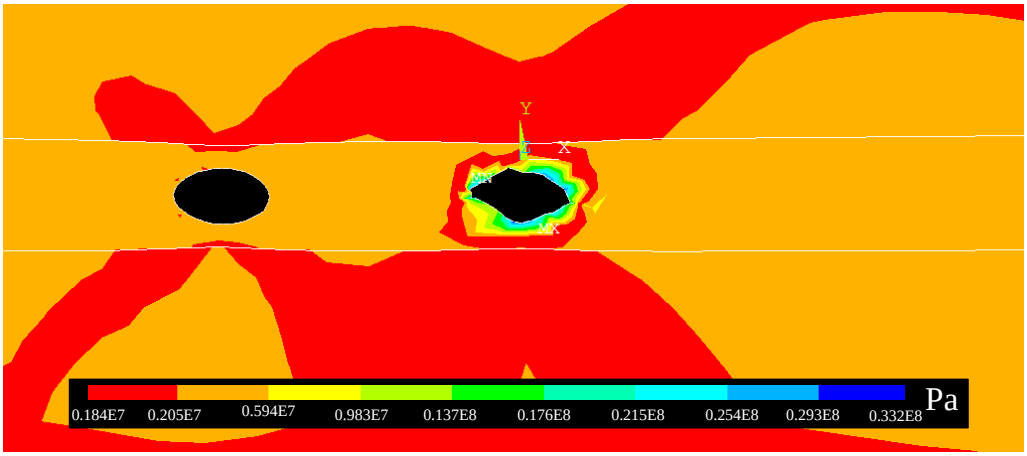

Figure 93. Contour map of minimum principal stress Phase 2, cavity radius = 2 m.

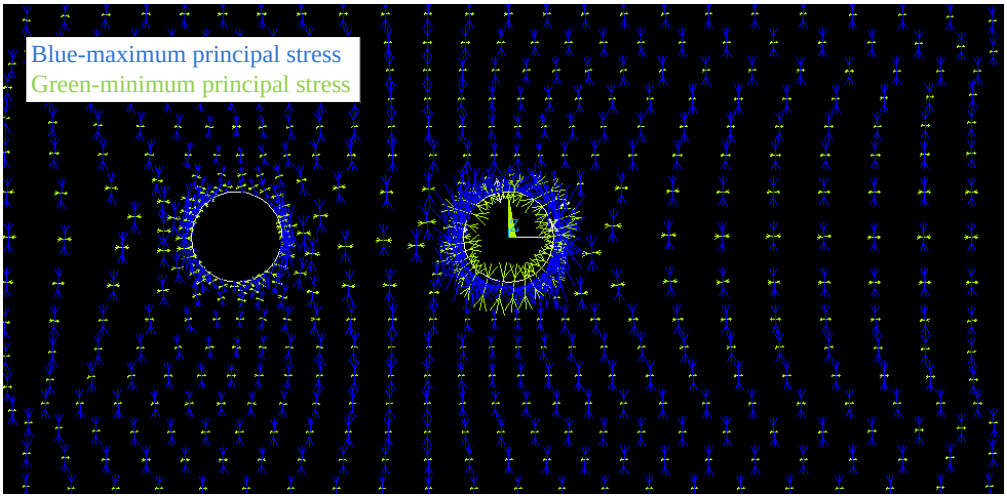

Figure 94. Vector map of principal stress, Phase 2, cavity radius = 2 m.

In Phase 3, all the three cavities are finished with the gasification process, and filled with groundwater. No high temperature boundary condition is applied on the wall of these cavities. Contour maps of the displacement are shown in Figures 95 and 96. Contour maps of the maximum and minimum principal stresses are shown in Figures 97 and 98. Because the thermal stress no longer exists, magnitudes of the displacement and induced stresses are much lower than those in Phase 2. The vector map of the maximum principal stresses is shown in Figure 99.

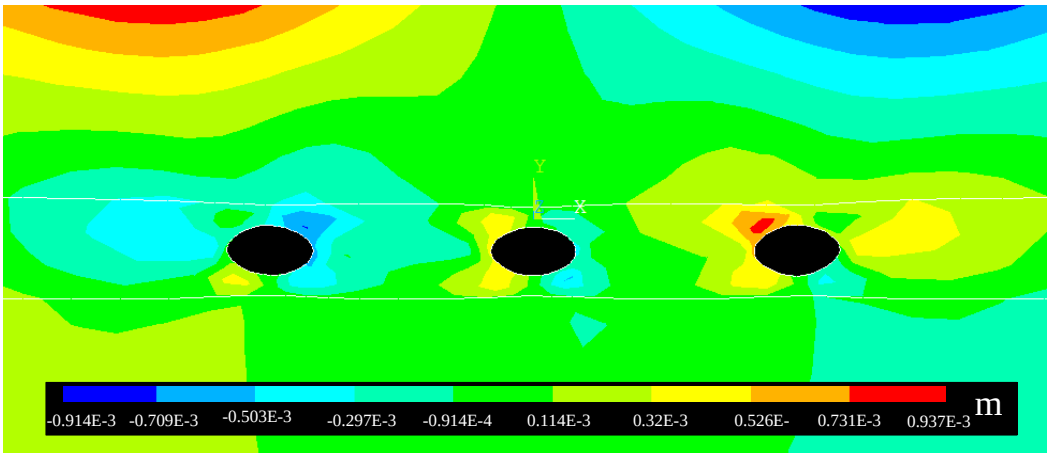

Figure 95. Contour map of displacement in X (horizontal) direction, Phase 3, cavity radius = 2 m.

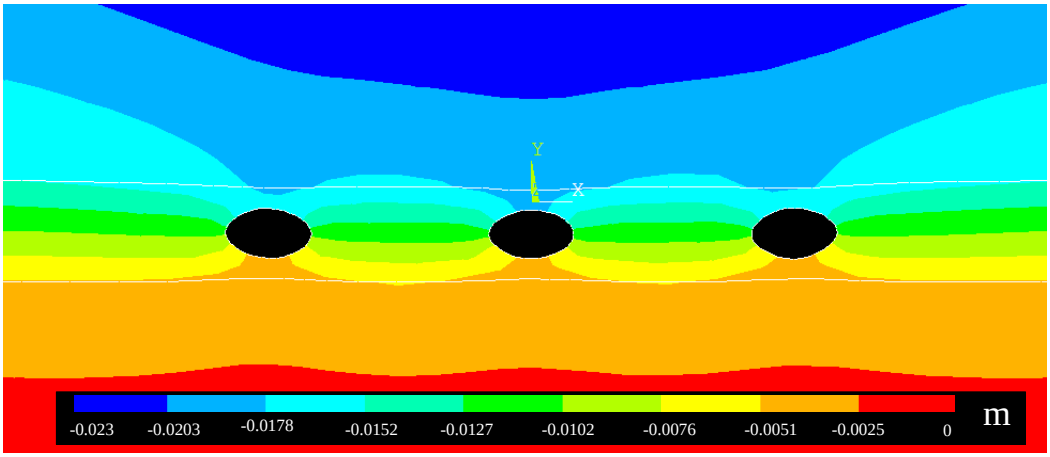

Figure 96. Contour map of displacement in Y (vertical) direction, Phase 3, cavity radius = 2m

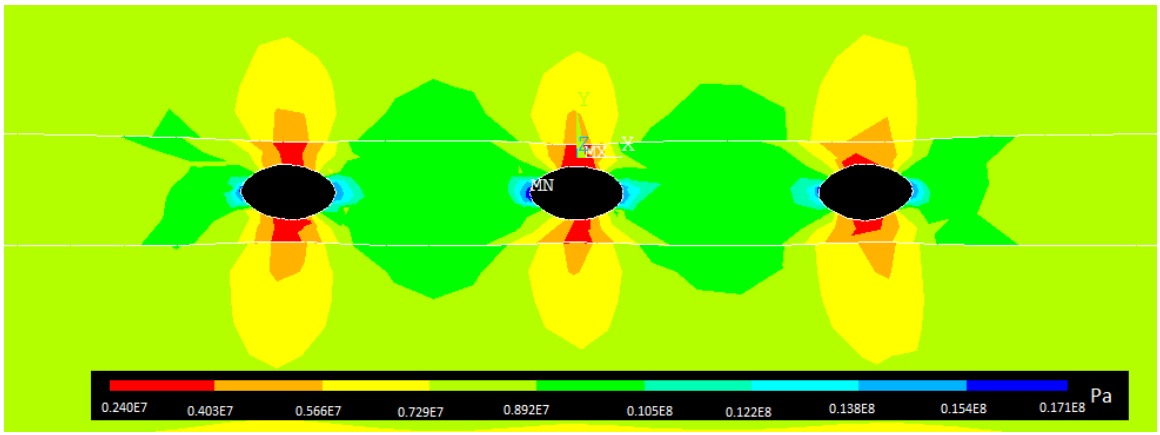

Figure 97. Contour map of maximum principal stress, Phase 3, cavity radius = 2 m.

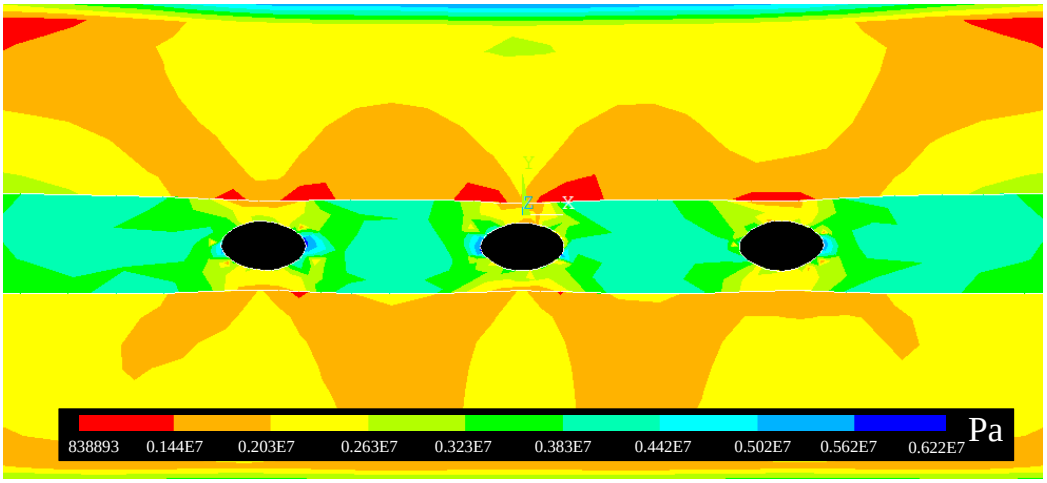

Figure 98. Contour map of minimum principal stress, Phase 3, cavity radius = 2 m.

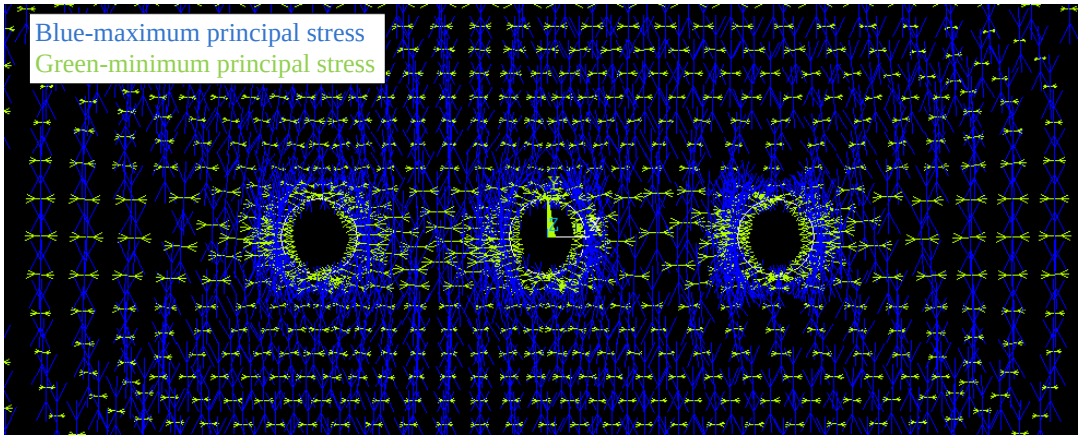

Figure 99. Vector map of principal stresses, Phase 3, cavity radius = 2 m.

5.5.2 Case 2: Cavity Radius Equal to 3 m

The structure of the UCG model with cavity a diameter of 3 m is shown in Figure 100. The thickness of the coalbed is 6 m and both the overburden and underlayer thicknesses are 10 m. The width of the model is 80 m to offset the impact of boundary conditions to the modeling results. Gasification cavities of a radius equal to 3 m are arranged in the coalbed with a spacing of 18 m. In the model, the overburden load is simulated by a pressure in the vertical (Y) direction is applying on the top boundary. The bottom boundary of the model is fixed in the Y direction, and the two vertical sides are fixed in the horizontal (X) direction. The origin of the coordinate is set at the center of the model, as in Figure 100. As mentioned above, the sign of the displacement agrees with the direction of the coordinate axis in ANSYS. Expansion along the X axis to left will be assigned a negative value; expansion along the X axis to right will be assigned a positive value. Table 15 lists the materials with different attributes representing the coalbed and adjoining rocks.

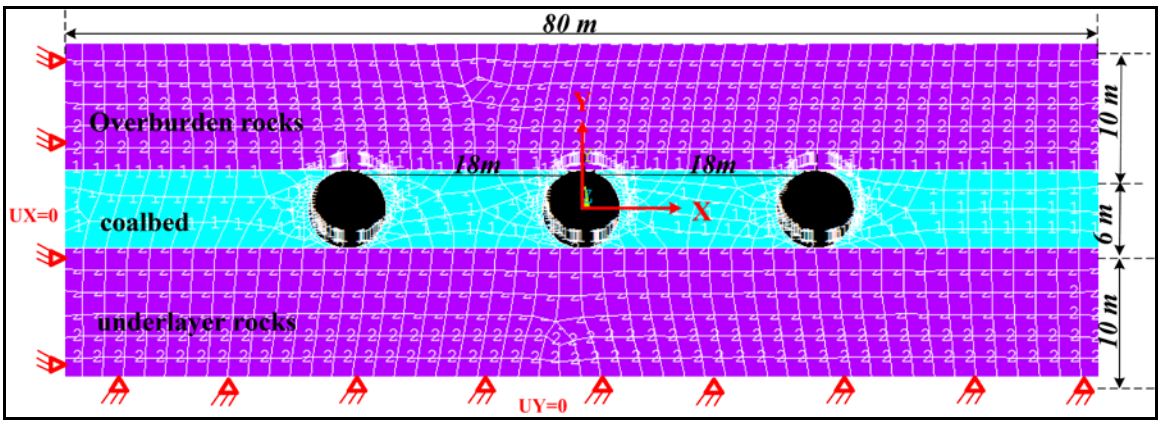

Figure 100. Structure of the UCG model, cavity radius of 3 m.

In Phase 1, gasification is undergoing in the first cavity, so thermal stress and internal-pressure induced stress exist around the cavity. Contour maps of the displacement are shown in Figures 101 and 102, the maximum expansion in X direction is about 0.0065 m, and the maximum subsidence in Y direction is about 0.025 m. The displacement in X direction is about two times of that in the case of cavity radius equal to 2 m, while the displacement in Y direction is almost the same. However, since the gasification cavity boundary reaches the adjoining rocks, severe displacement propagates from the coalbed to the overburden. The deformation in the overburden is more obvious than the case of cavity radius equal to 2 m. Contour maps of the maximum and minimum principal stresses are shown in Figures 103 and 104. The magnitude of the principal stresses are higher than that in the case of 2 m radius. The overburden above the cavity subjects to a higher induced stress comparing to the case of 2 m radius. The vector map of the maximum principal stresses is shown in Figure 105.

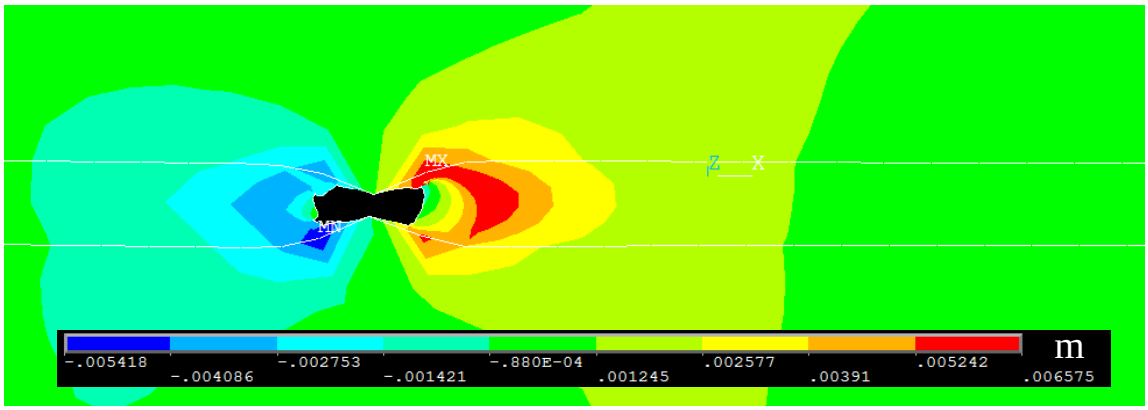

Figure 101. Contour map of displacement in X (horizontal) direction, Phase 1, cavity radius = 3 m.

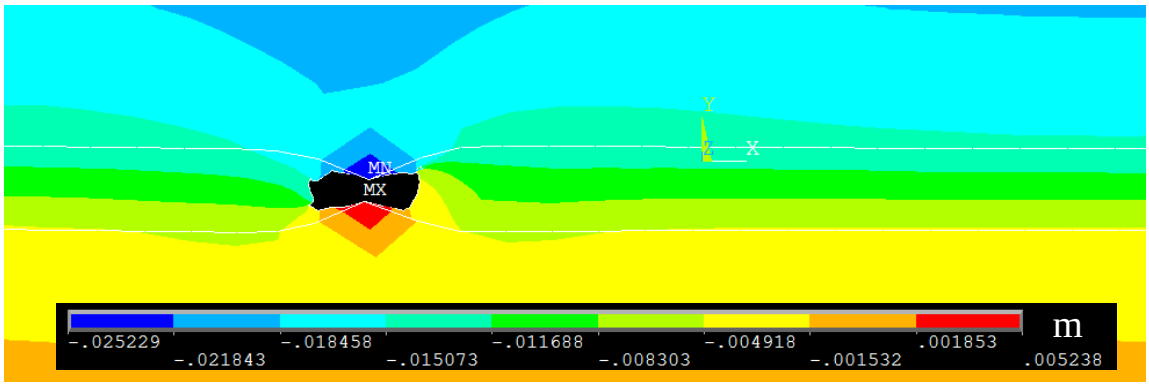

Figure 102. Contour map of displacement in Y (vertical) direction, Phase 1, cavity radius = 3 m.

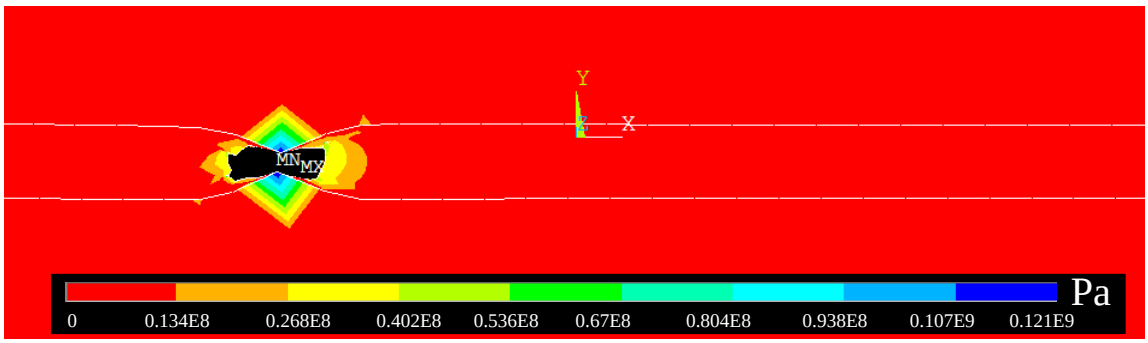

Figure 103. Contour map of maximum principal stress, Phase 1, cavity radius = 3 m.

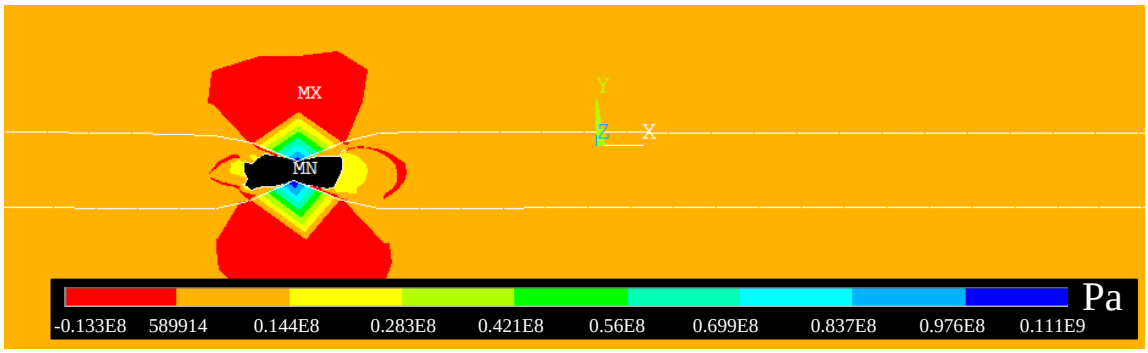

Figure 104. Contour map of minimum principal stress, Phase 1, cavity radius = 3 m.

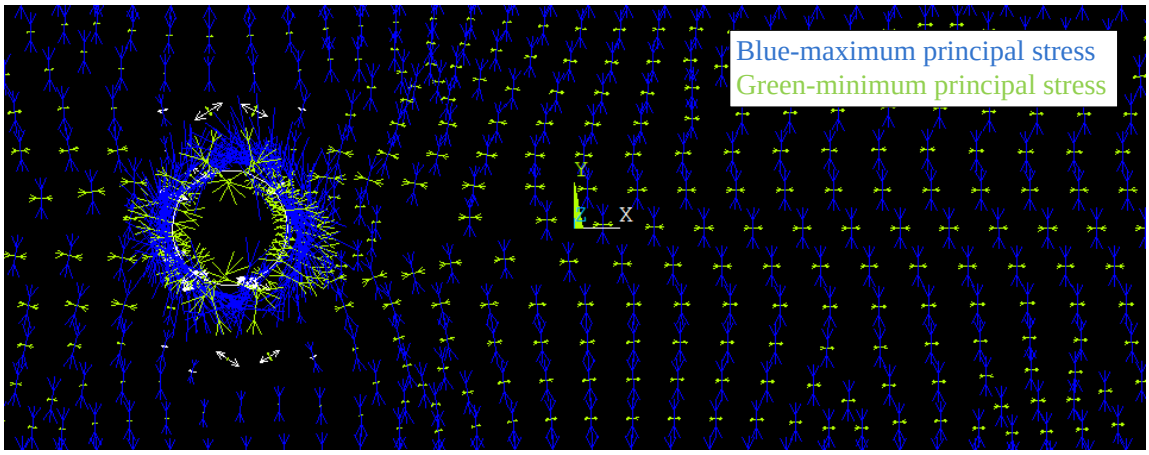

Figure 105. Vector map of principal stresses, Phase 1, cavity radius = 3 m.

In Phase 2, the first cavity is finished with the gasification process and filled with ground water. A high temperature boundary condition is only applied on the wall of the second cavity to simulate the gasification process. From the contour maps of the displacement shown in Figures 106 and 107, the maximum expansion in X direction is about 0.0047 m, and the maximum subsidence in Y direction is about 0.027 m. Contour maps of the maximum and minimum principal stresses are shown in Figures 108 and 109. The magnitude of principal stresses around the first cavity is much lower than that around the second cavity. The highest value of maximum principal stress is very close to that in the Phase 1. It can be seen that between the cavities, the stresses are of low magnitude, and pillar is in safe status. However, comparing to the case of cavity radius equal to 2 m,

severe induced stresses propagate from the coalbed to the overburden, as in Phase 1. The vector map of the maximum principal stresses is shown in Figure 110.

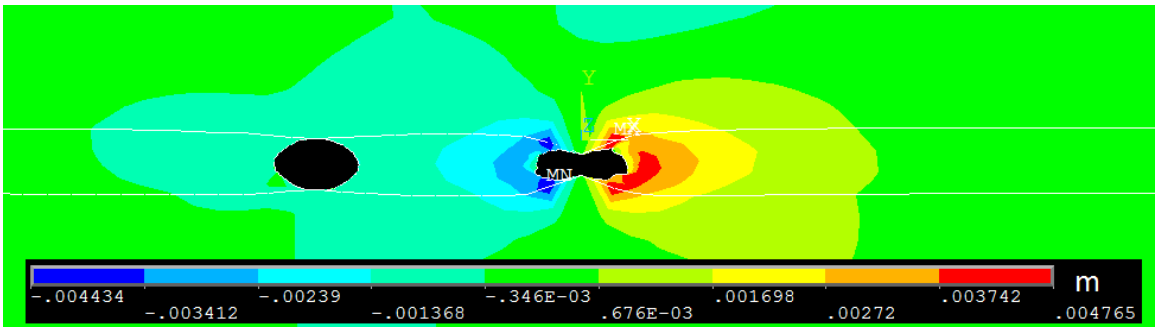

Figure 106. Contour map of displacement in X (horizontal) direction, Phase 2, cavity radius = 3 m.

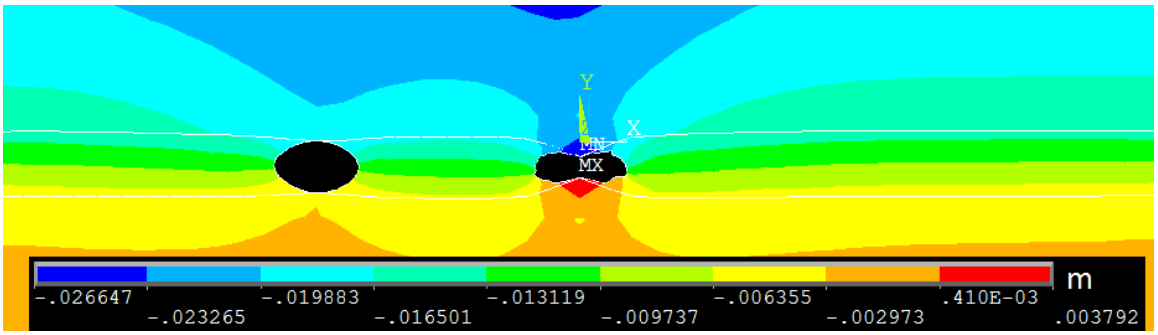

Figure 107. Contour map of displacement in Y (vertical) direction, Phase 2, cavity radius = 3 m.

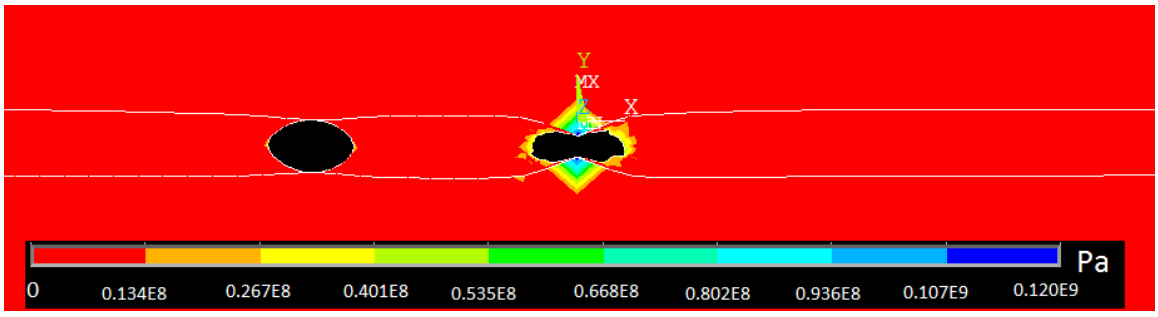

Figure 108. Contour map of maximum principal stress, Phase 2, cavity radius = 3 m.

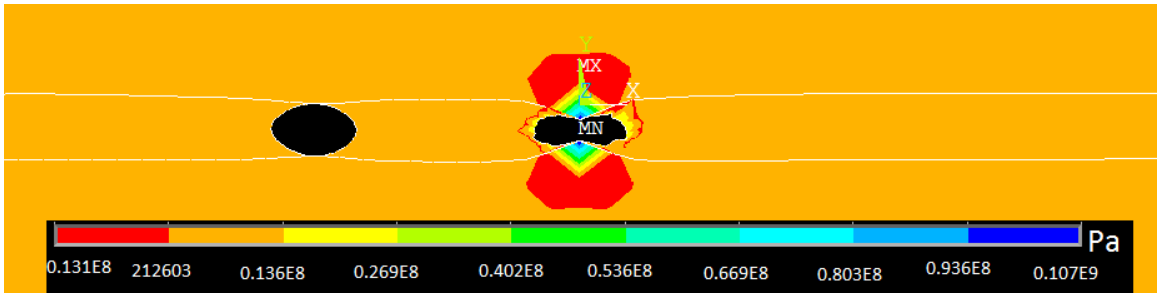

Figure 109. Contour map of minimum principal stress, Phase 2, cavity radius = 3 m.

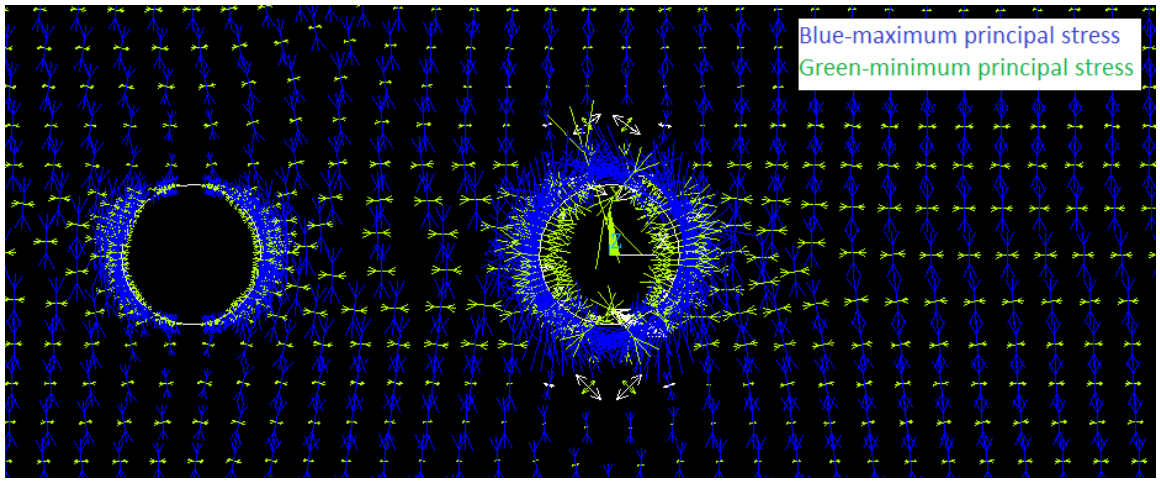

Figure 110. Vector map of principal stresses, Phase 2, cavity radius = 3 m.

In Phase 3, all the three cavities are finished with the gasification process, and filled with groundwater. No high temperature boundary condition is applied on the wall of these cavities. Contour maps of the displacement are shown in Figures 111 and 112. The maximum expansion is X direction is about 0.0127 m, and the maximum subsidence in Y direction is about 0.024 m. Contour maps of the maximum and minimum principal stresses are shown in Figures 113 and 114. Magnitudes of the displacement and induce stress are much lower than those in Phase 2. The vector map of the maximum principal stresses is shown in Figure 115.

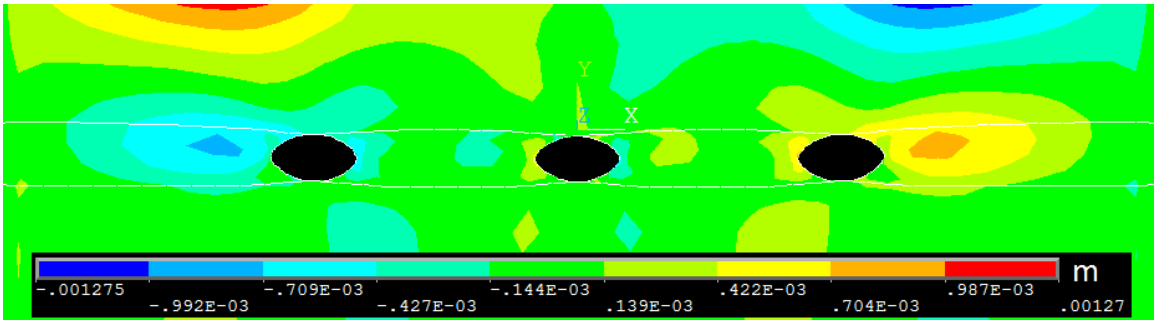

Figure 111. Contour map of displacement in X (horizontal) direction, Phase 3, cavity radius = 3 m.

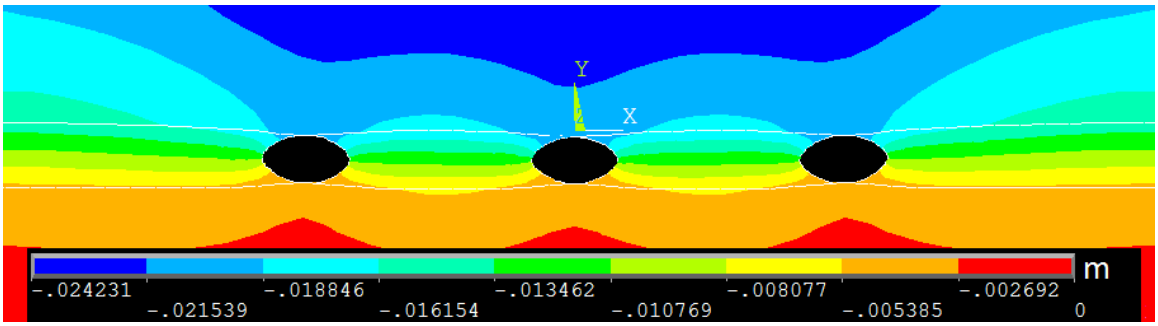

Figure 112. Contour map of displacement in Y (vertical) direction, Phase 3, cavity radius = 3 m.

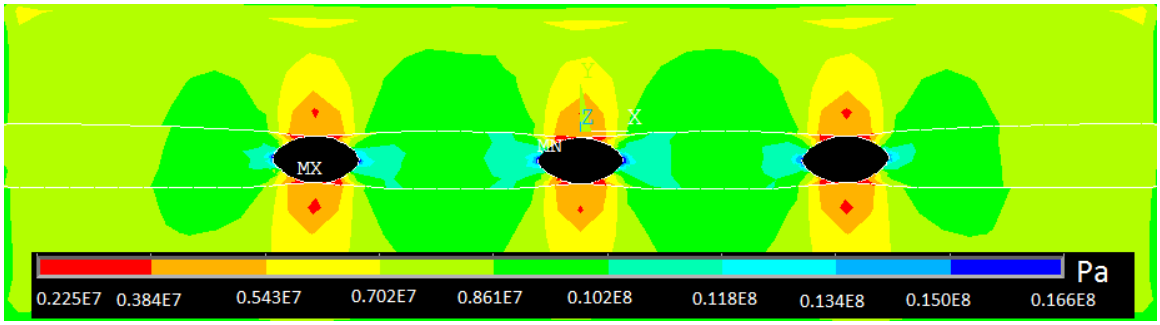

Figure 113. Contour map of maximum principal stress, Phase 3, cavity radius = 3 m.

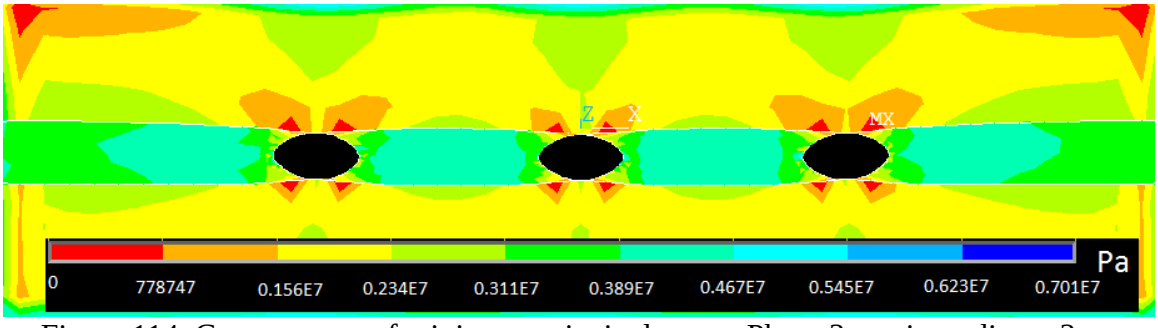

Figure 114. Contour map of minimum principal stress, Phase 3, cavity radius = 3 m.

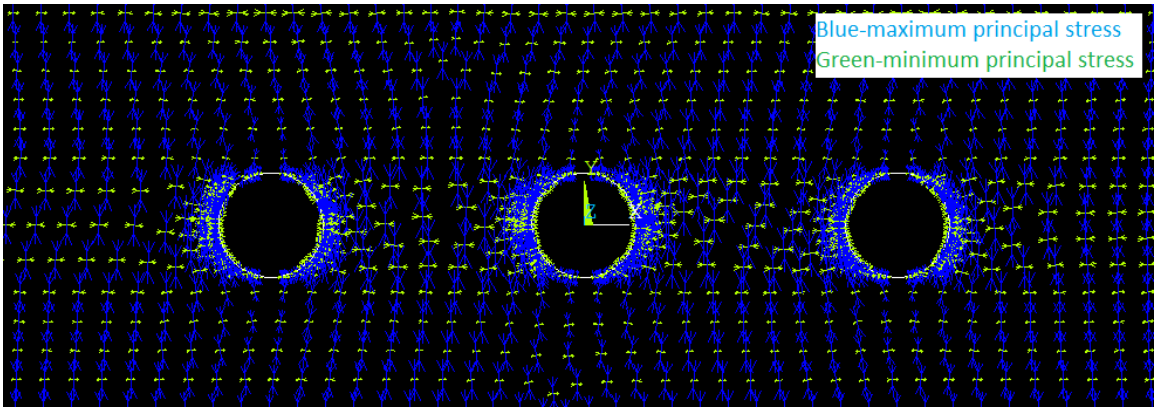

Figure 115. Vector map of principal stresses, Phase 3, cavity radius = 3 m.

From the results of numerical modeling, it can be concluded that the thermal stress is the largest part of the induced stress during the UCG process. The induced stress is much higher if an elevated temperature boundary condition is applied. With enough spacing, pillar between the cavities stays in safe status with low induced stresses. From the analytical solution in Section 5.4, it is suggested that plant arrangement with a cavity radius equal to 3 m can achieve a higher mining recovery factor. However, in the numerical modeling results, severe displacement and induced stresses propagate into the overburden in the case of 3 m cavity radius, and higher risk of subsidence may be induced compared to the arrangement with cavity radius of 2 m.

CHAPTER VI

SYNGAS PROCESSING AND POWER GENERATION

6.1 Process Description

The UCG-CCS system is similar to the IGCC plant, except that the surface gasifier in the IGCC plant is moved to the subsurface, and there is no requirement for coal storage and handling facilities. A pre-combustion process is applied to capture CO_2. To demonstrate the performance of a conceptual UCG-CCS plant, a simulation was run using the Integrated Environmental Control Model (IECM) 7.0 [80]. The simulation calculated the performance of an IGCC plant with pre-combustion CO_2 capture. Based on the calculation result, the cost associated with gasifier area is replaced by the drilling cost of gasification panel wells to figure out the cost of a UCG-CCS plant with the same net output. The economics of the two types of plant are compared.

A process diagram of the UCG-CCS system is shown in Figure 116. Oxygen is provided by the air separation unit (ASU) and injected with steam into the gasification cavity. Produced syngas is transported to the surface through the production well. The syngas is first cooled by a radiant cooler, and then sent to the WGS reactor, where CO is reacted with steam, and converted to CO_2 and H_2. At the outlet of the WGS reactor, the major components of the produced gases are CO_2 and H_2, with minor amount of H_2S as a

contaminant.

H_2S and CO_2 are removed by the "Double-Absorber" Selexol™ process. The separated CO_2 is compressed and sent through a pipeline to oil fields for EOR. The H_2S is sent to the sulfur recovery plant (Claus plant) to produce elemental sulfur as a sellable byproduct. The pure H_2 is combusted to drive a gas turbine to generate electricity. The waste heat in the exhaust gas from gas turbine is then recovered by a HRSG. Steam produced from the HRSG is used to produce additional electricity through a steam turbine. A detailed description for each of these processes is given as follows.

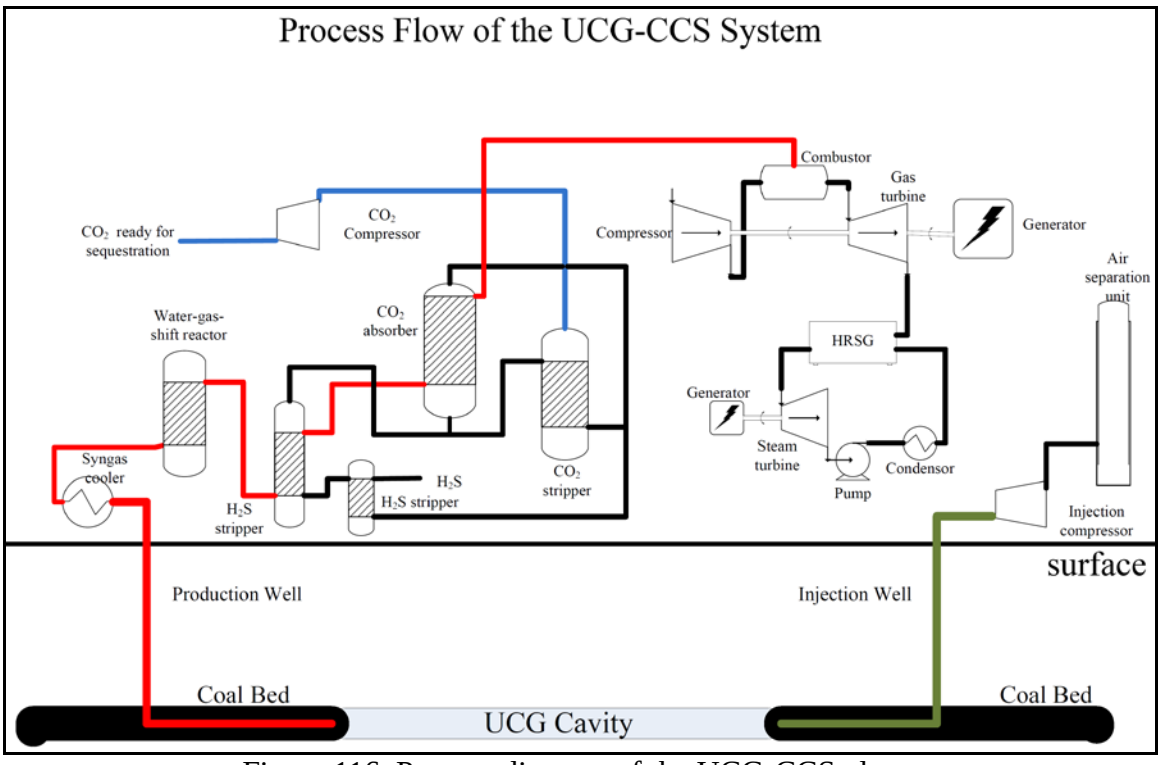

Figure 116. Process diagram of the UCG-CCS plant.

The ASU provides pure oxygen to the gasification at a high pressure via a cryogenic process. The final oxidant pressure is set as 4 MPa. In the IECM, the energy required by

the ASU to produce hydrogen is assumed to be 232 kWh per ton pure O_2 [80]. In this model, the ASU is not assumed to provide nitrogen to the gas turbine.

The WGS reaction is important for the CO_2 capture, since it converts the CO in the syngas into CO_2 and generates more hydrogen with the reaction:

$$CO + H_2O = H_2 + CO_2 \tag{33}$$

This is an exothermic reaction, which releases heat at a rate of 44.5 kJ/mol; so an environment of lower reaction temperature could facilitate the reaction [81, 82]. The released heat can be extracted to assist high pressure steam production for the steam cycle, similar to the radiant cooler and the convective cooler.

In the coal gasification process, most of the sulfur in the coal is converted to hydrogen sulfide (H_2S), instead of SO_x, as in most coal combustion processes [83, 84]. H_2S and CO_2 are removed by the "Double-Absorber" Selexol™ process.

The Selexol™ technology from UOP, LLC, a subsidiary of Honeywell, uses Dow Chemical's Selexol solvent, which is a mixture of dimethyl ethers of polyethylene glycol. The molecular formula is $CH_3(CH_2CH_2O)_nCH_3$ where n is between 3 and 9 [85]. The Selexol™ technology is a liquid physical solvent-based system for removing acid gases (H_2S, CO_2, and COS) from natural gas and syngas. It was developed over 35 years ago and more than 55 commercial Selexol™ units have been put into service. It is applicable at feed pressures greater than 2.4 MPa and acid gas concentrations above 5% by volume. In general, a CO_2 capture efficiency of over 85% can be achieved using the Selexol™

process. Selexol™ system has a minimum operating temperature of -18°C and is suitable for operation at temperatures up to 175°C [86, 87].

Figure 117 shows the single-stage Selexol™ process, which is used when the concentration of H_2S in the gas stream is low. The gas is contacted with the Selexol solvent in the absorber tower. The acid gas-rich solvent flows to the stripper tower, where it is heated to release the acid gases (primarily CO_2). The solvent is recycled back to the absorber tower.

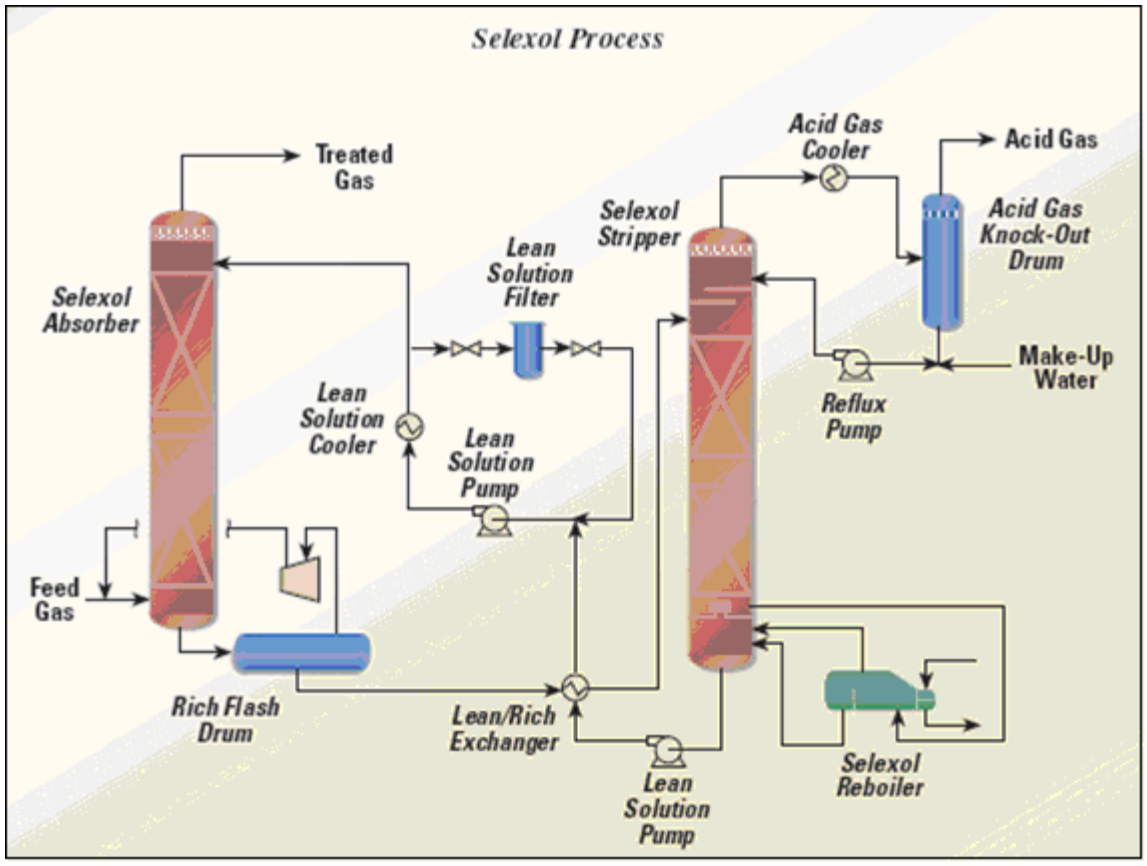

Figure 117. The UOP's Selexol™ Process [88].

The Selexol solvent preferentially removes H_2S over CO_2, so when H_2S is present with

CO_2 as more than a low-concentration contaminant (such as in syngas), a "Double-Absorber" Selexol™l process is used. This design uses the solvent "pre-loaded" by CO_2 from the downstream CO_2 absorption section to absorb the H_2S, which avoids taking both gases at the same time. With this design, the CO_2 to H_2S co-capture ratio can be limited at 1.75. Stripping the H_2S from the Selexol requires about 68 megajoule (MJ) per kg of sulfur stripped [82], and this heat can be provided by the waste steam from the low pressure steam turbine. Figure 118 shows the "Double-Absorber" Selexol™ process scheme which is used in the Kemper IGCC project in Mississippi, U.S.A.

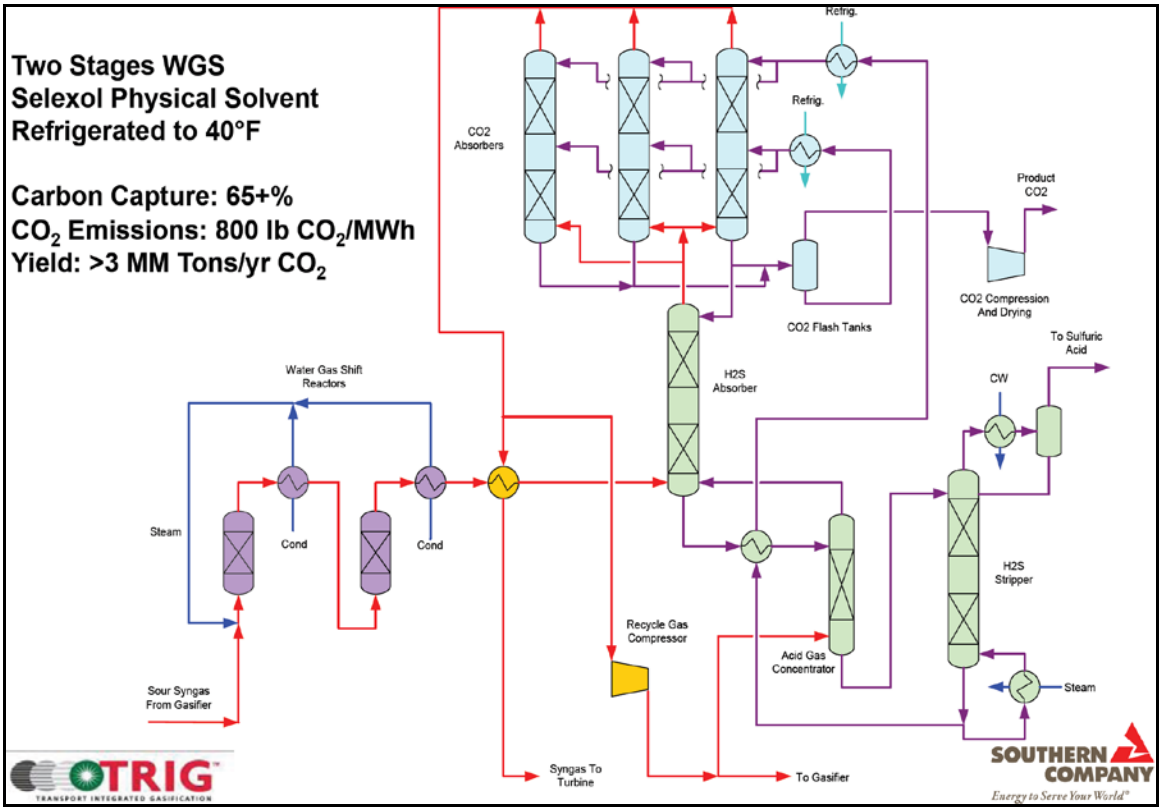

Figure 118. Scheme of the "Double-Absorber" Selexol™ process [89].

CO_2 in the syngas is removed by the Selexol™ process at an operation temperature of 30°C, or ambient temperature. As in the "Double-Absorber" mentioned above, 15% of

the solvent rich in CO_2 is recycled to the sulfur absorption tower. The rest goes through a series of flash drums. A series of flash drums are employed to decrease the pressure of the rich solvent to release the CO_2. The lean solvent is then pumped back to the absorption tower. Unlike the stripping of H_2S, there is no requirement for thermal stripping which consumes steam. Therefore, most of the energy consumption is due to the pumping power to recycle the solvent. The released CO_2 is then compressed to 13.7 MPa to send for sequestration.

In this model, a GE 7FB gas turbine is used. The total output of the gas turbine is 251.7 MW. Parameters of the gas turbine are listed in Table 16.

Table 16. Gas turbine parameters

Parameter	Unit	Value
Gas Turbine Model	-	GE 7FB
No. of Gas Turbines	-	1
Total Gas Turbine Output	MW	251.7
Fuel Gas Moisture Content	vol %	33
Turbine Inlet Temperature	°C	1371
Turbine Back Pressure	kPa	13.8
Adiabatic Turbine Efficiency	%	85.7
Shaft/Generator Efficiency	%	98
Pressure Ratio (outlet/inlet)	ratio	18.5
Adiabatic Compressor Efficiency	%	87.5
Combustor Inlet Pressure	kPa	1875
Combustor Pressure Drop	kPa	27.6
Excess Air For Combustor	% stoich.	136.3

The main components of the steam cycle include the HRSG, a high pressure turbine, an intermediate pressure turbine, a low pressure turbine, a condenser and a pump. The radiant cooler, convective cooler and WGS cooling system work as the high pressure boiler to generate additional high pressure steam. Operation parameters assumed are listed in Table 17.

Table 17. Operation parameter of the HRSG and steam cycle

Parameter	Unit	Value
HRSG Outlet Temperature	°C	121
Steam Cycle Heat Rate, HHV	kJ/kWh	9496
Aux. Heat Exch. Load	%	1.41
Total Steam Turbine Output	MW	107.1
Power Requirement	%	2

6.2 Modeling Results and Plant Performance

The coal used in the simulation is North Dakota lignite. Properties of the lignite (as received) are listed in Table 18. The plant has one GE 7FB gas turbine and one steam HRSG cycle. The Selexol™ process is used for CO_2 removal and H_2S removal. The plant is assumed to have a 30-year operation life. The discount rate (before tax) is assumed to be 7.9%. Performance of the power plant is listed in Table 19. The captured CO_2 is sold to the nearby oil fields, so the length of the pipeline is set as 20 miles. The coal gasification rate is 364 tons per hour to support a net electricity output of 232 MW.

Estimated financial results of the corresponding IGCC plant, including operation and

maintenance (O&M) cost, and capital costs are listed in Table 20. The total levelized annual cost is 2.22×10^8 $/year, of which the gasifier area shares more than 50%, or 1.30×10^8 $/year. The cost of electricity is 85.5 $/MWh.

Table 18. Properties of North Dakota lignite used in the model

Property	Unit	Value
Higher heating value	kJ/kg	14002.5
Carbon	wt%	35.04
Hydrogen	wt%	2.68
Oxygen	wt%	11.31
Chlorine	wt%	0.09
Sulfur	wt%	1.16
Nitrogen	wt%	0.77
Ash	wt%	15.92
Moisture	wt%	33.03

Table 19. Modeling result, plant performance

Parameter	Unit	Value
Coal feed rate	tonnes/hr.	364
Gross plant output	MW	359
Net electricity output	MW	232
Net plant efficiency	%	16.4
CO_2 emission rate	tonnes/hr.	27.0
Make up water	tonnes/hr.	165
CO_2 capture	Million tonnes/year	2.53
CO_2 storage method	-	EOR
Pipelien length	mile	20.0
capacity factor	%	75.0
CO_2 capture efficiency	%	93.6

Table 20. Modeling result, IGCC plant cost

Equipment	Fixed O&M, 10^6\$/year	Variable O&M, 10^6\$/year	Total O&M, 10^6\$/year	Annualized capital, 10^6\$/year	Total levelized annual cost, 10^6\$/year
ASU	8.68	44.5	53.2	29.6	82.8
Gasifier area	20.9	53.3	74.2	56.5	130
Sulfur control	5.81	3.7	9.51	14.7	24.2
CO_2 capture	10.6	-1.9	8.68	30.7	39.4
Power block	5.63	-81.6	-76	20.5	-55.5
Total	51.6	18	69.9	151.9	222
Cost of electricity	146 \$/MWh				
Cost of CO_2 captured	88.7 \$/metric ton				

To figure out the economics of a UCG-CCS plant of the same size, and compare it to the IGCC plant, the cost of surface gasifier is replaced by the drilling cost. Since both plants use the same surface facility, and achieve the same net electricity output, the fuel feed rate should be the same.

In most of the UCG pilot tests, the coal gasification rate ranges between 60~110 tons/day [90], which is too small to be used as reference for a commercial scale plant. In the report of GasTech [14], the model for a 200 MW UCG-CCS power plant was calculated. Twenty-five wells for start-up and 10 wells in addition annually are required for a 200 MW plant. The coal gasification rate is 227 tons per hour by using the Wyoming Power River Basin subbituminous. Considering differences of heating values between the

Wyoming subbituminous and North Dakota lignite, and scaling up by the plant size, about 19 new wells will be needed per year. Assuming the drilling cost is $580 per foot [91], and the average depth is 1200 ft, the UCG-CCS plant cost is listed in Table 21.

Table 21. Modeling result, UCG-CCS plant cost

Equipment	Fixed O&M, $10^6$$/year	Variable O&M, $10^6$$/year	Total O&M, $10^6$$/year	Annualized capital, $10^6$$/year	Total levelized annual cost, $10^6$$/year
ASU	8.68	44.5	53.2	29.6	82.8
Drilling wells	0.00	0.00	0.00	13.2	13.2
Sulfur control	5.81	3.7	9.51	14.7	24.2
CO_2 capture	10.6	-1.90	8.68	30.7	39.4
Power block	5.63	-81.6	-76	20.5	-55.5
Total	30.7	-35.3	-4.61	108	104
Cost of electricity	68.3 $/MWh				
Cost of CO_2 captured	88.7 $/metric ton				

Compared to the IGCC plant, the total levelized annual cost of a UCG-CCS plant is reduced to 104×10^6 $/year, or 47% of that for the IGCC plant. The cost of electricity is reduced to 68.3 $/MWh. Obviously the UCG-CCS plant shows a significant advantage in economics over the IGCC plant. This is attributed to the elimination of the gasifier area, which includes the surface gasifer and associated coal preparation facilities. The result also matches the prediction given by the GasTech Inc [14].

CHAPTER VII

SUMMARY AND CONCLUSIONS

7.1 Summary of Research Works

As only a small portion of the lignite reserves in North Dakota can be economically mined by conventional surface mining practices, UCG-CCS technology proposed in this study is expected to provide a clean and efficient way to recover this huge resource. UCG-CCS plants have a smaller footprint than IGCC plants have. High moisture content in the lignite is utilized favorably as a reactant in the gasification process, instead of functioning as a barrier during combustion in boilers. The produced syngas is versatile and can be used to generate electricity or upgrade to various chemical products and clean fuels such as hydrogen, substitute natural gas or liquid fuel through the Fischer-Tropsch process. Such a long industrial chain can generate job opportunities and tax revenues for the state. Successful UCG projects will help convert lignite resources beneath North Dakota into large economic benefits.

In this dissertation, a feasibility of the UCG technology in North Dakota has been conducted. A research roadmap was established. Finished works include literature review, site selection, geological formation modeling, laboratory geomechanical testing, induced stress analysis, stability assessment, estimate of mining recover factor, and

technical-economic analysis of a UCG plant.

As described in previous chapters, candidate sites in Dunn County, Golden Valley County and Slope County in North Dakota, which are suitable for a UCG-CCS project, have been selected out, and three-dimensional models were constructed to visualize the structure, lithological composition, clay content and hydrological condition of the lignite-bearing formation. In each of these sites, the coal seam is thick, deep, and expansive. The selected site in Dunn County has the best potential to host the UCG-CCS project for its appropriate geologic conditions and proximity to oil fields. Some aquifers exist in close distance to the lignite seam, and should be avoided during the UCG operation. Most parts of the surrounding strata, except areas where the aquifers are located, have high clay content; which would function as a seal for the gasification zone. The proposed area overlies with Little Knife Anticline, which is an active oil producing region in North Dakota. Major producing pools include Bakken, Duperow, Madison, and Red River Formations. Some oil fields in this region are now at the secondary or tertiary production phase, meaning a potentially big demand for CO_2 for EOR in the future. The CO_2 storage potential of nearby oil fields is estimated to be 18 million tones. The region is also tectonically stable, and no major faults exit at the selected site.

In the laboratory study, the mechanical and fluid transport properties of the surrounding rocks collected from the overburden of the Harmon coal bed were tested. Some interesting phenomena were observed. These results and observations can provide useful information to the assessment and design of UCG projects in the target coal bearing

formation. However, because of the limitation of laboratory facility, the tests were not carried out with heating. So the information about the behaviors of the specimens at high temperatures is missing.

First, the tested specimens had a low strength, which would be a disadvantage from the view of structural stability of the UCG plant. UCG process would result in significant induced stress around the cavity. The formation may be prone to fail due to the low strength of the rock. Some of the rock samples are very soft and behave like soil at failure, and this can be very risky to the gasification process.

The rocks had a low permeability; and the permeability tends to reduce with both increasing stresses perpendicular and parallel to the flow direction. The test results indicate that the overburden rocks may function well as a hydraulic seal to the gasification zone, and prevent escape of contaminants during and after the gasification process.

During the UCG process, groundwater may be drawn to the gasification zone from adjacent aquifers. As water flows in, formation around the gasification zone may become saturated with water. In the tests, we observed the rocks showing compressibility and a quasi-creeping behavior after being saturated with water; and the specimens were able to buffer the load. How such a characteristic would affect the gasification process needs further investigation. The overburden of the Harmon coal zone is described as mainly claystone, interbedded with sandstone and mudstone in literatures. However, only

claystone samples were collected from the outcrop and used in this study. These samples are weathered to different degrees, and the properties would be somewhat different from those underground.

A commercial UCG plant involves multiple gasification cavities, and the induced stresses would set limits for the mining recovery factor and plant economics. For a conceptual UCG plant in commercial scale, its developmental procedure has been classified into three major phases in this study. Phase 1 is the development of the first gasification cavity. In this phase, induced stresses only result from the cavity in gasification process, and the stress alternation is based on the natural in-situ stress field. Phase 2 is the development of the next cavity based on the disturbed stress field. Phase 3 is the post gasification, and all the cavities have been gasified and cool down. Both analytical and numerical approaches were employed to investigate stress field and displacement profiles associated with these development phases. The mining recovery factor and structural stability were studied.

The results indicate that the properties of the coal seam and the presence of the discontinuities have a significant effect on the mining recovery factor, and hence on the economics of the plant. The safety and the achievable mining recovery factor are always in tension with each other. For safety purposes, a conservative value may be assigned to the sacrifice of the mining recovery factor. The analytical solution suggests that the mining recovery factor increases with the radius of the gasification cavity. As the diameter of the gasification cavity reaches the thickness of the coal bed, the maximum recovery factor can be achieved. However, the numerical modeling result shows that,

when the cavity diameter is equal to the coal bed thickness, severe induced stresses and displacement may propagate into the caprock. This would increase the risks of structural stability. In general, as indicated in the examples, by understanding the properties of the formation, and designing reasonable cavity radius and spacing, the stability of the cavities can be guaranteed, with improved recovery efficiency.

In the last section of this study, the performance and cost of the proposed UCG-CCS plant were studied by analogue to the IGCC system of the same size. The calculated results indicate that the UCG-CCS plant present advantages over the IGCC plant in both investment and operation cost. Because of the removal of coal mining, transportation, storage, handling, and surface gasifier, the total annual cost of a UCG-CCS plant with 30-year operation life is reduced to 104×10^6 $/year; the cost of electricity is reduced to 68.3 $/MWh, or 47% of that for the IGCC plant.

7.2 Discussion and Conclusion

More than 30 UCG trial projects were conducted in the U.S. during 1970 – 1980s, but currently no commercial or trial project is in actual operation. Environmental pollution and disappointing economic returns are the major issues. However, in recent decades, thanks to great technological advances such as directional drilling, process monitoring, well linkage, computer modeling, as well as expectation on reduction of CO_2 emission and energy cost, UCG technology has received renascent interest; and several successful UCG pilot projects have been conducted in the world. These projects have provided large

economic and environmental benefits, as well as valuable information concerning UCG site selection, process design and operation. With the significant unmineable lignite resource, there exist opportunities in North Dakota of developing the UCG combined with CCS and EOR, and development of this process helps to contribute to the “energy independence” of the United States. All above together gives a motivation to assess the possibility of using UCG in North Dakota.

As mentioned in previous chapters, there are several challenges associated with the application of UCG in North Dakota, including coincidence of aquifers and the Harmon lignite bed, lack of information about the geomechanical properties of coal-bearing formation, and uncertainty of the economic performance of a UCG plant of commercial scale. These challenges have been discussed and answered in this dissertation study. The applicability of the proposed UCG-CCS system in North Dakota, utilizing the Harmon lignite bed, is confirmed. Careful site selection, detailed facies modeling, good understanding of formation properties, and optimized gasification pressure can be used to eliminate the risk of groundwater pollution. Regarding to structure safety, enough knowledge about the geomechanical properties and optimized cavity arrangement can be applied to minimize the subsidence, guarantee stability, and obtain improved mining recovery factor. Based on knowledge about the specific geological formation in North Dakota, techniques, information, and suggestion are given from this dissertation to make sure the UCG technology will function safely and effectively.

To ensure consistent UCG researches based on North Dakota lignite resources and to

realize commercialization of UCG in North Dakota, the research work is moving forward. Cores and samples in the Harmon bed, overlayer and underlayer will be obtained. Proximate and ultimate analysis and swelling test of the lignite will be carried out once the samples are available. A gasification test to simulate the underground conditions and measure the product composition is also in the plan. Mechanical properties of adjoining rock samples will be tested before and after heating to investigate the changes, and predict the effects on structural stability. Transport properties of the lignite beds and adjoining rocks will also be tested. The test results will be used to predict possible environmental risks and how the UCG process will affect the flow patterns of groundwater.

REFERENCES

1. BP. 2012. Statistical review of world energy 2012, http://www.bp.com/subsection.do?categoryId=9037151&contentId=7068607 (accessed July 2012).

2. U.S. Energy Information Administration. 2012. Energy explained – electricity in the United State, http://205.254.135.7/energyexplained/index.cfm?page=electricity_in_the_united_states (accessed June 2012).

3. U.S. Energy Information Administration. 2012. Data of coal, http://205.254.135.7/coal/data.cfm#summary (accessed June 2012).

4. U.S. Energy Information Administration. 2012. Energy explained – coal, http://205.254.135.7/energyexplained/index.cfm?page=coal_home (accessed June 2012).

5. U.S. Energy Information Administration. 2012. Energy in brief – what is the role of coal in the United States? http://205.254.135.7/energy_in_brief/role_coal_us.cfm (accessed June 2012).

6. Linc Energy Ltd. 2008. Underground coal gasification: Industry review and an assessment of the potential of UCG and UCG value added products, http://www.lincenergy.com/data/media_news_articles/relatedreport-02.pdf (accessed May 2012).

7. Metz, B., Davidson, O., de Coninck, H., Loos, M. and Meyer, L. 2005. *IPCC special report on carbon dioxide capture and storage*. New York: Cambridge University Press.

8. Burton, E., Friedmann, J. and Upadhye, R. 2006. Best practice in underground coal gasification. Project Report, Contract No. W-7405-Eng-48, US Department of Energy, Washington, DC.

9. Friedmann, S., Upadhye, R and Kong, F. 2009. Prospect for underground coal gasification in carbon-constrained world. *Energy Procedia* **1** (1): 4551-4557.

10. Shafirovich, E. and Varma, A. 2009. Underground coal gasification: a brief review of current status. *Industrial and Engineering Chemistry Research* **48** (17): 7865-7875.

11. Blinderman, M.S. and Friedmann, S. 2006, UCG with CCS: a pathway to a low-cost, low-carbon gas for power generation and chemical syntheses. Presentation at the 5th Annual Conference on Carbon Capture and Sequestration, Alexandria, Virginia, 8-11 May.

12. UCG Association. 2012. Worldwide UCG projects and development, http://www.ucgassociation.org/index.php?option=com_content&view=article&id=70&Itemid=219 (accessed July 2012).

13. Kempka, T., Nakaten, N., Azzam, R. and Schluter, R. 2009. Economic viability of in-situ coal gasification with downstream CO_2 storage. *Glückauf Mining Reporter* **1**: 43-50.

14. GasTech, Inc. 2007. Viability of underground coal gasification in the “deep coals”

of the Powder River Basin, Wyoming. Report prepared for the Wyoming Business Council, Business and Industry Division State Energy Office, Cheyenne, Wyoming.

15. Perkins, G. and Shahajwalla, V. 2007. Modeling of heat and mass transport phenomena and chemical reaction in underground coal gasification. *Chemical Research and Design* **85** (3): 329–343.

16. Biezen, E. and Bruining, J. 1995. An integrated 3D model for underground coal gasification. Proceedings of the SPE Annual Technical Conference& Exhibition, Dallas, Texas. 22-25 October.

17. Blinderman, M.S., Saulov, D.N. and Klimenko, A.Y. 2008. Exergy optimisation of reverse combustion linking in underground coal gasification. *Journal of the Energy Institute* **81** (1): 7-13.

18. Ergo Exergy Inc. 2012. What is εUCG process? http://www.ergoexergy.com/eucg.htm (accessed July 2012).

19. Britten, J. A. 1985. Modeling thermal and material interactions between a re acting char bed and a gasifying/spalling coal roof. Project Report, Contract No. W-7405-ENG-48. US Department of Energy, Washington, DC.

20. Hadro, J. 2008. A new approach to the coalbed methane exploration in the Upper Silesian Coal Basin. Presented at the 2008 International Mining Forum, Wieliczka, Poland, February 2008.

21. Brunner, D.J. and Schwoebel, J.J. 2009. Directional drilling for methane drai nage and exploration in advance of mining: recent advances and applications.

REI Drilling, http://www.reidrilling.com/uploads/files/1247/REI-Drilling-Technical-Paper.pdf (accessed June 2012).

22. Bowen, B.H. 2008. Underground Coal Gasification (UCG), Presentation to Heritage Research Laboratory, Indianapolis, Indiana, 21st October 2008, http://www.purdue.edu/discoverypark/energy/assets/pdfs/cctr/presentations/UCG-HeritageLab-10-21-08.pdf. Accessed June 2012 (accessed May 2012).

23. Olovyanne, A.G. 2005. Mathematical modeling of hydraulic fracturing in coal seams. *Journal of Mining Science* **41** (1): 61-67.

24. U.S. Environmental Protection Agency. 2004. Evaluation of impacts to underground sources of drinking water by hydraulic fracturing of coalbed methane reservoirs. National study final report, US EPA, Washington, DC.

25. Zhu, Y. 2004. Evaluation of Gas Turbine and Gasifier-Based Power Generation System. PhD Dissertation, North Carolina State University, Raleigh, North Carolina (August 2004).

26. Haslbeck, J., Michael, D., Rutkowski, M., Buchanan, T., Goldstein, H., Klett, M., Schoff, R. and White, J. 2002. Evaluation of fossil fuel power plants with CO2 recovery. Final report, task No. 50802 /Subtask No. 01200, US Department of Energy, Washington, DC.

27. Geosite, R. and Schmoe, L. 2005. IGCC – The Challenge of integration. Proceedings of GT2005 ASME Turbo Expo 2005: power for land, sea, and air, Reno-Tahoe, Nevada, 6-9 June.

28. Martelli, E., Kreutz, T. and Consoni, S. 2009. Comparison of coal IGCC with and

without CO_2 capture and storage: Shell gasification with standard vs. partial water quench. *Energy Procedia* **1** (1): 607-614.

29. Wender, I. 1996. Reaction of synthesis gas. *Fuel Processing Technology* **48** (3): 189-297.

30. Liu, S., Li, J., Mei, M. and Dong, D. 2007. Groundwater pollution from underground coal gasification. *Journal of China University of Mining & Technology* **17** (4): 467-472.

31. Yang, L. and Zhang, X. 2009. Modeling of contaminant transport in underground coal gasification. *Journal of Energy & Fuels* **23** (1): *193–201*.

32. Mead, S., Wang, F., Ganow, H., Stuermer, D. and Stone, R. 1979. Ground-water effects of underground coal gasification experiments in Northeastern Wyoming. Proceedings of the Annual Fall Technical Conference and Exhibition of the Society of Petroleum Engineers, Las Vegas, Nevada, 23-28 September.

33. Heck, T. J., LeFever, R. D., Fischer, D. W. and LeFever, J. 2007. Overview of the petroleum geology of the North Dakota Williston Basin. *North Dakota Geological Survey Report*, Bismarck, North Dakota.

34. Fred, F. M. 1978. Petroleum Geology of the Bakken Formation, Williston Basin, North Dakota and Montana. Presentation at the Williston Basin Symposium. Montana Geological Society 24th Annual Conference, Billings, Montana.

35. Fischer, D., Smith, S., Peck, W., LeFever, J., LeFever, R., Helms, L., Sorensen, J., Steadman, E. and Harju, J. 2005. Overview of Williston Basin geology as it relates to CO_2 sequestration. Report of the Plains CO_2 Reduction Partnership Report,

Energy & Environmental Research Center, The University of North Dakota, Grand Forks, North Dakota.

36. Flores, R.M., Keighin, C.W., Ochs, A.M., Warwick, P.D., Bader, L.R. and Murphy, E.C. 1999. 1999 Resource assessment of selected tertiary coal beds and zones in the Northern Rocky Mountains and Great Plains Region, Part II: Williston Basin, Chapter WF, Framework of coal geology of the Fort Union coals in the Williston basin. In *U.S. Geological Survey Professional Paper 1625-A.*

37. Murphy, E.C., Kruger, N.W., Goven, G.E., Vandal, Q.L., Jacobs, K.C. and Gutenkunst, M.L. 2006. The lignite resources of North Dakota. Report of Investigation No. 105, North Dakota Geological Survey, Bismarck, North Dakota.

38. Stricker, G.D., and Ellis, M.S. 1999. 1999 Resource assessment of selected tertiary coal beds and zones in the Northern Rocky Mountains and Great Plains Region, Part II: Williston Basin, Chapter WQ, Coal quality and geochemistry, Williston basin, North Dakota. In *U.S. Geological Survey Professional Paper 1625-A.*

39. Cvancara, A.M. 1976. Geology of the Cannonball Formation (Paleocene) in the Williston Basin, with reference to uranium potential. Report of Investigation No. 57, North Dakota Geological Survey, Bismarck, North Dakota.

40. Winczewski, L.M. 1982. Paleocene coal-bearing sediments of the Williston Basin North Dakota: an interaction between fluvial systems and intracratonic basin. Ph.D dissertation, University of North Dakota, Grand Forks, North Dakota.

41. Smith, S. A., Sorensen, J.A., Steadman, E.N., Harju, J.A. and Fischer, D.W. 2009. Estimates of CO_2 storage capacity in selected oil fields of the northern Great Plains

region of North America. In *Carbon dioxide sequestration in geological media—State of the science: AAPG Studies in Geology* **59**, eds. M. Grobe, J. C. Pashin and R. L. Dodge, 87– 97.

42. Sury, M., White, M., Kirton, J., Carr, P., Woodbridge, R., Mostade, M., Chappell, R., Hartwell, D., Hunt, D. and Rendell, N. 2004. Review of environmental issues of underground coal gasification. Report COAL R272 DTI/Pub URN 04/1880, Department of Trade and Industry Technology (DTI), London, United Kingdom.

43. Shafirovich, E., Mastalerz, M., Rupp, J. and Varma, A. 2008. The potential for underground coal gasification in Indiana, Phase I report to the Indiana Center for Coal Technology Research (CCTR), West Lafayette, Indiana.

44. Topuz, E. 1982. Methane resources of the unmineable coal seams in the Richmond Basin. Proceedings of the SPE Unconventional Gas Recovery Symposium, Pittsburgh, Pennsylvania, 16-18 May.

45. North Dakota Geological Survey. 2009. Coal maps of North Dakota. https:// www.dmr.nd.gov/ndgs/Coalmaps/pdf/100K/bwmn_100k_c.pdf (accessed Februar y 2010).

46. Linc Energy. 2006. Groundwater use in UCG, Technical Report LINC-ENV-06.2, Linc Energy, Brisbane, Australia.

47. Ellis, M.S., Gunther, G.L. Ochs, A.M. Keighin, C.W. Goven, G.E., Schuenemeyer, J.H., Power, H.C., Stricker, G.D. and Blake, D. 1999. 1999 Resource assessment of selected tertiary coal beds and zones in the Northern Rocky Mountains and Great Plains Region, Part II: Williston Basin, Chapter WN, Coal Resource. In *U.S.*

Geological Survey Professional Paper 1625-A.

48. US Geological Survey. 2000. Williston Basin stratigraphic data, supporting d ata of the National Coal Resource Assessment, Region 4, Rocky Mountains and Great Plains Supporting data, http://energy.cr.usgs.gov/coal/coal_assessme nts/reg4gis.html (accessed December 2009).

49. Schlumberger. 2010. Petrel. Houston, Texas. http://www.slb.com/services/soft ware/geo/petrel.aspx.

50. IHS Inc. Petra. 2009. Douglas County, Colorado. http://www.ihs.com/products /oil-gas-information/analysis-software/petra.aspx.

51. Senergyworld. 2009. Interactive Petrophysics. Houston, Texas. http://www.sen ergyworld.com/software/interactive-petrophysics.

52. U.S. Geological Survey. 2010. Lower Tertiary Aquifers, Northern Great Plain s aquifer system, USGS H730-I Ground Water Atlas of the United States, h ttp://pubs.usgs.gov/ha/ha730/ch_i/index.html (accessed May 2011).

53. Klausing, R. 1979. Ground-water resources of Dunn County, North Dakota. Prepared by the U.S. Geological Survey in cooperation with the North Dakota Geological Survey, North Dakota State Water Commission, and Dunn County Water Management District.

54. Oil and Gas Division, Department of Mineral Resources, North Dakota Industrial Commission. 2010, https://www.dmr.nd.gov/oilgas/ (accessed June 2010).

55. Buscheck, T.A., Hao, Y., Morris, J.P. and Burton, E.A. 2009. Thermal-hydrological sensitivity analysis of underground coal gasification. Proceedings of the 2009

International Pittsburgh Coal Conference, Pittsburgh, Pennsylvania, September 20 – 23.

56. Shoemaker, H., Advani, S. Gmeindi, F. and Lin, Y. 1978. The influence of bituminous coal and overburden thermo-mechanical properties on subsidence associated with underground coal conversion, *ACE Fuel*, **23**: 233-244.

57. Morris, J.P., Buscheck, T.A. and Hao, Y. 2009. Coupled geomechanical simulation of UCG evolution. Proceedings of the 2009 International Pittsburgh Coal Conference, Pittsburgh, Pennsylvania, September 20 – 23.

58. Advani, S.H., Lin, Y.T. and Shuck. L.Z. 1977. Thermal and structural response evaluation for underground coal gasification. *SPE Journal* **17** (6): 413 – 422.

59. Younger, P. 2011. Hydrogeological and geomechanical aspects of underground coal gasification and its direct coupling to carbon capture and Storage. *Mine Water and the Environment* **30** (2): 127 – 140.

60. Tan, Q., Luo, X. and Li. S. 2008. Numerical modeling of thermal stress in a layered rock mass. Proceedings of the 42nd US Rock Mechanics Symposium and 2nd US-Canada Rock Mechanics Symposium in San Francisco, 29 June – 2 July.

61. Fjar, E., Holt, R.M. Horsrud, P. Raaen, A.M. and Risnes. R. 1992. *Petroleum Related Rock Mechanics*. 1st ed. Oxford, United Kingdom: Elsevier.

62. Hudson, J.A., and Harrison. J.P. 1997. *Engineering Rock Mechanics, An Introduction to the Principles*. 1st ed. London, United Kingdom: Pergamon.

63. Sheng, M. 1998. *Rock Mass Mechanics.* 1st ed. Shanghai, China: Tongji University Press.

64. Barcaly, V. 1974. Geological map and lignite deposits of the Dengate Quadrangle, Morton County, North Dakota. Coal investigation map, MAP C-67, U.S. Geological Survey, Denver, Colorado.

65. Zeng, Z. 2006. Multipurpose tri-axial core flooding system. Research report, Grand Forks, North Dakota: University of North Dakota.

66. MTS Inc. 2012. Geomaterials test systems, http://www.mts.com/en/products/producttype/test-systems/load-frames-uniaxial/servohydraulic/geomaterial/index.htm (accessed July 2012).

67. Fetter, C.W. 2001. *Applied Hydrogeolgoy.* 4th ed. Upper Saddle River, New Jersey: Prentice-Hall, Inc.

68. Zhu, W., Montesi, L.G. and Wang. T. 1997. Shear-enhanced compaction and permeability reduction: triaxial extension tests on porous sandstone. *Mechanicals of Materials* **25**: 199 – 214.

69. Zhou, X., Zeng, Z. and Liu, H. 2010. Laboratory testing on Pierre Shale for CO_2 sequestration on clayey caprock. Proceedings of the 44th US Rock Mechanics Symposium and 5th US-Canada Rock Mechanics Symposium in Salt Lake City, June 27 – 30.

70. Gueguen, Y and Bouteca, M. 2004. *Mechanics of Fluid Saturated Rocks*. Maryland Heights, Missouri: Academic Press.

71. Brewer, R.E, 1942. Plastic and swelling properties of bituminous coking coals. In *BuMines Bulletin*.

72. Macrae, J. C. and Mitchell. A.R. 1957. The response of bright bituminous coal to

undirectional compression. *Fuel* **36**: 423-441.

73. Sanda, Y. and Honda, H. 1963. Creep in coal over the temperature range 200 to 370^{o}C. *Fuel* **42**: 479-486.

74. Lin, Y.T. 1978. Structural mechanics simulations associated with underground coal gasification. Project report MERC/CR-78/4, US Department of Energy, Washington, DC.

75. Friedmann, J. 2007. Fire in the hole. *Science and Technology Review.* Lawrence Livermore National Laboratory, Livermore, California.

76. Stakgold, I., 1987. *Boundary Value Problems of Mathematical Physics*. New York: Macmillan.

77. Chen, G., Chenevert, M.E. Sharma, M.M. and Yu. M. 2003. A study of wellbore stability in shales including poroelastic, chemical, and thermal effects. *Journal of Petroleum Science & Engineering* **38** (3-4): 167 – 176.

78. Zipf, R.K. 2001. Toward Pillar Design To Prevent Collapse of Room-and-Pillar Mines. Proceedings of the 108th Annual Exhibit and Meeting, Society for Mining, Metallurgy, and Exploration, Denver, Colorado, February 26-28.

79. ANSYS, Inc. 2010. ANSYS Version 13.0. 2010. Canonsburg, Pennsylvania.

80. Integrated Environmental Control Mode, version 7.0. 2012. Pittsburgh, Pennsylvania: The Carnegie Mellon University.

81. Chiesa, P., Consonni, S., Thomas Kreutz, T. and Williams, R. 2005. Co-production of hydrogen, electricity and CO_2 from coal with commercially ready technology, Part A: Performance and Emissions. *International Journal of Hydrogen Energy* **30**

(7): 747-767.

82. Probstein, R.F., and Hicks, R.E. 2006. *Synthetic Fuels*. Mineola, New York: Dover Publication.

83. Takematsu, T. and Maude, C. 1991. *Coal gasification for IGCC power generation*. London, United Kingdom: International Energy Agency Coal Research.

84. Clarke, L.B. 1991. *Management of by-products from IGCC power generation.* London, United Kingdom: International Energy Agency Coal Research.

85. Kuryachiy, V.G., 2007, Coal power plants—IGCC process description: www. carboncapture.us/docs/IGCC_UNITS.ppt (accessed August 2010).

86. Bucklin, R.W. and Schendel, R.L. 1984. Comparison of Fluor solvent and Selexol processes. *Energy Progress* **4** (3): 137–142.

87. Ciferno, J., Klara, J., Schoff, R. and Cpicotto, P. 2006 cost & performance comparison of fossil energy power plants. Presented at the 5th Annual Conference on Carbon Capture & Sequestration, Alexandria, Virginia, May 8–11.

88. UOP. 2009. Selexol process: www.uop.com/objects/97%20Selexol.pdf (accessed July 2010).

89. Rush, R. 2012. Overview of the Kemper County IGCC Project Using Transport Integrated Gasification (TRIGTM). Presentation given to the Research Experience of Carbon Sequestration 2012, Birmingham, Alabama, 5 June.

90. Neville, A. 2011. Underground coal gasification: another clean coal option. *Power Magazine,* July 2011: 36-42.

91. U.S. Energy Information Administration. 2012. Cost of crude oil and natural gas wells drilled, http://www.eia.gov/dnav/pet/pet_crd_wellcost_s1_a.htm (accessed July 2012).

Nomenclature

ASU: air separation unit

bbl: barrel

^{o}C: degree Celsius

CCS: carbon capture and storage

CBM: coalbed methane

cm: centimeter

CRIP: controlled retraction injection point

DME: Diemthyl Ether

EIA: Energy Information Administration

EOR: enhanced oil recovery

EPA: Environmental Protection Agency

FCL: Foward Combustion Linking

FE: finite element

ft: foot

GPa: gigapascal

GR: gamma ray

HRSG: heat recovery steam generator

IECM: Integrated Environmental Control Model

IGCC: integrated gasification combined cycle

IPCC: Intergovernmental Panel on Climate Change

K: kelvin

kJ: kilojoule

kg: kilogram

km^2: square kilometer

kPa: kilopascal

KWh: kilowatt-hour

LLNL: Lawrence Livermore National Laboratory

m: meter

m^3: cubic meter

mD: millidarcy

mm: millimeter

MJ: megajoule

mol: mole

MPa: megapascal

M.R.F.: mining recovery factor

MW: megawatt

MWh: megawatt-hour

m/d: meter per day

NDGS: North Dakota Geological Survey

NDIC: North Dakota Industry Commission

O&M: operation and maintenance

OOIP: original oil in place

PC: pulverized coal

PJ: petajoule

ppmv: parts per million by volume

R/P: reserve-to-production ratio

RCL: Reverse Combustion Linking

RQD: rock quality designation

scf: standard cubic feet

S.F.: safety factor

SNG: synthetic natural gas

THCM: Thermal-hydrological-chemical-mechanical

UCG: underground coal gasification

UCG-CCS: underground coal gasification coupled with carbon capture and storage

UND: University of North Dakota

USGS: United States Geological Survey

WGS: water gas shift